Defects in Ge and GeSn and their impact on optoelectronic properties 🅕

View Online   Export Citation   CrossMark

Andrea Giunto[1,a] 🆔 and Anna Fontcuberta i Morral[1,2,a] 🆔

AFFILIATIONS

[1]Laboratory of Semiconductor Materials, Institute of Materials, School of Engineering, École Polytechnique Fédérale de Lausanne, Lausanne, Switzerland

[2]Institute of Physics, School of Basic Sciences, École Polytechnique Fédérale de Lausanne, Lausanne, Switzerland

[a]Authors to whom correspondence should be addressed: andrea.giunto@epfl.ch and anna.fontcuberta-morral@epfl.ch

ABSTRACT

GeSn has emerged as a promising semiconductor with optoelectronic functionality in the mid-infrared, with the potential of replacing expensive III–V technology for monolithic on-chip Si photonics. Multiple challenges to achieve optoelectronic-grade GeSn have been successfully solved in the last decade. We stand today on the brink of a potential revolution in which GeSn could be used in many optoelectronic applications such as light detection and ranging devices and lasers. However, the limited understanding and control of material defects represents today a bottleneck in the performance of GeSn-based devices, hindering their commercialization. Point and linear defects in GeSn have a strong impact on its electronic properties, namely, unintentional doping concentration, carrier lifetime, and mobility, which ultimately determine the performance of optoelectronic devices. In this review, after introducing the state-of-the-art of the fabrication and properties of GeSn, we provide a comprehensive overview of the current understanding of GeSn defects and their influence on the material (opto)electronic properties. Where relevant, we also review the work realized on pure Ge. Throughout the manuscript, we highlight the critical points that are still to solve. By bringing together the different fabrication techniques available and characterizations realized, we offer a wholistic view on the field of GeSn and provide elements on how it could move forward.

TABLE OF CONTENTS

I. INTRODUCTION

GeSn is nowadays recognized as a promising absorber and emitter that can be integrated monolithically on the Si platform, operating in the short-wave infrared (SWIR) wavelengths (1.5–3 μm), potentially down to the medium-wave infrared (MWIR) (3–8 μm) and long-wave

infrared (LWIR) (8–15 μm).[1] The addition of Sn to the Ge lattice induces a red-shift in the material bandgap (BG), extending the absorption cutoff wavelength toward the infrared. In addition, it has been shown that above 7–9 at. % Sn,[2–4] the GeSn alloy acquires a direct BG, enabling its use as active material in light-emitting devices. Ge-rich GeSn alloys have been demonstrated in a plethora of optoelectronic devices including photodetectors,[5–8] lasers,[4,9–11] and light emitting diodes (LEDs).[12–14] Furthermore, the high theoretical mobility of GeSn[15,16] has motivated its development in field-effect transistors (FETs).[17–19] The possibility of monolithic integration on Si platforms has also pushed the investigation of GeSn in silicon photonics and for on-chip thermoelectric applications.[20,21] To date, despite more than 15 years of intensive research in the field, there exists no commercial device based on GeSn. In fact, there are numerous challenges hindering the rise of this material for the next-generation (opto)electronics.

In this review, we provide an overview of the withstanding challenges in the field of GeSn for (opto)electronic devices. Specifically, we illustrate the defects arising during material processing, and we discuss the current, albeit limited, understanding of their impact on the GeSn electrical properties. While our primary focus is on the GeSn alloy, we also address and explore studies on Ge as they pertain to understanding GeSn. In Sec. II, we provide a concise review of the historical development of GeSn as an optoelectronic grade semiconductor. This is accompanied by a description of the GeSn physical properties and the challenges associated with the material, respectively, in Secs. III and IV. In Sec. V, we investigate the general efforts in GeSn epitaxy, as well as the challenges associated with increasing the Sn content in the alloy. Additionally, we provide a detailed review of magnetron sputtering epitaxy of Ge and GeSn, complementing existing literature reviews that focus on growth of these materials by chemical vapor deposition (CVD) and molecular beam epitaxy (MBE). In Sec. VI, we discuss the defects arising during epitaxial growth of Ge and GeSn, considering both point defects and extended defects such as dislocations and stacking faults. In Sec. VII, we undertake a comprehensive examination of the optoelectronic characterization of Ge and GeSn films reported in the literature. This consists in compiling measurement data into detailed tables and condensing key findings to establish a coherent understanding of the subject. Finally, in Sec. VIII, we conclude with a brief discussion of the open questions in the field.

II. HISTORICAL PERSPECTIVES
A. Early days of c-GeSn

In 1982, Goodman first proposed crystalline GeSn (cGeSn) as a group-IV direct-BG material, hypothesizing alloy properties governed by Vegard's law between Ge and the diamond cubic phase of Sn (i.e., α Sn).[22] High mobility values were predicted due to the absence of polar scattering, typical in III–V and II–VI compounds. The Ge-Sn solid solution was, thus, suggested as alternative to III–V and II–VI materials for high-mobility FETs and infrared photodetectors in the SWIR, MWIR, and LWIR wavelengths. Challenges in experimental realization of this material were expected due to the low solubility limit of 1 at. % of Sn in Ge (and vice versa)[23,24] and the lack of a lattice-matched substrate to stabilize metastable GeSn phases. Metastable, micro-crystalline GeSn with more than 20 at. % Sn was demonstrated one year later, thanks to the use of out-of-equilibrium synthesis.[25] $Ge_{0.78}Sn_{0.22}$ was crystallized from amorphous $Ge_{0.70}Sn_{0.30}$ by means of a UV pulsed laser. The first epitaxial metastable GeSn film appeared in

1987, with growth up to 8 at. % Sn on a Ge(001) substrate by sputtering.[26] The growth temperature was maintained at 150 °C to prevent Sn segregation due to the reduced solubility in Ge.

B. First monocrystalline GeSn films

Slow, but notable progress in out-of-equilibrium synthesis processes was obtained in the 20 years following the demonstration of epitaxial GeSn on Ge(001). In 1989, Pukite *et al.*[31] employed the MBE method to push the Sn content to 30 at. % in polycrystalline GeSn films on Si(100) at 170 °C. Despite the successful sputtering growth of GeSn epitaxial films, MBE became the growth method of choice in the 1990s, hence seeing considerable improvements in the following years. After a few more studies reporting polycrystalline growth,[32,33] monocrystalline MBE-grown GeSn was obtained in 1992 on Ge(001), but only up to thicknesses of 2 nm. Thicker layers could not be obtained due to Sn segregation and the low growth temperatures employed.[34] Low growth temperatures ($T < 200$ °C) reduce the adatom mobility, causing kinetic roughening and strain-induced roughening,[35] limiting the epitaxial thickness to tens of nm for Sn fractions higher than 10 at. %.[36–38] Issues with Sn segregation and low-temperature growth were overcome in 1995 with the introduction of ion-assisted (Ar^+) MBE.[39] Mimicking the analogous effect in sputtering, it was found that slight Ar bombardment induced collisional mixing of Sn adatoms with the film, increasing Sn incorporation and limiting its segregation.[28] With this method, He *et al.*[28] obtained 20-nm-thick monocrystalline GeSn films on Ge-buffered Si(001) substrates with Sn contents up to 34 at. %. The same research group realized the first pseudomorphic GeSn film on Ge(001) in 2000, using standard thermal MBE.[40]

C. Demonstration of GeSn direct bandgap behavior

In 1997, He *et al.*[41] experimentally observed direct-BG behavior in GeSn for the first time. The BG crossing from indirect to direct character was found to occur for a Sn content of around 11 at. %. This constitutes a Sn alloy fraction considerably lower than the crossover composition expected at the time. The first theoretical studies of the GeSn alloy band structure using tight-binding models predicted in fact an indirect-to-direct BG transition around 20 at. % Sn,[42] similar to what expected from Vegard's law. This discrepancy between theory and experiments was understood in the 2000s with first-principle computations[43] and confirmed with subsequent experimental observation.[44] It was found that the behavior of the GeSn band energies follows a positive deviation from Vegard's law, described with the use of a bowing parameter (b),

$$E_{GeSn} = (1-x)E_{Ge} + xE_{\alpha Sn} - b(1-x)x, \quad (1)$$

where E is the BG energy of the respective materials.[45] Numerous measurements and computations of b have been reported in the literature since then, with values generally spanning between 2.0 and 2.5 eV (see Table I, discussed in Sec. III). The positive value of b implies that the BG crossover occurs at lower x compared to what predicted by Vegard's law, explaining the early disagreement between theoretical and experimental data. The discovery of a positive BG bowing behavior significantly boosted the prospects of the GeSn alloy, as it signified that the Ge BG can be strongly red-shifted with only a few at. % of Sn. This makes GeSn well-suited for optoelectronic applications in the

TABLE I. Summary of bowing parameters determined by experiments and computations. In the header row, $x_{Sn,max}$ refers to the maximal Sn fraction considered in the study. Acronyms: contactless electroreflectance (CER), variable angle spectroscopic ellipsometry (VASE), photoreflectance (PR), optical transmittance (OT), degree of strain relaxation (DSR).

	Ref.	b_Γ (eV)	b_L (eV)	Method	$x_{Sn,max}$	Comments
Experiments	Zelazna et al.[138]	1.8	⋯	CER	0.11	MBE, pseudomorphic on Ge. Compressive strain compensated in fits.
	Gallagher et al.[3]	$2.66 - 5.4x_{Sn}$	$1.11 - 0.78x_{Sn}$	PL	0.11	UHV-CVD, on Ge/Si. Compressive strain compensated in fits.
	Jiang et al.[139]	2.46	1.03	PL	0.06	CVD, on Si. Compressive strain compensated in fits.
	Lin et al.[140]	2.43	⋯	PR	0.064	MBE, on lattice-matched $In_yGa_{1-y}As$/GaAs.
	Pérez Ladrón et al.[141]	2.30	⋯	OT	0.14	MS, on Ge(100). Strain unspecified, thickness of few hundred nm.
	D'Costa et al.[44]	2.3	⋯	VASE and PR	0.20	UHV-CVD, on Si(100). Slight compressive (DSR > 90%).
	He and Atwater[41]	2.8	⋯	OT	0.15	MBE, on Ge/Si(100). Fully relaxed within experimental error.
Computations	Song et al.[126]	2.28	2.86	30-band k · p	0.3	Strain-free. Less precise than DFT.
	Polak et al.[112]	3.02	1.23	DFT	1	Strain-free. 54-atom supercell, fully random alloy
	Zelazna et al.[138]	1.97	0.26	DFT	0.08	Strain-free. 54-atom supercell, non-random
	Eckhardt et al.[135]	3.1	⋯	DFT	1	Strain-free. 216-atom supercell, fully random alloy
	Chibane and Ferhat[129]	1.94	0.90	DFT	0.25	Strain-free. 16-atom supercell, Sn-clustered and non-clustered cells.
	Yin et al.[45]	2.55	0.89	DFT	0.75	Strain-free. 64-atom supercell, fully random alloy.

SWIR range and potentially longer wavelengths in spite of its metastability.

D. First CVD-grown GeSn films

To overcome the limitations of MBE associated with low-temperature growth and kinetic roughening,[35] in the 2000s the attention was shifted toward alternative growth methods. Magnetron sputtering (MS) was successfully employed to grow few-hundred-nm-thick GeSn films on Ge(001) up to 14 at. % Sn,[46,47] while CVD growth was demonstrated in 2001 by Taraci et al. thanks to the introduction of stable Sn precursors;[48–50] films up to 200 nm with 20 at. % Sn were obtained on Si(100) by ultrahigh vacuum (UHV) CVD.[44] At the same time, the first SiGeSn films were demonstrated[51] with the potential of delivering a higher thermal stability and a decoupling of lattice parameter and BG energy.[52]

E. First GeSn-based (opto)electronic devices

These promising advances in epitaxy led to a growing interest in GeSn in the research community, evident in Fig. 1 from the increase in number of published works on GeSn from 2009 onward. With this increase in the number of studies, researchers gained a deeper understanding of GeSn synthesis processes and properties. For example, it was found that the Ge surface reconstructs in the presence of Sn,[53] and the misfit strain in GeSn films influences Sn precipitation during post-growth thermal processing.[54] A method to calculate the alloy BG dependence on composition and strain was also proposed.[55] Furthermore, the introduction of doping methods of GeSn[56] led to the first demonstration of a GeSn-based optoelectronic device in 2009 by Mathews et al.,[30] with the fabrication of a CVD-grown n-i-$Ge_{0.98}Sn_{0.02}$/p-Si photodiode (PD), sensitive up to 1750 nm. This detector possessed quantum efficiencies lower than 0.1% but, only 2 years later, an improved design in MBE-grown p-i-$Ge_{0.97}Sn_{0.03}$/n-Si demonstrated a responsivity in the SWIR comparable to commercial Ge devices.[57] In 2011, GeSn p-type metal-oxide-semiconductor field-effect transistors (MOSFETs) were demonstrated with a higher hole mobility than conventional Ge MOSFETs.[58,59] Furthermore, following demonstration of GeSn photoluminescence (PL),[29] the first GeSn-based LED was fabricated, demonstrating room-temperature electroluminescence and a clear red-shift in light emission with respect to Ge LEDs.[60,61] In the same year, Vincent et al. achieved GeSn epitaxial growth by atmospheric-pressure chemical vapor deposition (CVD) with commercially available precursors, demonstrating the viability of vacuum-free alloy growth, thus significantly simplifying the synthesis process.[62] The growth of epitaxial GeSn on Si(100) with industry-compatible reduced-pressure chemical vapor deposition (CVD) was published in

04 January 2025 10:11:00

2013 by Wirths et al.[63] These studies catalyzed additional momentum in the field, which gained even more interest from scientists and engineers. This heightened interest is evident from the corresponding growing number of publications dedicated to GeSn, appreciable in Fig. 1.

F. GeSn-based lasers

One of the most remarkable steps in the development of GeSn-based technology was the demonstration of the first optically pumped GeSn laser operating at $T < 90$ K with 12 at. % Sn at wavelengths of $\sim 2.3 \mu$m.[4] This was the last long-sought building block required for SWIR monolithic group-IV on-chip Si photonics,[64] setting off a race toward the achievement of an electrically pumped GeSn laser operating at room temperature, yet to be realized. Breakthroughs were reached in 2020 with the first electrically injected laser operating up to 100 K,[65] and in 2022 with room-temperature lasing obtained in optically-pumped $Ge_{0.86}Sn_{0.14}$ devices.[66] These works currently set the state-of-the-art of the operating temperatures in the respective injection modes. Factors limiting laser performance are the low carrier lifetimes in GeSn due to the presence of defects, and the limited direct nature of the GeSn BG. The latter, known as "directness" of the bandgap, is quantified via the difference in energy between the indirect L- and direct Γ-valleys.[4] These factors have the effect to increase the lasing threshold and to decrease the maximum operating temperature.[67] Common strategies to increase the BG directness, and thus the lasing temperature, are to induce tensile strain in the GeSn gain material or increase the Sn fraction in the alloy.[66,68,69] The former is preferable to avoid the increase in defect concentration associated with large Sn contents.[66] Material defects affecting the lasing thresholds may originate at the bulk,[70] surface,[11] and interface[68] of the active material. Some approaches have been proposed to limit the detrimental effects of these defects. Surface traps can be prevented via proper passivation

of the material, although no absolute passivation scheme has been established for GeSn, resulting in each group using different methods.[7,71–73] Interface defects arise from the arrays of misfit dislocations forming during GeSn epitaxy. They are physically unavoidable when growing on mismatched substrates. In microdisk laser architectures, misfit dislocations have been etched away to improve the lasing threshold.[68] Alternatively, type-I GeSn/SiGeSn and GeSn/Ge multi quantum well (MQW) structures have been employed to confine carriers away from the epitaxial interface.[70,74,75] On the other hand, there is no clear strategy to decrease the material bulk defect concentration, mainly because GeSn bulk defects and electrical properties are poorly understood, as elaborated later in Sec. VII.

G. Other GeSn-based devices

The highlighted challenges prevent room-temperature operation of electrically injected GeSn lasers, hindering the commercialization of these devices. The very same factors limit the performance of GeSn as active material in photodetectors, although promising improvements have been achieved in the latest years. GeSn PDs have been fabricated using various methods, including CVD,[5,76,77] MBE,[8,78,79] and magnetron sputtering (MS).[80] An extensive review of GeSn PDs is present in Ref. 81. At a wavelength of 2μm, GeSn PDs have demonstrated a responsivity of several tens of mA/W[82,83] and operation frequencies up to 30 GHz.[76,83,84] Dark currents as low as a few tens of mA/cm^2 were obtained,[76,85] also thanks to the use of pseudomorphic Ge/GeSn MQW absorber stacks to suppress strain relaxation of the GeSn alloy.[76,86] These studies employed GeSn alloys with a Sn content of 8 at. % or less. Attempting to extend the wavelength sensitivity range with larger Sn contents results in the degradation of GeSn quality due to increased defect concentration.[1] This leads to an increase in leakage currents and concurrent decrease in detectivity. For example, employing an all-GeSn p-i-n PD with Sn contents up to 12 at. %, Atalla et al.[5]
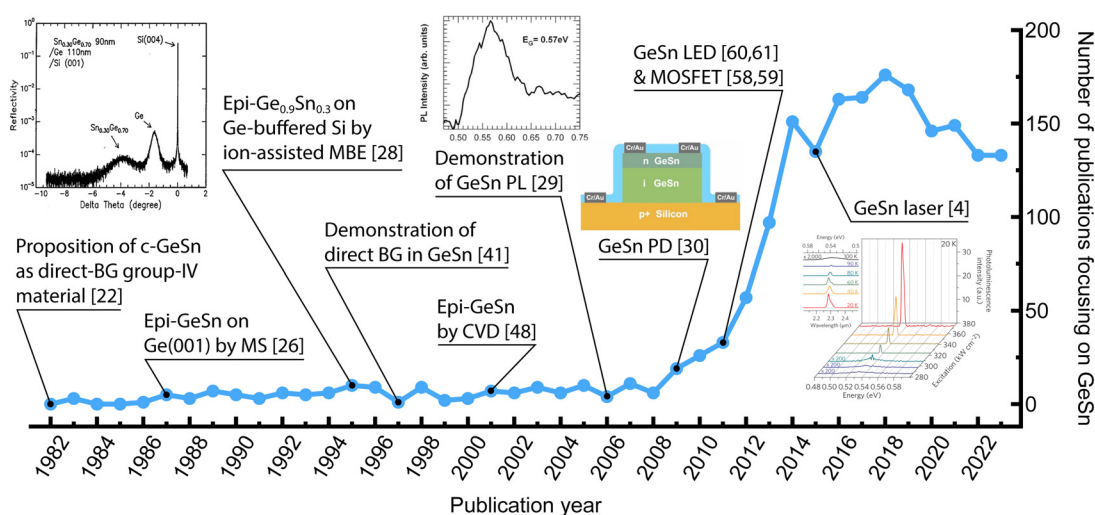
FIG. 1. Plot of number of publications per year focusing on GeSn, with selected milestones achieved in the field. Publication data were selected using the web tool *Scopus Analytics*,[27] searching with the "OR" operator among the following keywords in the title or abstract: "GeSn", "SnGe", "Ge$_{1-x}$Sn$_x$", "Sn$_x$Ge$_{1-x}$", "Ge$_{1-x}$Sn$_x$", and "Sn$_x$Ge$_{1-x}$", accessed in March 2024. Figures in the insets are reprinted with permission from the corresponding authors: respectively, from left to right, He et al.,[28] Nucl. Instrum. Methods Phys. Res. Sect. B **106**, 126–132 (1995). Copyright 1995 Elsevier; Soref et al.,[29] MRS Proc. **958**, 0958-L01-08 (2006). Copyright 2006 Springer Nature; Mathews et al.,[30] Appl. Phys. Lett. **95**, 1–4 (2009), with the permission from AIP Publishing; Wirths et al.,[4] Nat. Photonics **9**, 88–92 (2015). Copyright 2015 Springer Nature.

achieved sensitivity up to 2.8 μm. However, the average dark current in these PDs was 2.5 A/cm^2 at -1 V. The authors identified bulk material defects as the main contributors to these currents, with their presence in large concentrations likely attributed to the higher Sn content. These devices, with a diameter of 10 μm, exhibited a cutoff frequency of 12.5 GHz at -5 V, with a peak responsivity of 0.18 A/W at a wavelength of 2.5 μm.[5] In general, the literature evidence that so far dark currents generated by defects in GeSn alloys remain too high to be competitive with III–V technology.[87]

Despite the potential of GeSn suggested by theoretical studies to reach the MWIR (i.e., 3–8 μm) wavelengths,[55,88] the inherent epitaxial compressive strain on Ge and Si substrates increases the BG energy, significantly complicating the experimental realization of MWIR devices. As a consequence, there are only a handful of studies focusing on operation in this wavelength range.[77,89] Strain engineering is, thus, an essential point to consider to extend the wavelength operation range into the MWIR.[1] Waveguides[90–92] and photonic crystals[93] have been proposed to enhance absorption and thus improve responsivity. To the same goal, GeSn avalanche photodiodes (APDs) have been fabricated,[8,78,79,94] demonstrating responsivities close to 5 A/W at 1550 nm. On the other hand, GeSn single-photon avalanche photodiodes (SPADs) have been proposed theoretically[95,96] and attempted experimentally.[97,98] As of the date of this publication, single-photon detection with GeSn is yet to be demonstrated.

While GeSn laser devices fabricated to date employ exclusively CVD-grown materials, LEDs have been realized with both CVD and MBE methods.[99] Emission at 3.3 μm has been achieved with Ge$_{0.85}$Sn$_{0.15}$/Ge heterostructures,[12] and a simple gas detector has been demonstrated employing a GeSn LED.[100] Though comparable with commercial MWIR LEDs,[1] the GeSn LED quantum efficiency remains suboptimal due to trap recombination mechanisms caused by material defects.[100,101] GeSn-based LEDs, including alternative architectures such as waveguides[102] and SiGeSn/GeSn MQW,[101,103] have been reviewed in Refs. 1 and 104. For a comprehensive review of GeSn-based optoelectronic devices, the reader is referred to the work of Reboud et al.[105]

In the realm of GeSn electronic devices, a significant milestone was recently achieved by Liu et al.,[106] who successfully fabricated GeSn FETs for complementary metal-oxide-semiconductor (CMOS) beyond-Si electronics with improved performance with respect to the pure Ge counterpart. In the past decade, significant advancements have also been made in the field of GeSn nanostructures, which include nanowires, quantum wells, and quantum dots. These works have been thoroughly reviewed by Doherty et al.[107] Finally, GeSn has also been proposed for thermoelectric applications,[21] as a platform to host quantum spin Hall phases,[108] and as a THz emitter.[109]

III. PHYSICAL PROPERTIES OF GeSn

In Sec. III A, we introduce the basic physical properties of GeSn. We review the GeSn phase diagram and the metastability of the alloy, and then introduce recent discoveries on the arrangement of Sn solute atoms in the Ge matrix. Finally, we describe the band structure of GeSn, and its dependence on the alloy composition and strain state of the material.

A. GeSn: A metastable alloy

GeSn is an alloy obtained from a solid solution of two group-IV elements, namely, Ge and Sn. The Ge-Sn phase diagram is shown in Fig. 2(a). Ge is an indirect-BG semiconductor with diamond face-centered cubic (FCC) crystal structure (space group (SG): $Fd\bar{3}m$), shown in the inset of Fig. 2(b), with lattice constant of 5.658 Å.[22] Sn instead can be found in two phases, the high-temperature metallic β Sn phase, and the low-temperature semi-metallic α Sn phase, with a thermodynamic phase transition of 13.2 °C. In the case of GeSn alloys, α Sn is the phase of reference, since it also has a diamond FCC crystal structure, with a lattice constant of 6.489 Å.[22] Ge and Sn can, thus, be mixed in a solid solution to obtain a non-polar semiconductor (or semi-metal, depending on the composition), with the same diamond

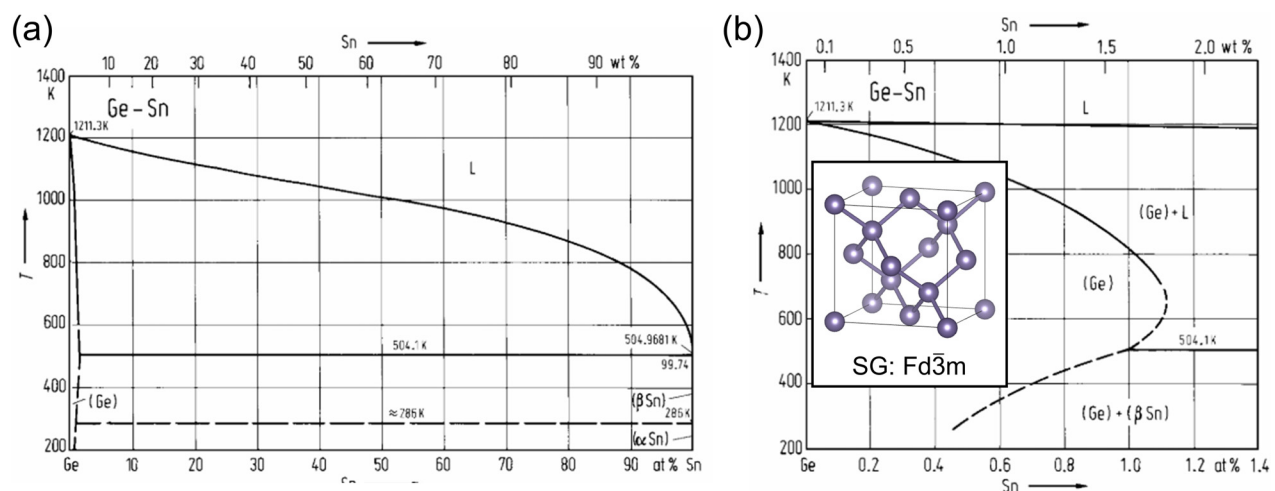**FIG. 2.** (a) Phase diagram of the Ge-Sn alloy, and (b) zoom on the Ge-rich compositions. In the inset of (b) is the diamond FCC crystal unit cell with space group $Fd\bar{3}m$, produced with the software *VESTA*.[110] Figures (a) and (b) reproduced with permission from Predel, in *Ga-Gd – Hf-Zr*, edited by O. Madelung (Springer-Verlag, Berlin/Heidelberg, 1996), pp. 1–4. Copyright 1996 Springer Nature.[111]

FCC crystal structure of the two elemental materials. A consequence of the large lattice mismatch between Ge and α Sn of 14.7% is that the solubility of one element in the other is low. Evident from the Ge-rich zoomed region of the phase diagram in Fig. 2(b), the solubility of Sn in Ge is limited to a bare 1.1 at. % at 400 °C, and drops well below 1 at. % at room temperature. Ge-Sn are mostly immiscible, with an eutectic temperature of 231 °C. The single-phase GeSn is, therefore, metastable across most of its composition range. Hence, phase-separation during growth or post-growth thermal processing is of concern. If not kinetically hindered by out-of-equilibrium processes, Sn will tend to segregate out of the Ge crystal, forming a metallic β Sn phase that is detrimental for optoelectronic devices. In this review, we discuss the Ge-rich phase of the GeSn alloy, as it is technologically more relevant for the targeted optoelectronic applications in the SWIR, MWIR, and LWIR wavelength ranges.

B. Crystal Lattice

The diamond FCC lattice parameter of GeSn follows Vegard's law,[112–115] i.e., it varies linearly with composition between the lattice constants of Ge and α Sn. In agreement with *ab initio* calculations,[116] extended x-ray absorption fine structure (EXAFS) studies found that the Sn-induced strain in the GeSn alloy is accommodated by both bond stretching and bond bending, with a slightly larger contribution from the latter.[117,118]

For years, GeSn has been considered to be a homogeneous random solid solution following both computational predictions of the alloy properties[55,112] and experimental studies.[119] A fully random solution implies the absence of any short- or long-range atomic order of the solute species. However, recent works showed that the GeSn alloy may possess a short-range order (SRO).[120,121] Combining statistical sampling and *ab initio* calculations, Cao *et al.*[120] suggested the presence of a SRO at Sn atoms, with the first coordination shell nearly devoid of other Sn atoms. With this assumption, they provided better predictions of the GeSn BG energy at high Sn contents, comparing it with experimental results previously fit with the random alloy assumption. With the latter model, the reduction in bandgap associated with increasing Sn content tends to be overestimated. The SRO was later demonstrated experimentally by EXAFS characterization of strain-free $Ge_{0.906}Sn_{0.094}$ nanowire shells grown around a compliant Ge core by CVD.[121] The observed SRO may be rationalized in terms of the larger size of Sn atoms compared to Ge. One can expect that self-repulsion of Sn atoms is favored to drive local strain accommodation with reduced bond distortions. This intuition is backed by a study from Fuhr *et al.*,[122] which through density-functional theory (DFT) computations observed a significant Sn-Sn repulsion in the first coordination cell of Sn.[122] The repulsion energy quickly drops moving away from the first coordination shell, becoming negligible at the fourth coordination cell.[122]

A previous experimental study by atom probe tomography (APT) reported the absence of SRO in CVD-grown $Ge_{0.82}Sn_{0.18}$.[119] The lack of observation of SRO has been suggested to be owed to the high temperatures employed during growth of the material.[123] In Ref. 123, Windl *et al.* employed Monte Carlo methods to simulate the effect of growth temperature on the alloy by relaxing an 8000-atom cell with average composition corresponding to $Ge_{0.86}Sn_{0.14}$; they observed a significant reduction in SRO at the growth temperatures of 300–400 °C, typically used in CVD epitaxy of GeSn. Furthermore, Lentz *et al.*[121] suggested the employed growth rate may also play a role in the

final alloy SRO, as their GeSn layer was grown at 275 °C at a slow rate of 1 nm/min in contrast with the rate of 1.5–2.8 nm/min employed in the GeSn film stack studied by APT in Ref. 119. Additional experimental studies on GeSn films are required to confirm the presence of SRO and to assess its dependence on growth conditions.

Finally, APT studies suggested that compressive strain in GeSn may favor the presence of Sn-Sn bonds,[124] in contrast with the SRO observed in strain-free GeSn.[121] If confirmed, this would suggest the importance of strain engineering to prevent phase separation, especially in the case of GeSn with Sn content at the high end. It should be kept in mind, however, that compositional measurement artifacts may arise during APT characterization of compound semiconductors and alloys.[125] For instance, the thermal energy introduced into the system during APT sample preparation and measurements could promote the (surface) diffusion of Sn, leading to atomic rearrangement with respect to the original sample, and possibly local Sn segregation.

C. Band structure

The evolution of the band structure of GeSn with the composition can be qualitatively understood first by extrapolating from the band structure of the constituent elements—Ge and α Sn—shown in Fig. 3(a). Ge is an indirect-BG semiconductor with a BG energy of 0.66 eV at the L-valley, and a direct Γ-valley energy of 0.80 eV.[126] α Sn, on the other hand, is a semi-metal with a direct BG energy of −0.41 eV, and BG energy at the L-valley of 0.09 eV.[126] The Ge-Sn energy differences at Γ- and L-valleys are, respectively, of 1.21 and 0.55 eV. Assuming the bandgap energies vary linearly with compositions, one can therefore expect that by adding Sn to Ge the Γ-point energy will red-shift faster than the L-point, inducing a crossover from indirect to direct BG behavior in the material. Experimentally, this is indeed the case, although we have seen in Sec. II that the crossover occurs at lower Sn fractions compared to the linear prediction, with the bandgap energies following a bowing behavior described in Eq. (1). This bowing behavior is shown in Fig. 3(b) for Sn contents lower than 40 at. %. In this plot, Lan *et al.*[127] computed the dependence of the direct and indirect bandgaps (indicated respectively with $E_{g\Gamma}$ and E_{gL}) using the nonlocal empirical pseudopotential method, calculating a BG crossover for a Sn fraction of 8.5 at. %. The authors additionally observed that relaxed GeSn with Sn contents greater than 41 at. % may exhibit characteristics of a topological semimetal, opening up the possibility of entering the realm of quantum materials with GeSn.

The bowing behavior of the GeSn alloy is the result of coupling of states through a non-diamond-like potential.[45] This asymmetric potential originates from the difference in electronegativity of the constituent elements and the lattice distortions (i.e., bond stretching and bending[128]) due to their different atomic sizes.[45] This explains why early works using highly symmetric potential-averaged virtual crystal approximations, such as that from Jenkins *et al.*,[42] failed to capture the large bowing behavior of the material. On a side note, DFT studies by Yin *et al.*[45] found that the total bowing behavior originates equally from Ge-Sn charge and structural differences, while Chibane *et al.*[129] determined a dominant contribution from the latter. Discrepancies in the result may have arisen from the different GeSn compositions and supercell sizes considered in the studies (see Table I).

In Table I, we report the measured and computed values of bowing parameters of the GeSn Γ- and L-energy gaps (b_Γ, b_L). From these results, it is clear that there is no close agreement on these values in the
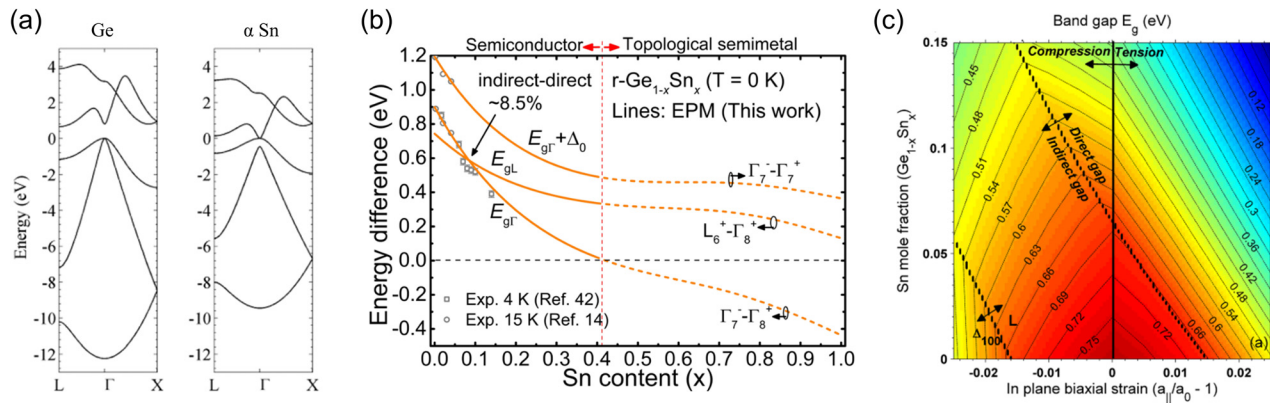
FIG. 3. (a) Band structures of Ge and α Sn. (b) Computed evolution of direct and indirect BG s ($E_{g\Gamma}$, E_{gL}) with the GeSn alloy composition, reporting bandgap inversion at 8.5 at. % Sn, and a transition to topological semi-metal at 40 at. % Sn. (c) Calculations of BG energy dependence on strain, using $b_\Gamma = 2.1$ eV. Figure (a) adapted from Moontragoon et al., J. Appl. Phys. **112**, 073106 (2012), with permission from AIP Publishing.[130] Figure (b) reprinted from Lan et al., Phys. Rev. B. **95**, 201201 (2017), with permission from AIP Publishing.[127] Figure (c) reprinted from Gupta et al., J. Appl. Phys. **113**, 073707 (2013), with permission from AIP Publishing.[55]

literature. In general, $2\,\text{eV} < b_\Gamma < 3\,\text{eV}$, while $b_L \sim 1$ eV. The large variability of the reported experimental values of b_Γ comes from the complexity of the material system: In addition to possible experimental systematic errors coming from the different employed techniques, the atomistic structure of the alloy may vary depending on the employed growth technique and parameters, resulting in different physical properties. For example, Sn-clustering has been observed in GeSn,[124,131] and it has been predicted to lower the material bandgap,[129] consequently inducing an apparent larger bowing parameter. Additionally, the strain state of the material affects BG energies shifts, as shown in Fig. 3(c). In particular, compressive strain has the opposite effect of Sn alloying on the conduction band (CB) valleys,[55,132] increasing the BG energy, and thus decreasing the apparent bowing behavior. Strain also splits the heavy-hole (HH)-light-hole (LH) degeneracy, with compressive strain lifting the HH, and tensile strain producing the opposite effect.[133,134] Failure of appropriately taking into account the strain state of the material will result in experimental errors. Concerning theoretical computations of the alloy bowing parameter, the DFT model on strain-free material considered the GeSn alloy to be fully random, while recent works demonstrated the presence of a SRO in GeSn.[120,121] The absence of Sn atoms in the first coordination shells of Sn yields a larger BG energy,[120,129] and thus, b is overestimated when fitted over the entire alloy spectrum; this is the case for Refs. 112 and 135, which report $b_\Gamma > 3$ eV. Finally, Gallagher et al.[3] found their data were better fitted with composition-dependent bowing parameter, also proposed with DFT-based calculations by Chibane et al.[129] On the other hand, Yin et al.[45] computed by DFT a negligible dependence on composition of the bowing parameter. Furthermore, D'Costa et al.[136] argued that with the composition-dependent b_Γ from Gallagher et al. pseudomorphic GeSn would not show a direct-bandgap behavior for any composition. Fernando et al.[137] predicted the indirect-to-direct crossover behavior of pseudomorphic GeSn on Ge(001) to be at 26 at. %, though extrapolated from samples with $x_{Sn} < 0.11$, and calculated without considering any SRO. The latter is expected to further push the crossover composition to larger Sn contents.[120] More theoretical work is necessary to determine the exact behavior of the bowing parameter.

On the other hand, one needs to consider that experimentally derived GeSn bowing parameters may exhibit variations because of inherent differences in the atomic configurations of the alloy, which may be influenced by the specific growth technique and growth parameters utilized.[121]

Until recently, GeSn was expected to show a hard crossover from an indirect to direct BG behavior. Several groups have tried to measure and/or compute the crossover alloy composition. Inevitably, the large scatter in the reported values of bowing parameter (see Table I) resulted in an equally large scatter in the reported alloy crossover compositions, spanning between 6 and 10 at. % Sn.[142] In fact, recent works demonstrated that GeSn has a soft transition from an indirect to a direct BG behavior due to band mixing.[1,143,144] In GeSn, the CB edge states were found to consist in a linear combination of the Γ (Γ_{7c}) and L states (L_{6c}). This behavior originates from the large differences in covalent radius and electronegativity of the alloy constituent elements and was demonstrated by measuring the GeSn bandgap hydrostatic pressure coefficient (dE_g/dp) of GeSn:[143] In Ge, the pressure coefficient of the direct BG ($\Gamma_{7c} - \Gamma_{8v}$) is three times that of the indirect BG ($L_{6c} - \Gamma_{8v}$). By measuring dE_g/dp, it is thus simple to discern the BG behavior of the material. In GeSn, experimental values of dE_g/dp progressively increase from dE_L/dp to dE_Γ/dp for increasing Sn content ($x_{Sn} < 0.15$[1]) indicating that the band mixing evolves progressively with x_{Sn}.[143] DFT computations confirmed the progressive increase in dE_g/dp in GeSn, corroborating the experiments.[143,144] Furthermore, O'Hallaran et al.[144] found evidence of band mixing also in the previously reported DFT calculations, e.g., from Polak et al.,[112] emphasizing the importance of atomistic computations in capturing the electronic behavior of the GeSn alloy. The band mixing behavior may explicate to some extent the variability in the reported experimental crossover alloy compositions.

In general, we can conclude that the lattice ordering and band structure of the GeSn alloy are fairly well understood qualitatively, but still lack accurate quantitative interpretation. Nevertheless, the data acquired until now allowed significant progress in the performance of GeSn-devices, reviewed in Sec. II.

IV. CHALLENGES OF THE GeSn ALLOY

The main challenges associated with GeSn processing are discussed in the following two sections. First, we provide a brief introduction to the challenges related to epitaxial strain relaxation via dislocation formation. This subject is further elaborated in Secs. VI and VII. Second, we delve into the processes of Ge-Sn phase separation and Sn segregation, which may occur during and after growth as a result of the alloy metastability. We review the efforts toward understanding the driving forces at play in this process.

A. Epitaxial relaxation defects

In this section, we introduce the mechanism for epitaxial strain relaxation via the formation of misfit and threading dislocations. We furthermore review simple models for critical thickness prediction for the GeSn-on-Ge material system. Additionally, we address the challenges associated with the presence of dislocations in GeSn, and a few methods proposed to overcome them.

To maximize the material performance, GeSn should be integrated in devices as a monocrystal, since group-IV grain boundaries are known to be sources of trap states[145–148] and they act as scattering centers during charge transport.[149] Monocrystalline GeSn can be obtained by epitaxial growth on substrates with a suitable crystal structure and similar lattice parameter. Undoubtedly, the ideal substrate from the technological point of view is Si, which is widely commercially available and has a diamond cubic FCC structure with a lattice constant of 5.431 Å, which corresponds to a lattice mismatch of 4.18% with pure Ge. GeSn, possessing a lattice parameter larger than Ge, will thus grow in a compressive strain on Si substrates. With such large lattice mismatch, as the epitaxial film grows coherently on the substrate, it accumulates enough elastic energy to overcome the nucleation energy of dislocations, and the strain is thus (partially) relaxed via the formation of misfit dislocations (MDs) and threading dislocations (TDs), as shown in Fig. 4(a). The critical thickness of strain relaxation (t_{cr}) on Si is only a few nm,[150] and thus relaxation defects in epitaxial GeSn are unavoidable for any film thickness that would be technologically relevant for optoelectronic applications.

1. Critical thickness for strain relaxation (t_{cr})

To partially accommodate compressive strain, GeSn is grown on Ge-buffered Si substrates [also called Ge virtual substrate (vGe)], or directly on Ge wafers. This yields considerably larger t_{cr}, which however drops as the lattice mismatch increases with the Sn fraction in the alloy. The dependence of t_{cr} on GeSn composition is plotted in Fig. 4(b) using the Matthews and Blakeslee (M-B) and People and Bean's (P-B) models, and assuming the strain is released by 60° misfit dislocations (MDs). The solid coloring indicates regions where the film grows pseudomorphically—i.e., no strain relaxation occurs in the film—according to the corresponding model. The M-B model is based on a mechanical equilibrium approach and assumes that threading dislocations are already present in the film, inherited from the substrate.[151] This is the case of GeSn grown on vGe. In this model, t_{cr} is found by equating the force felt by a threading dislocation (TD) segment under misfit stress to the tension in the dislocation core. The M-B model is an *equilibrium* model. It turns out that it does not describe accurately the relaxation process and the critical thickness of group-IV semiconductors[152] because their t_{cr} is in fact dominated by the kinetics of dislocation nucleation and motion. These kinetic factors, which are dependent on growth temperature and rate, can be taken into account with more complex models capable of describing metastable strain states of the epitaxial films, reviewed in Ref. 153. An alternative, simpler model has been proposed by People and Bean to describe the metastable critical thickness of epitaxial group-IV films.[154,155] The P-B model is based on a thermodynamic energy-balance approach, where the t_{cr} is obtained by equating the misfit strain energy density to the self-energy of a dislocation. This model assumes that this condition is sufficient for the nucleation of a dislocation, ignoring the effective
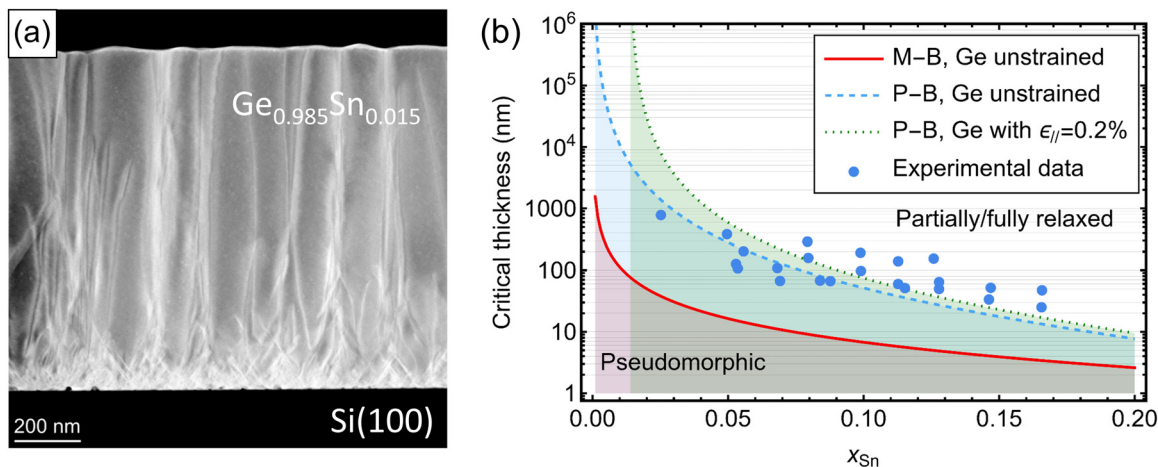
FIG. 4. (a) XTEM of Ge$_{0.985}$Sn$_{0.015}$ epitaxially grown on Si(100) by MS by the authors. The film is rich in dislocations due to epitaxial strain relaxation phenomena, elucidated in detail in Sec. VI. (b) Plot of the Matthews and Blakeslee (M-B) equilibrium model and People and Bean's (P-B) thermodynamic model for GeSn critical thickness (t_{cr}) on Ge (100) substrates, respectively in red (whole) and blue (dashed). The blue dots represent experimentally measured values of t_{cr} from Refs. 119 and 156–161. The green, dotted line represents the P-B model calculated for GeSn growth on a tensile-strained Ge layer, with in-plain strain ($\epsilon_{//}$) of 0.2%. On tensile-strained Ge, the GeSn t_{cr} is increased as a consequence of the reduced lattice mismatch.

kinetics of dislocation nucleation. Despite of this, the P-B model is widely used. It predicts relatively accurately the experimental critical thickness of GeSn grown on Ge,[46,156,157] especially for Sn contents below 10 at. %, as illustrated in Fig. 4(b). The higher accuracy of the P-B model compared to the M-B can be explained by the fact that GeSn growth occurs far from equilibrium, where kinetics of dislocations play a major role in determining strain relaxation. This leads to GeSn films retaining a metastable strain state, implying that strain relaxation may occur when the material is heated to temperatures exceeding those utilized during its growth.

2. The need for dislocation engineering

Dislocations not only limit the thermal stability of GeSn,[162,163] but they are also a source of electronic deep trap states,[164–166] which are detrimental for the performance of GeSn-based optoelectronic devices. For example, in GeSn PDs, trap states increase the dark currents via Shockley-Read-Hall (SRH) and trap-assisted tunneling (TAT) carrier generation mechanisms in the junction depletion regions.[167] Hence, epitaxial relaxation defects require appropriate management for the optimization of optoelectronic device performance. Extensive research on dislocation engineering showed that the threading dislocation density (TD) in Ge and GeSn films can be reduced via nano- and micro-patterning of the substrate,[168,169] thick (graded) buffers,[161] thermal processing,[170,171] or any combination of these strategies.[169] A more thorough discussion of strain relaxation mechanisms and defects will follow in Secs. VI and VII. Because of the technological relevance of Ge buffers in the realization of GeSn devices, the growth of Ge, its relaxation phenomena, and its electrical properties are presented as well throughout this review.

3. SiGeSn alloys

To reduce the epitaxial strain with Ge and Si substrates, it may be desirable to employ the SiGeSn alloy, as the addition of Si decreases the overall lattice parameter. The latter also induces a blue-shift in the bandgap. Consequently, the use of SiGeSn allows us to decouple the lattice parameter of the material from its bandgap.[52] This can be advantageous in applications where specific band alignments are required, such as quantum wells and quantum dots, to improve the efficiency of photonic devices.[172] The SiGeSn alloy is also predicted to exhibit greater thermal stability compared to the binary GeSn alloy.[52,173] This prediction still requires experimental validation, as the currently limited experimental data do not support this assertion.[174] Challenges with this ternary system stem from the low solubility of Sn in Ge (<1 at. %) and in Si (<0.1 at. %), which complicates epitaxial growth due to segregation and difficulties in achieving high crystal quality.[1] Reviewing SiGeSn further is out of the scope of this manuscript and the reader is referred to other reviews on the topic.[1,52,172,175]

4. The Nanowire case

Finally, we should add some words on a particular case that enables the growth of GeSn without dislocations and or stacking faults. This is the case of GeSn obtained around ultra-thin Ge nanowires (NWs). NWs are filamentary crystals with a tailored diameter ranging from the few to few tens of nm. Their aspect ratio renders them new properties and enables a large variety of functional applications that include electronics, optoelectronics, and sensing.[176–179] Their reduced diameter also enables the combination of materials along or across the axis that would not otherwise be possible in a planar substrate. This is due to the more facile strain relaxation both axially and laterally.[180]

The most common method to obtain NWs is the so-called vapor–liquid(solid)–solid growth (VLS/VSS). Here, a liquid (or solid) metal droplet is used as a catalyst to preferentially gather and decompose growth precursors. Upon supersaturation of the droplet, there is precipitation underneath. Continuous precipitation leads to the formation of the filamentary crystal.[181] Free-standing GeSn NWs with Sn content upto 4% have been obtained by VLS using a mixture of AuAg or Au that facilitates the dissolution of both Ge and Sn.[182,183] More commonly, Ge NWs are used as a template to grow GeSn shells around them.[184,185] Using ultra-thin Ge NWs strongly avoids strain relaxation via structural defects.[186,187] As a consequence, Ge/GeSn core/shell NW systems constitute a benchmark for the functional properties of GeSn free of extended defects. Several studies reveal that indeed the properties of such GeSn are better than in thin films, including room temperature luminescence, photodetection, and high carrier mobility.[89,121,188–190] For example, CVD-grown VLS GeSn NWs with Sn fractions up to 19 at. % exhibited room-temperature PL emission beyond 4 μm, highlighting the crystal quality of the material.[190] The NW geometry brings advantages both in the understanding of GeSn as a semiconductor and in the foresight and potential of GeSn technology. For the device integration of GeSn NWs, the challenges remain multiple,[191] e.g., the influence of dopants on the droplet Sn supersaturation, or the precise control of NW positioning on wafer-scale.

B. Sn segregation and thermal (In)stability

In this section, we discuss the driving forces at play in Sn segregation in metastable GeSn, with the implications on the material thermal stability. We review the current understanding of Sn diffusion phenomena, the mediating role of defects in GeSn, and the efforts to elucidate the interplay between the alloy composition, strain relaxation, and Sn out-diffusion.

GeSn is metastable for all compositions with $x_{Sn} > 1$ at. %. According to the Ge-Sn phase diagram in Fig. 2, at room temperature, thermodynamics predict a phase separation of GeSn into a Ge-rich phase with less 1 at. % Sn, and a β Sn phase. This process is kinetically hindered by the low atomic diffusivity of Sn and Ge at room temperature. On the other hand, upon thermal processing of the material, may it be for annealing, doping, or any CMOS post-growth process that requires heating, Sn atoms may acquire sufficient thermal energy to diffuse to the surface of the material,[174,192] and/or cluster in the bulk into a β Sn phase.[192] Sn segregation may also occur during growth if the substrate temperatures are too elevated.[193–195] The resulting film will show several Sn droplets on surface, similar to the one reported in the scanning electron microscopy (SEM) image of Fig. 5(a). The Sn out-diffusion from the Ge matrix increases the effective bandgap of the material, defeating the purpose of alloying with Sn. Additionally, the metallic behavior of the segregated β Sn phase is detrimental for optoelectronic devices. Hence, in general, it is necessary to prevent the Sn segregation by maintaining a low thermal budget both during growth and post-growth processes. Exceptions where the Ge-Sn phase separation is sought exist.[196]
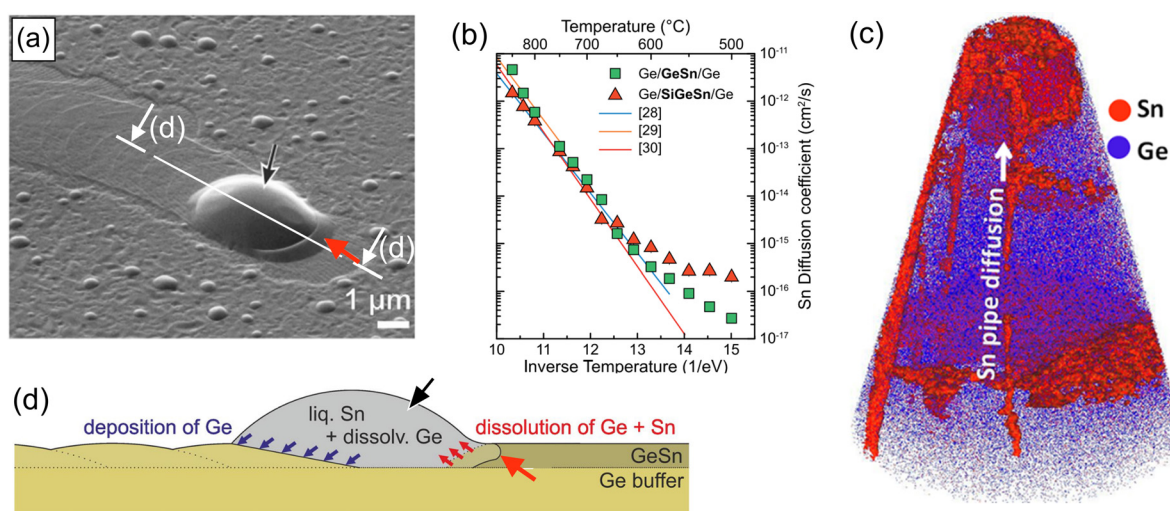
FIG. 5. (a) SEM image of a β Sn segregation droplet on the surface of a GeSn film. (b) Activation energy of Sn diffusion in GeSn alloys in function of the annealing temperature, evidencing two regimes of diffusion: (1) vacancy-mediated Sn diffusion at high temperatures, and (2) metastability-enhanced Sn diffusion at low temperatures. References 28–30 in this figure correspond to Refs. 197–199 here. (c) Pipe diffusion of Sn along a dislocation core, as measured by APT. (d) Cross section schematic view of a Sn droplet on surface. Figures (a) and (d) adapted from Groiss et al., Sci. Rep. **7**, 16114 (2017). Copyright authors, licensed under a Creative Commons Attribution (CC BY) license.[193] Figure (b) reprinted from Ref. 174, von den Driesch et al., Phys. Rev. Mater. **4**, 033604 (2020). Copyright authors, licensed under a Creative Commons Attribution (CC BY) license. Figure (c) reprinted with permission from Nicolas et al., Cryst. Growth Des. **20**, 3493–3498 (2020). Copyright 2020 American Chemical Society.[162]

1. Driving forces for Sn segregation

Several experimental investigations have elucidated the driving forces for Sn segregation and the influence of material defects on the latter. It is widely accepted that Sn diffusion in Ge is mediated by vacancies,[197,199,200] whose formation energy in group-IV semiconductors is known to depend on the strain state of the material.[201–203] In particular, the vacancy formation energy decreases under compressive strain. Therefore, in compressively strained GeSn films, the associated increase in vacancy concentration is expected to increase the Sn diffusion coefficient, facilitating Sn segregation. However, a study from von den Driesch et al.[174] in nearly dislocation-free GeSn films showed that this cannot be the only contributor to Sn out-diffusion. In fact, they observed that given an equal Sn composition and film compressive strain, Sn out-diffusion in $Si_{0.040}Ge_{0.895}Sn_{0.065}$ is accelerated compared to $Ge_{0.94}Sn_{0.06}$ due to the larger metastability of the ternary alloy, concluding that the main driving force for Sn out-diffusion is given by the thermodynamic instability of the material. In support of this conclusion, they further observed two regimes of Sn diffusion depending on the annealing temperature, shown in Fig. 5(b). By gradually increasing the annealing temperature (T) from 500 °C, they first found a low activation energy[204] regime with enhanced diffusion due to the large metastability of the material. Around 650 °C, as the Sn progressively diffused out of the Ge matrix, its diffusion activation energy increased and the diffusion coefficient matched that of Sn in non-metastable, Sn-doped Ge. The latter is plotted in Fig. 5(b) using activation energies from three different Refs. 197–199, and it is shown to match the Sn diffusion coefficients measured during annealing of $Si_{0.040}Ge_{0.895}Sn_{0.065}$ and $Ge_{0.94}Sn_{0.06}$ above 650 °C in Ref. 174. The authors attributed the increase in activation energy at high temperatures to the loss of metastability-enhanced diffusion as the Sn concentration decreased to values within the solubility limit in Ge.[174] They ruled out this effect

was purely from a composition-dependent diffusion coefficient as they did not observe the typical Gaussian shapes of composition-dependent diffusion profiles.[174]

As a consequence of the strong influence of the alloy metastability on Sn segregation, the thermal stability of GeSn decreases with increasing Sn content, making it progressively more difficult to achieve large Sn fractions in GeSn. Zaumseil et al.[205] showed that the decrease is almost linear with Sn content, with phase-separation temperatures reported to be between 600 and 350 °C for Sn fractions, respectively, between 4.8 and 11.7 at. %. This is in close agreement with other reports.[206,207]

2. Influence of extended defects on Sn segregation

The presence of extended defects in GeSn has been found to strongly affect the Sn segregation behavior during thermal treatments. In pseudomorphic GeSn, Sn segregation occurs gradually via vacancy-mediated diffusion,[174,205] while in strain-relaxed GeSn the segregation process is considerably different due to the presence of MDs and TDs in the film. By investigating the atomic structure of segregated GeSn by APT, Mukherjee et al.[163] observed that during annealing of GeSn—with step-graded increase in the Sn content from 8 to 18 at. %—Sn atoms tend to diffuse and accumulate at the cores of both at MDs[205] and TDs.[162,163] This is rationalized in terms of larger space available for Sn atoms at the dislocation cores, with consequent lower lattice local strains with respect to substitutional Sn atoms in the bulk. Figure 5(c) shows a Sn-decorated TD, as reconstructed from APT in the work of Nicolas et al.[162] The upward increase in Sn concentration in the TD core along the epitaxial growth direction allowed to confirm that TDs act as preferential pathways for Sn diffusion to the film surface, a mechanism referred to as *pipe diffusion*.[163] The Sn diffusion coefficient

04 January 2025 10:11:00

is estimated to increase up to 4 orders of magnitude in the presence of linear defects.[162,205] Moreover, Mukherjee et al.[163] observed that, for a short annealing time, while Sn was accumulating at dislocation cores, the GeSn film was pristine far from the core, with no sign of Sn clustering. This observation allowed to conclude that dislocations do not merely facilitate Sn segregation, but they also act as initiators of phase separation as a consequence of the local strain fields generated around their core. Similarly, it has been suggested that during strain relaxation Sn is harvested by TDs as they diffuse in the film, further accelerating Ge-Sn phase separation.[208] Hence, Sn segregation is enhanced in the presence of relaxation defects, also confirmed by other systematic studies: Stanchu et al.[209] showed that Sn segregation increased with higher density of dislocations, while Bonino et al.[210] demonstrated an improved thermal stability by etching relaxation defects in microstructured GeSn, achieving stability of $Ge_{0.831}Sn_{0.169}$ for temperatures as high as 400 °C. This thermal stability range is considerably higher than what observed by Zaumseil et al. for relaxed films of similar alloy compositions.[205] Finally, the presence of a GeSn surface oxide—formed by annealing GeSn in rough vacuum—has also been found to affect the Sn segregation behavior, inhibiting Sn out-diffusion and improving the material thermal stability.[211]

3. Model of Sn segregation

The Sn segregation behavior during annealing of GeSn has been modeled by Groiss et al.[193] The authors showed that, once a consistent amount of Sn atoms out-diffuse and accumulate on surface, they nucleate liquid Sn droplets. These droplets move on surface through a self-maintained segregation process, schematized in Fig. 5(d); liquid droplets of Sn have a tendency to dissolve the metastable GeSn film at their leading edge, which leads to the deposition of a Ge layer at the trailing edge as a result of Ge supersaturation in the Sn droplet. This Ge layer contains a Sn concentration near its solubility limit. Due to a better wetting of Sn on the GeSn film compared to Ge, the droplet tends to advance in the opposite direction from the Ge deposited layer, often along the ⟨110⟩ and ⟨100⟩ crystal orientations. The wetting behavior explains the motion of droplets on the surface of the GeSn film, which leave a trail of precipitated Ge at the back, similarly to the vapor–liquid–solid process.[212] This results in characteristic trails associated with β Sn segregation droplets on the surface of phase-separated GeSn films, visible in Fig. 5(a). In addition to the surface phenomena modeled by Groiss et al.,[193] upon annealing of (partially) relaxed films, Sn clustering has been observed in the bulk[192] and at the film/substrate interface.[205] Bulk Sn clustering has been linked with a large concentration of vacancies induced by the low-temperature growth of GeSn,[205] while clustering at the interface occurs due to accumulation of Sn at the core of MDs.[205]

4. Interplay between alloy composition, strain relaxation, and Sn segregation

In light of the above results, several studies tried to elucidate the interplay between alloy composition, strain relaxation and Sn segregation during annealing of GeSn. With in situ annealing x-ray diffraction (XRD) studies, Zaumseil et al.[205] observed a gradual Sn out-diffusion with increasing temperature in RP-CVD-grown $Ge_{0.95}Sn_{0.05}$ pseudomorphic films on fully relaxed vGe. In these pseudomorphic samples, the epitaxial strain was progressively released as a consequence of the

reduction in lattice parameter of the film as Sn diffused out of the Ge matrix. Comrie et al.[213] demonstrated, however, that strain relaxation in GeSn can occur without any Sn out-diffusion, and thus that the material metastability is not a driving force for plastic strain relaxation. The latter is governed purely by dislocation nucleation and diffusion dynamics. By annealing $Ge_{0.935}Sn_{0.065}$ on a vGe substrate, Comrie et al. observed by XRD a change in lattice parameter for $T > 400$ °C, with no change in Sn substitutional fraction, as evidenced by Rutherford backscattering spectrometry (RBS) channeling contrast measurements. They could, thus, conclude that plastic strain relaxation in GeSn occurred without any Sn out-diffusion, which instead took place for $T > 600$ °C. In agreement with these results, Zaumseil et al.[205] showed that partially relaxed films with the Sn content from 5 to 12 at. % underwent an initial strain relaxation stage starting at approximately 300 °C, with no Sn segregation. This occurred via the elongation of MDs at the GeSn/Ge interface, and was followed by a "sudden" complete Sn segregation out of the Ge matrix when a higher critical temperature was reached.[205] The latter critical temperature decreased with increasing Sn content, shifting from 640 °C for 5 at. % to 350 °C for 12 at. % of Sn. The sudden Sn segregation was attributed to the activation of fast Sn pipe diffusion through TDs. In the study from Zaumseil et al.,[205] the onset of vacancy-mediated Sn out-diffusion occurred at the same temperature in pseudomorphic and metamorphic $Ge_{0.95}Sn_{0.05}$ ($T \sim 500$ °C), but the segregation initially took place at a higher rate in the former, suggesting the existence of a driving force from the compressive strain present in the pseudomorphic film. Despite these differences, it is interesting to notice that both samples reached the equilibrium Sn concentration of 1 at. % at approximately 650 °C. On the other hand, in metamorphic films with larger composition—i.e., $x_{Sn} = 0.09, 0.12$—the critical temperature for pipe diffusion was lower than the onset of vacancy-mediated diffusion, and therefore, the latter was not observed prior to full Sn segregation. In agreement with Ref. 205, strain relaxation through solely Sn out-diffusion was also observed in Ref. 174 in pseudomorphic RP-CVD-grown GeSn with 6 and 9 at. % Sn on fully relaxed vGe. Here, no dislocation nucleation took place during the process. On the other hand, in GeSn grown by MBE on vGe substrates, relaxation of $Ge_{0.92}Sn_{0.08}$ pseudomorphic films was observed to occur first via dislocation formation up to temperatures of ~ 550 °C, and then also through Sn out-diffusion.[192,214] Contrary to Ref. 205, no sudden segregation of Sn through pipe diffusion was observed, possibly due to the different experimental time scales in play (40-s-rapid thermal annealing (RTA) in Ref. 214 and 5-min-RTA in Ref. 192, as opposed to 15–20 min for each 12.5 °C step in in situ XRD in Ref. 205). The different GeSn strain relaxation behavior in these works may arise from the different TDDs present in the employed Ge buffers. In particular, in Ref. 205, they specify the Ge buffer TDD to be $< 1 \times 10^7$ cm^{-2}, while in Refs. 192 and 214, the Ge buffers have a thickness of, respectively, 210 and 250 nm, in which we can expect in the best case a TDD of $\sim 4 \times 10^8$ cm^{-2}.[170,171] This TDD is transferred to the epitaxial GeSn, facilitating its strain relaxation via TD bending, as elucidated briefly in Sec. IV A. In addition, to explain the discrepancies in the reported studies, the presence of vacancies generated by the low-temperature MBE growth may also have played a role in the interplay between relaxation and segregation, favoring Sn diffusion or conversely decreasing the metastable driving force for segregation due to local stabilization through the formation of Sn-vacancy complexes. Altogether, the above-cited

studies converge in that the critical temperatures for Sn out-diffusion and plastic strain relaxation in GeSn are independent of each other. Nevertheless, it is important to note that these two processes do exert mutual influences. On the one hand, strain can be relaxed purely via Sn out-diffusion in pseudomorphic films; on the other hand, the presence of dislocations can facilitate Sn out-diffusion via pipe diffusion phenomena. Finally, systematic studies with comparable time scales are required to shed light on the role of point defects arising from the different growth conditions of GeSn.

5. Sn segregation during epitaxial growth

Until now we have discussed phase separation of the metastable GeSn alloy during post-deposition annealing (PDA) of the material. It is, however, important to make a distinction with the Sn segregation behavior during the growth process itself. While phase separation during PDA requires bulk Sn diffusion, during epitaxy Sn segregation can occur via adatom surface diffusion and nucleation of β Sn droplets. Surface adatom diffusion rates are considerably more elevated than Sn bulk diffusion, as the latter requires breaking of covalent bonds. As a result, the processing temperatures withstood by GeSn during growth are lower than the thermal stability after growth.[163,215]

During epitaxy, Sn segregation is evidently facilitated by higher Sn fluxes, which increase the concentration of Sn adatoms and consequently the β Sn nucleation probability.[215] This introduces a fundamental limit to the Sn fraction achievable in epitaxial GeSn films. This issue, along with strategies implemented to address it, is discussed in Sec. V A. Briefly, Sn segregation can be mitigated by adjusting the growth parameters, primarily by lowering the growth temperature. Additionally, increasing the film's growth rate (e.g., increasing the atomic/gas fluxes of all elements) reduces the adatom diffusion length, hindering Sn segregation.[216] It is also worth noting that Sn surface segregation can be further enhanced during *in situ* doping of GeSn due to co-segregation with dopant species.[217]

6. Subsection conclusion

The above-cited works illustrate the physics of Ge-Sn phase separation and its driving forces. The interplay between strain state of the material, defects, and alloy composition influences its thermal stability. During growth, the thermal stability of GeSn is decreased further.

V. EPITAXIAL GROWTH OF GeSn, Ge

In this section, we outline the primary advancements in GeSn epitaxy, and the efforts toward achieving a higher incorporation of Sn in the alloy for MWIR and LWIR devices. While epitaxial growth by CVD and MBE methods has been extensively reviewed,[1,52,218–220] we aim to complement these works by reviewing the state of art of sputtering epitaxy of Ge and GeSn. Additionally, we outline the general strategy employed to grow Ge buffer layers on Si substrates, necessary to prevent 3D growth and islanding.

A. Epitaxy of GeSn toward higher Sn content

1. The need of out-of-equilibrium growth

GeSn must be grown epitaxially in monocrystalline form to obtain the desired optoelectronic properties in the material. For technologically relevant studies, GeSn growth is investigated on Si(100) substrates, with or without Ge buffer. To study pseudomorphic GeSn free of linear defects, GeSn is sometimes grown directly on Ge(001). Since the early studies on GeSn thin-film growth, researchers emphasized the need of out-of-equilibrium synthesis methods to prevent Sn segregation. Several epitaxial techniques have been thereby successfully reported with compositions up to 10 at. % Sn, mostly focusing on CVD and MBE growth as widely recognized standard epitaxial methods, reviewed in Refs. 1, 52, and 218–220. A handful of groups employed different techniques, including MS epitaxy,[80,221–224] solid-phase epitaxy (SPE),[225–228] and a few more exotic methods such as liquid-phase epitaxy (LPE)[229,230] and flashlamp annealing (FLA) of Sn-implanted Ge.[231] The main focus of the more recent studies on GeSn epitaxy has been to improve the material crystal quality and push the Sn content to access the MWIR and LWIR wavelengths. Assuming a strain-free material, Sn fractions of $\sim$16 and $\sim$26 at. % are, respectively, required to access these wavelength ranges.[126] However, GeSn crystal quality and thermal stability quickly degrade with increasing Sn fractions, posing major challenges to the synthesis and use of these materials in actual devices.[1]

2. Strategies to increase the Sn content

In Table II, the highest Sn compositions achieved in epitaxial, monocrystalline GeSn films are reported, together with a few representative films grown with more than 15 at. % Sn. A common strategy to maximize Sn incorporation avoiding segregation is the use of low substrate temperatures ($T < 150\,^\circ C$) in physical vapor deposition (PVD) growth processes.[232–236] While low substrate temperatures prevent Sn segregation, the associated reduced adatom mobility is detrimental for the material crystal quality[236,237] and limits the maximal epitaxial thicknesses due to kinetic roughening phenomena.[35,38] The latter take place at low temperatures due to the presence of a potential barrier at atomic terrace steps, termed *Erlich* barrier.[238] With low thermal energy available from the system, adatoms cannot overcome this potential barrier and are forced to remain on their atomic plane. This leads to an unbalance of flux between atomic planes, and to increased nucleation of 2D islands on terraces, with consequent progressive 3D roughening and faceting of the film.[35] After a certain *critical thickness*, the film roughness prevents filling of trenches and the epitaxial growth breaks down, with the film growing first in highly defective[38] or polycrystalline fashion, and then purely amorphous.[239] In the presence of Sn, the Ge adatom mobility and interlayer mass-transport (i.e., adatom up- or down-stepping at terraces) is increased,[38] and therefore, kinetic roughening is partially suppressed.[38] Nonetheless, with increasing Sn content, compressive strain increases in the film—on Ge and Si substrates—leading to a hybrid strain-roughening mode, where the reduced kinetics induce the surface oscillations necessary to allow strain relaxation through roughening.[35] Pure strain-induced roughening effects are normally observed at high temperature due to the large mass-transport involved.[240] Hybrid kinetic-strain roughening is exacerbated with larger Sn contents, as the compressive epitaxial strain increases in the film.[38] This poses a fundamental limit to the maximal epitaxial thickness achievable with large Sn contents at low growth temperatures. Hence, all experimental GeSn films with the highest Sn content ever achieved are only a few tens of nm thick, as reported in Table II. The epitaxial critical thickness increases with higher growth temperatures, yet these temperatures are constrained by the elevated

TABLE II. Summary of the epitaxial, monocrystalline GeSn films with the highest fractions of Sn achieved in the literature. Acronyms: graded GeSn buffer (grGeSn), monolayer (ML).

Sn at. %	Growth method	Substrate	Thickness (nm)	Growth, T (°C)	Ref.
35.4	UHV-CVD	Si(100)	49	220	Mircovich et al.[237]
34	Ar$^+$ MBE	Ge/Si(100)	20	150	He and Atwater[39]
30	UHV-CVD	Si(100)	40	245	Xu et al.[241]
28	MS	grGeSn/Ge(100)	20	100	Zheng et al.[232]
27	MBE	Ge(100)	120	100	Imbrenda et al.[233]
25	MBE	Si(100)	48	120	Oehme et al.[234]
22.3	RP-CVD	grGeSn/Ge/Si(100)	Few MLs[a]	200	Dou et al.[159]
18.3	MBE	Ge(100)	100	90	Hickey et al.[235]
18	LP-CVD	grGeSn/Ge/Si(100)	40	280	Assali et al.[160]
16	MBE	Ge/Si(100)	250	150	Rathore et al.[242]
15	UHV-CVD	Si(100)	245	285	Xu et al.[241]

[a]The composition of this film is not uniform over its thickness. Only the top few MLs of the film showed the max Sn content of 22.3 at. % reported in the table.

tendency of Ge-Sn phase separation, in particular with higher Sn contents.

On the other hand, CVD growth can take place at higher deposition temperatures thanks to the different growth dynamics involving gaseous species. This has been the motivation since the early studies on CVD growth of GeSn.[48] Common precursors are Ge and Sn hydrides/chlorides.[52] In CVD growth, Sn incorporation depends on the strain state of the film and increases for decreasing compressive strain, a phenomenon known as strain-relaxation enhancement of Sn incorporation.[157,159,160,243] This does not occur in MBE films.[242] Strain engineering is therefore key in maximizing Sn incorporation in CVD-grown GeSn.[1] Hence, graded GeSn buffers with progressively increasing Sn content have been proposed to gradually relax the film, preventing Sn segregation, to maximize the Sn content at the top of the GeSn stack.[128,160,161,244,245] On the other hand, other groups argued that growing directly on Si(100) allows for increased strain relaxation, which leads to a higher degree of Sn incorporation during growth by CVD,[237] and additionally reduces strain-induced roughening, leading to a larger critical epitaxial thickness.[234] Recently, by growing directly on Si(100) and switching the Sn precursor from SnD$_4$ to SnH$_4$, Mircovich et al.[237] demonstrated a record 35.4 at. % Sn content in UHV-CVD 49-nm-thick GeSn.

3. Accessing MWIR and LWIR ranges

Achieving the large compositions from Table II is not necessarily sufficient to access the MWIR (3–8 μm) and LWIR wavelengths (8–15 μm). In fact, the inherent compressive strain induced by epitaxial mismatch during growth on Ge or Si substrates causes a blue-shift in the GeSn film BG energy.[55,132,246] This implies that a compressive strained film requires higher Sn content to red-shift its BG to the desired energies. Strain engineering thus becomes essential in achieving full relaxation of the compressive strain to operate at long wavelengths.[237] In addition, the crystal quality of GeSn is known to degrade with increasing Sn contents,[57] complicating the realization of optoelectronic devices. For these reasons, while numerous GeSn film-based optoelectronic devices have been demonstrated to operate in the SWIR wavelengths (1.4–3.0 μm), only a handful of them could reach the

MWIR[119,247] despite the large Sn contents achieved in GeSn epitaxial films, as reported in Table II. The alloy compositions in the works reported in Table II are also in principle sufficient to access the LWIR; nevertheless, to date, there exists only a few studies of bandgap energy measurements that barely reach the edge of the LWIR wavelength range,[233,241] and the fabrication of devices in the LWIR is lacking. Employing GeSn of such large Sn contents in devices remains an open challenge.

The factor currently hindering the commercialization of GeSn-based devices is the material crystal quality. The main challenge remains the thorough understanding and management of linear and point defects in GeSn alloys. While the former can be avoided to some extent by engineering the growth processes, e.g., with (graded) buffer layers, the latter are poorly understood. In Secs. VI and VII, we review the research done toward the understanding of defect nucleation, and their influence on carrier trap states in the material.

B. State-of-Art of GeSn sputtering epitaxy

1. MS as an alternative method for GeSn growth

Despite its poor reputation for thin film epitaxy, magnetron sputtering (MS) may represent a plausible solution for industrial scale-up of GeSn. Compared to mainstream epitaxial methods such as MBE and CVD, MS tools are relatively simple, and they allow large growth rates, film homogeneity over large substrates and the use of nontoxic Ge and Sn targets. An additional advantage related to MS growth of GeSn is that ion impingement enhances the incorporation of Sn adatoms via collisional mixing inhibiting segregation, as demonstrated in early works with ion-assisted MBE[28] and sputtering growth.[26] This allows to employ higher substrate temperatures compared to other PVD methods such as MBE, leading in principle to a lower concentration of point defects.[248,249] Experimental verification is required to confirm this hypothesis. However, while CVD and MBE have been extensively studied for epitaxy of GeSn, MS was investigated only by a handful of groups.[26,46,80,97,221–224,250–252] A summary of the works on sputtering epitaxy of GeSn is reported in Table III. Monocrystalline GeSn with Sn content up to 28 at. % has been demonstrated,[232] among the highest Sn fractions observed in

TABLE III. Summary of monocrystalline GeSn films grown by the magnetron sputtering (MS) method, except for Ref. 26, where DC diode sputtering was employed. Acronyms: film thickness (t_f), graded GeSn buffer (grGeSn), low-temperature GeSn buffer (LT-GeSn), growth rate (GR), root mean square roughness (R_{rms}), radio-frequency (RF), high-power impulse (HiPI), and secondary-ion mass spectroscopy (SIMS).

Ref.	Comp. Sn at. %	Substrate	Growth T (°C)	t_f (nm)	Power Ge	(W) Sn	Gas	p (mTorr)	GR (nm/min)	R_{rms} (nm)	Claims
Lin et al.[253]	6.2	vGe	405	266	DC 86.6	DC 7.3	Ar	3.75	26.5	0.93	Obtained room-temperature PL, enhanced by high T growth.
Lin et al.[251]	16.2	(grGeSn/) /Ge(001)	259	60, 120	DC 51	DC 6.5	Ar	3.7	12	~ 1	High DSR. Relaxation mechanisms w/o grGeSn buffer.
Tsukamoto et al.[256]	9	Ge(001)	215–250	70, 390	DC 70	DC 5	Ar + 5% H$_2$	3	24	~ 0.4	Uniform Sn profile, and limited diffusion in substr.
Huang et al.[224]	13	Ge/Si(001)	180–300	350	DC 140	RF 40	Ar	3	8.4	> 4	Highest x_{Sn} on Si(100) by sputtering.
Khelidj et al.[257]	~ 10	Ge/Si(001)	< 360	100	DC 150	DC 15	Ar	2.25	62.5	1.24	96-s growth during cooling from 360 °C. O, C contamination $< 2 \cdot 10^{19}$ cm^{-3}.
Qian et al.[250]	~ 13	Ge(001) Si(001)	$\cdots$	330	RF 100	RF 20	Ar	3	5.5	~ 1	Direct-BG demonstrated via OT and PL.
Dascalescu et al.[223]	~ 12.5	Ge/Si(001)	200–250	~ 120	HiPI	DC	Ar + 5% H$_2$	3	1	$\cdots$	First growth by HiPI sputtering. Polycrystalline defects.
Tsukamoto et al.[258]	9	(LT-GeSn) /Si(001)	300	100	$\cdots$	$\cdots$	Ar + 5% H$_2$	$\cdots$	$\cdots$	~ 1.7	Low-T GeSn buffer allows to prevent Sn segregation.
Yang et al.[259]	7	Ge(100)	160	400	RF 120	RF	Ar	3	12–30	0.8	TDD $\sim 10^9$ cm^{-2}.
Miao et al.[222]	< 3	Ge/Si(100)	160	400	RF 120	RF	Ar	3	12–30	0.74	SIMS shows non-uniform Sn distribution along thickness. Showed GeSn PL.
Zheng et al.[232]	20 28	grGeSn/ /Ge(100)	100–160	20	RF 70	RF 9–30	Ar	3	10–14.5	< 0.5	Thermal stability of 350 °C for Ge$_{0.80}$Sn$_{0.20}$. Highest x_{Sn} achieved by sputtering.
Zheng, et al.[260]	12	grGeSn/ /Ge(001)	140	140	$\cdots$	$\cdots$	Ar + H$_2$ 0%–40%	3	$\cdots$	$\cdots$	Sn uniform along z. H$_2$ decreases Sn diff. length and helps strain relaxation.
Tsukamoto et al.[215]	8.5 11.5	Si(001)	250–300	100	DC	DC	Ar + 5% H$_2$	$\cdots$	$\cdots$	$\cdots$	Sn segregation occurs more easily during growth.
Tsukamoto et al.[221]	≤ 11.5	Si(001)	200–300	100	DC	DC	Ar + 5% H$_2$	$\cdots$	25.2	< 1	High GR allows high gr. T => better cryst. quality.
Zheng et al.[80]	≤ 6	Ge/Si(001)	150	450	RF 70	RF 5–15	Ar	3	~ 10.2	$\cdots$	Thermal stability of 700 °C for Ge$_{0.975}$Sn$_{0.025}$, 500 °C for Ge$_{0.94}$Sn$_{0.06}$.
Pérez Ladr et al.[46]	≤ 14	Ge(001)	150–170	≤ 800	RF	$\cdots$	Ar	$\cdots$	$\cdots$	$\cdots$	P-B model[154] describes well $t_{cr,GeSn}$ on Ge.
Shah et al.[26]	≤ 8	Ge(001) GaAs(001	90–150	1000	DC	DC	Ar	25	12		First epi-GeSn. Absence of magnetron required substrate bias for low-energy ion bombardment.

the literature with any growth technique. GeSn films are generally sputtered using Ar gas and substrate temperatures between 100 and 300 °C, which are higher than MBE, but lower than CVD. Macroscopic structural properties of the layers are well documented, with reported values of alloy composition, film roughness, and degree of strain relaxation (DSR). However, while structural characterization may give good indications of the promise of a material, it does not offer a full picture of its potential for use in optoelectronic devices. The latter is given exclusively by accurate optoelectronic characterization of the layer, currently lacking in the literature for

sputtered epitaxial GeSn. To date, there has been only one report demonstrating direct-BG in $Ge_{0.87}Sn_{0.13}$ grown on Si, Ge and GaAs substrates.[250] No study focused on the BG crossover composition. Room-temperature PL was shown in MS $Ge_{0.97}Sn_{0.03}$ by Miao *et al.*[222] and in $Ge_{0.938}Sn_{0.062}$ by Lin *et al.*[253] Zheng *et al.*[254] demonstrated the use of MS GeSn in an optoelectronic device. They fabricated a *p-i-n* photodetector using $Ge_{0.94}Sn_{0.06}$ as active material and showed performances comparable with devices realized with MBE or CVD at the time. Despite the promising results, only one additional GeSn-based device made from MS has been documented in the literature since then.[255]

Historically, sputtering machines frequently lacked the capability for substrate heating, hindering their use for epitaxial growth. In addition, sputtering tends to have a poor reputation as technique for epitaxy. This is likely owed to the association of the ion impingement occurring during sputtering to the detrimental effects taking place during ion implantation processing, e.g., for material doping. In the latter, implanted species accelerated at energies of few keV are known to generate defects and even amorphization in the implanted layer.[261] However, energies of sputtered atoms impinging on surface during MS are considerably lower, of a few tens of eV,[262,263] and thus the interaction with the film is fundamentally different. With these kinetic energies, impinging atoms will only influence the surface layers of the film, inducing some atomic displacement.[264] In addition, ion impingement can both enhance[263] or suppress[28] surface diffusion, depending on the ion impingement rate and energies. It is true that ions from the working gas (i.e., Ar) neutralized and reflected at the target can possess higher energies up to a few hundred of eV,[262,263] but with appropriate cathode design the acceleration voltages at the target can be kept low enough to limit the Ar energy to values similar to the sputtered atoms,[262] limiting bombardment and implantation effects. Furthermore, being the growing film and substrate heated during growth, the thermal energy will allow for crystal reorganization and annihilation of the eventual defects caused by ion surface impingement. Auret *et al.*[265,266] showed that while Ar plasma exposure of Ge at room temperature generated some trap levels in Ge, no electrically active Ar-related defects could be observed in the material. Additionally, all traps generated by the process were removed by annealing at 250 °C. Hence, with growth temperatures well above 250 °C and appropriate cathode design, MS should yield films free of ion-impingement-induced defects, though this conclusion should be experimentally verified for GeSn alloys.

2. Takeaways from literature on GeSn growth by MS

From the works reported in Table III, the investigations of GeSn MS epitaxy have allowed to establish a few guidelines for optimization of the material crystal quality.

- **Substrate T:** As explained in the above paragraph, it should be kept as high as possible while avoiding Ge-Sn phase separation.[221]
- **Sputtering gas:** H_2 is often added to the Ar sputtering gas, as reactive H species from the plasma are expected to passivate dangling bonds and prevent Sn segregation.[260] In MBE, the presence of H_2 during growth has been found to be beneficial in reducing adatom diffusion length.[267,268] Via DFT-based calculations, Johll

et al.[269] showed that hydrogenated epi-surface promotes Sn incorporation in the film, preventing Sn segregation. H_2 has also been found to induce strain relaxation in sputtered films.[260]

- **Growth rate:** Large growth rates reduce adatom diffusion length, promoting Sn incorporation, hindering phase separation.[221]

To the best of our knowledge, systematic studies on the effect of gas pressure have not been reported, despite its role in determining the ion impingement energy through scattering mechanisms in the gas phase. Several other questions regarding GeSn MS epitaxy remain open. For example, contrasting observations have been reported regarding Sn distribution uniformity along the epitaxial thickness, with studies showing both uniform[256] and non-uniform[222] distributions. Both theoretical and experimental investigations in defect levels and electronic properties in sputtered GeSn are missing.

C. Ge buffer epitaxial growth on Si substrates

Epitaxial growth of Ge has been investigated for years, with well-established recipes for MBE and CVD methods.[270] As for the GeSn alloy, MS epitaxy of Ge has been investigated to a lesser extent.

1. General strategies for Ge growth on Si

Due to the large epitaxial mismatch of 4.2%, strain-induced roughening and islanding tend to occur during Ge heteroepitaxy on Si.[35,271] Ge is, therefore, generally grown in a 2-step method, introduced by Colace *et al.*[272] A first flat Ge layer is grown at low-temperature (LT) as the film relaxes the epitaxial strain. The LT serves to reduce the adatom mobility to hinder 3D growth. This layer is typically thinner than 100 nm, since $t_{cr,Ge}$ on Si is of the order of few nm.[150] A second Ge layer is then grown to the desired final thickness at a high-temperature (HT) to maximize the crystal quality. Growth of the Ge buffer is followed by thermal annealing at T typically higher than 800 °C to fully relax the film and reduce the TDD,[270] as elucidated in Sec. VI B. In addition to the reduced TDD, the annealing of the Ge buffer has an additional benefit for GeSn epitaxy. Thanks to the high temperatures used during annealing, after cooling, the Ge buffer will be left with a $\sim 0.2\%$ in-plane tensile strain due to the differential thermal expansion coefficients (TECs) of the Ge film and the Si substrate.[273–275] The tensile strain built in the Ge layer will provide a decrease in lattice mismatch for GeSn epitaxy, increasing the t_{cr} for strain relaxation and thus extending the thickness limits for GeSn pseudomorphic growth. This is important to avoid additional nucleation of relaxation defects to optimize the material performance in optoelectronic devices. For a qualitative understanding of the effect of tensile-strained vGe substrate, the improvement in t_{cr} in epi-GeSn is shown in Fig. 4(b), using the P-B model for GeSn grown on Ge with 0.2% in-plane tensile strain. One should however note that relaxation of GeSn films on Ge-buffered Si will be eased by the presence of TDs inherited from the Ge buffer layer.[153] Hence, one can expect a lower t_{cr} of GeSn on vGe substrates compared to Ge substrates.

2. Takeaways from literature on Ge growth by MS

We now briefly review the literature on Ge MS epitaxy summarized in Table IV. Surprisingly, we did not find any study reporting the growth via a 2-step deposition, despite being well known to yield higher crystal quality. Monocrystalline Ge films on Si(100) have been

TABLE IV. Summary of monocrystalline Ge films grown by the magnetron sputtering (MS) method, except for Ref. 285, where RF diode sputtering was employed. Acronyms: growth rate (GR), pulsed direct current (pDC), continuous-wave (CW), stacking fault (SF), unintentional doping concentration (n_{un}), gas-source molecular beam epitaxy (GS-MBE).

Ref.	Growth T (°C)	t_f (nm)	Power (W)	Gas	p (mTorr)	GR (nm/min)	R_{rms} (nm)	Claims
Zeng et al.[279]	600	450	RF 75–125	Ar + H$_2$ 0–15%	1.2	· · ·	0.58	Improved crystal quality and R_{rms} with positive substrate bias to reduce Ar$^+$ ion impingement energy. H$_2$ enhanced relaxation.
Liu et al.[280]	400	100–200	RF	· · ·	1.1	4	· · ·	Reduction of 3 orders of magnitude in TDD upon CW laser annealing above $T_{m,Ge}$.
Otsuka et al.[283]	350	6	DC	Ar	2	17.4	0.39	RTA at 720 °C annihilates SFs in Ge film, though slightly degrading R_{rms} to 0.54 nm.
Tsukamoto et al.[278]	450	200	DC 100	Ar + 5%H$_2$	3	20	0.23	TDD $\sim 2 \cdot 10^9$ cm^{-2}. Higher sputtering power decreases adatom diffusion length, limiting islanding. Si-Ge interface intermixing observed at low power.
Yeh et al.[281]	< 360	1000	DC 100	Ar	2.5	126	· · ·	Demonstrate TDD reduction with annealing at 800 °C. μ_p improves to > 1000 cm^2/Vs; n_{un} decreases at LT, but increases at $T \gtrsim 150$ K.
Tsukamoto et al.[277]	350	≤ 100	DC 10	Ar + 5%H$_2$	3	2	0.3	B-doping of Si sub. has same effect as P in Ref. 276. Doping type of sub. not important.
Steglich et al.[284]	380	120	DC 10	Ar	7.5	4.5	· · ·	Oxide contamination on surface did not prevent epitaxy at 380 °C, but did at 320 °C. Measured n_{un}(300 K) $\sim 10^{17}$ cm^{-3}.
Hanafusa et al.[276]	350	≤ 60	DC	Ar + 5%H$_2$	3	2.2	0.31	Si sub. P-doping reduces adatom diff. length, influencing Ge islanding and strain relxn. Si-Ge intermixing observed at low Si doping. Sub. doping has no effect in GS-MBE.
Pietralunga et al.[282]	170 370	100–200	pDC 550 800	Ar	13 17	4.5	~ 1	Unintentional p-type doping observed in Ge. RTA at 400 °C improved crystal quality.
Bajor et al.[285]	470	1500	RF	Ar	15	14.5	· · ·	Strong Si-Ge interface intermixing, likely due to initial ion etching. n_{un}(300 K) $\sim 10^{17}$ cm^{-3}, μ_p= 1280 cm^2/Vs

achieved using both direct current (DC) and radio frequency (RF) power sources. With DC sputtering, root mean square roughness (R_{rms}) $\sim$ 0.3 nm was obtained, optimal for the use of Ge as an epitaxial buffer layer. Root mean square roughness (R_{rms}) for sputtered Ge was noticeably better than for GeSn (see Table III) likely due to the higher Ge growth T that limits kinetic roughening. In a few studies, the resistivity of the Si substrate has been found to play a major role in achieving flat Ge layers.[276,277] In particular, highly doped Si substrates, independently on their doping type, reduced Ge surface adatom mobility, preventing Si-Ge intermixing and strain-induced roughening at 350 °C. This phenomenon is not yet well understood and would need further investigation. A reduction in adatom mobility was also observed at high sputtering powers as a result of the increased growth

rate,[278] analogously to GeSn.[221] Zeng et al.[279] showed an improvement in crystal quality with the application of a positive substrate bias to reduce ion bombardment by decelerating Ar$^+$ ions from the plasma. This work highlighted the importance of tuning the ion impingement energy, an aspect often overlooked. The annealing of sputtered Ge was demonstrated to reduce TDD[280–282] and annihilate stacking fault (SF)s.[283] A few studies reported also the electrical properties of the films, showing p-type unintentional doping concentration (n_{un}) of $10^{16} - 10^{17}$ cm^{-3} (Refs. 281 and 284) and room-temperature hole mobility (μ_p) values of 1000 cm^2/Vs,[281] which are not too far from intrinsic bulk Ge μ_p of $\sim$ 1900 cm^2/Vs. These properties are in line with other epitaxial techniques, as discussed in Sec. VII.

VI. STRAIN RELAXATION MECHANISMS AND DEFECTS IN GeSn, Ge

In this section, we explore the defects typically found in Ge and GeSn films. A thorough comprehension of electrically active defects is crucial for assessing the electrical properties of these materials. We begin by outlining the extended defects that emerge during epitaxial growth of Ge on Si substrates. Subsequently, we analyze the annealing processes proposed to reduce the density of these defects. Annealing is commonly performed on Ge buffer films prior to GeSn growth. Next, we discuss defect formation during epitaxial growth of GeSn on Ge. Finally, we review the point defects that may form in both Ge and GeSn.

For an extensive summary of the different types of dislocations in the group-IV FCC lattice, the reader is directed to the work from Arroyo Rojas Dasilva et al.[286] It contains detailed explanations on the different types of extended defects in group-IV materials and their visualization at transmission electron microscopy (TEM).

A. Strain relaxation during epitaxial growth of Ge on Si (001)

This section provides a brief review of the phenomena occurring during strain relaxation in epitaxial Ge growth on Si(001) substrates.

1. 60° and 90° misfit dislocations

Models of critical thickness of strain relaxation predict a t_{cr} of few nm for epitaxial growth of Ge on Si.[151,153,154] These models have been briefly introduced in Sec. IV A. During growth, as the epitaxial film reaches its t_{cr}, 60° MDs nucleate on surface to plastically release the misfit strain. Driven by the misfit stress field, the 60° MDs form dislocation half-loops and in this configuration they glide down along the {111} planes.[287] This picture is represented schematically in Fig. 6(a). When a half-loop reaches the Ge/Si interface, it will form a misfit dislocation (MD) with Burger's vector (**b**) along one of the ⟨110⟩ directions. The dislocation will thread to the surface via two segments of mostly screw character,[287] the latter being known as threading dislocations (TDs). The Burger's circuit around a 60° MD dislocation core with **b**= $a/2\langle011\rangle$ is shown in Fig. 6(b). Since **b** has an in-plane edge component, the formation of a such MDs will contribute to the release of the epitaxial strain. On the other hand, due to their antiparallel **b**, the TD pair does not release misfit strain.[288] However, TDs are electrically active, i.e., source of trap states, and are therefore undesired.

A representative cross section transmission electron microscopy (TEM) image of a Ge epitaxial film on Si(001) along the ⟨110⟩ zone axis is shown in Fig. 6(c), with MDs and TDs indicated by arrows and
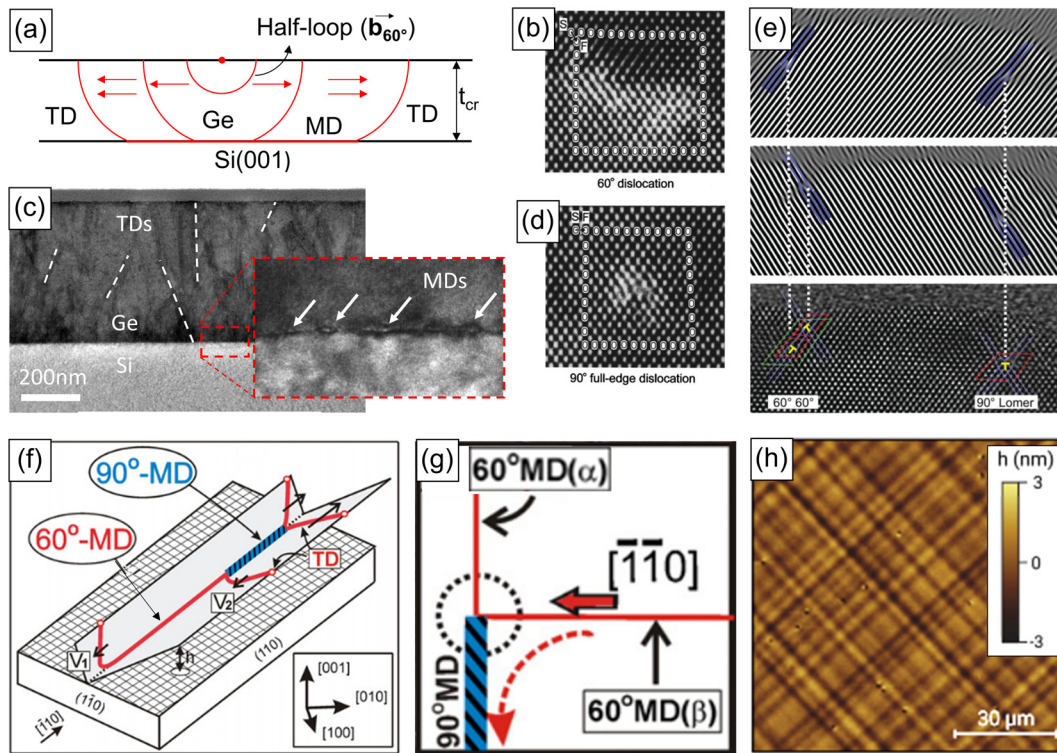
FIG. 6. (a) Schematics of 60° dislocation half-loops nucleating on surface at t_{cr}, and gliding to the Ge/Si interface to form a 60° MD + two screw TDs. (b) and (d) XTEM image parallel to the dislocation core (zone axis ⟨110⟩) of respectively a 60° and 90° MD showing their Burger's circuit and **b**. (c) XTEM of epi-Ge on Si(001), grown by MS by the authors. (e) XTEM showing the subtle difference between a 90° MD and a pair of 60° MDs having the same **b**. (f) and (g) Schematics of two 60° MDs, with (f) parallel and (g) perpendicular dislocation cores, recombining in one 90° MD. (h) Cross-hatch patterns on the surface of an annealed Ge film grown on Si(001), visualized by means of atomic force microscopy (AFM). Figures (b) and (d) are adapted from Sakai et al., Appl. Phys. Lett. **71**, 3510–3512 (1997), with permission from AIP Publishing.[291] (e) is reprinted with permission from Marzegalli et al.,[289] Phys. Rev. B. **88**, 165418 (2013). Copyright 2013 American Physical Society. (f) and (g) are adapted with permission from Bolkhovityanov et al.,[287] Semicond. Sci. Technol. **27**, 043001 (2012). Copyright 2012 IOP Publishing. (h) is reprinted with permission from Rovaris et al., Phys. Rev. B. **100**, 085307 (2019). Copyright 2019 American Physical Society.[292]

lines, respectively. In addition to the aforementioned 60° MDs and TDs, at the Si-Ge interface we also find several 90° full edge dislocations with $\mathbf{b}=\pm a/2[1\bar{1}0]$ or $\mathbf{b}=\pm a/2[110]$, known as Lomer dislocations.[287] A 90° MD is imaged by XTEM in Fig. 6(d), with its Burger's circuit showing that $\mathbf{b}$ lies in the (001) plane. Thanks to their full edge character, Lomer dislocations release twice the misfit strain of 60° MDs.[289] However, while 60° MDs are glissile as their slip plane[290] is the {111} family, Lomer MDs are sessile as their slip plane is the (001) plane, which is not a close-packed slip plane of the FCC lattice. 90° MDs therefore cannot nucleate directly as half-loops on surface and glide to the Si/Ge interface.[289] At high processing temperatures, Lomer dislocations can move perpendicularly to their slip plane by *climb*, involving vacancy-assisted atomic diffusion, but this does not explain their presence at the Ge/Si interface at the growth T used for Ge epitaxy,[287] since their *climbing* would require the presence of extremely large concentrations of vacancies. In fact, Lomer MDs have been found to be the result of the reaction

$$a/2[10\bar{1}] + a/2[011] = a/2[110], \qquad (2)$$

which describes the recombination of two 60° MDs with parallel dislocation cores,[287] shown in Fig. 6(f) after Ref. 287. Perpendicular 60° MDs may also recombine into a Lomer MD, as schematized in Fig. 6(g) for specific combinations of $\mathbf{b}$.[287]

The large occurrence of 90° MDs in epitaxial Ge on Si(001) has been explained by the fact that in high-misfit epitaxial systems the nucleation of a first 60° MD induces the nucleation of a second 60° MD in the near vicinity. In a 3-nm Ge thin film grown on Si(001) by CVD, Marzegalli *et al.*[289] showed the formation of 60° MD pairs at the film interface in Fig. 6(e). They reported an occurrence of 88% of these pairs, with the remaining 12% being isolated 60° or 90° MDs, and they elucidated this phenomenon with dislocation dynamics simulations. They found that after a first MD has nucleated and glided to the interface, its strain field is sensed at the film surface, and the surface nucleation of a *complementary* 60° MD becomes energetically favored. Its most likely position is off the gliding plane of the first 60° MD, explaining the large occurrence of the MD pair, with dislocation cores distanced by ~ 1 nm. On the other hand, nucleation of the complementary dislocation can statistically still occur in the mirror-like gliding plane of the *parent* MD, with consequent gliding and recombination into a Lomer MD. At high processing temperatures, e.g., during growth of the HT Ge layer in a 2-step process, or during annealing, the 60° MD pair can recombine via short-range climbing, explaining the predominance of Lomer dislocations observed at high processing temperatures.[289] The authors, however, point out that the experimental reports of statistics of Lomer MDs could be affected by the difficulty of discerning a 60° pair from a Lomer dislocation. In Fig. 6(e), they show that the Burger's vectors of a 60° MD pair and a Lomer MD are the same, and that the two can be easily confused given the small distance between the dislocation cores in the 60° MD pair. Finally, it should be mentioned that the elucidated mechanism of 60°-MD-induced nucleation is typical of only largely mismatched heteroepitaxial systems, such as the 4.2% of Ge on Si substrates. At low misfit ($< 1.5\%$[293]) such as that of Si-rich SiGe grown on Si, the t_{cr} is too large for this phenomenon to occur; as the first 60° MD nucleates and glides to film/substrate interface, its strain field will not be felt at the surface. Hence, there will be no preferential nucleation of a complementary MD. In this system, Lomer dislocations are thus not observed after growth.[287]

2. Stacking faults

Stacking faults (SFs) has also been observed in epitaxial Ge on Si (001) in few-nm-thick films,[267,283] Ge islands,[294] as well as on growth on patterned substrates.[295,296] The presence of stacking faults (SFs) is due to the splitting of a 60° MD into two Shockley partial dislocations (90° + 30°).[286] This process is driven by the reduction in energy associated with the MD self-energy, proportional to $\mathbf{b}^2$.[34] After dissociation of the 60° MD, the two partials split apart, connected by a SF, reaching an equilibrium distance determined by the interplay between the mutually exerted repulsive force from two partials, and the attractive force due to energetically unfavorable lengthening of the SF.[34] Of course, the misfit strain also plays a role in the stability of this dislocation complex. In particular, in compressively strained Ge films on Si (001), after a critical thickness of a few nm the two partials are expected to glide under the driving force of the misfit stress and recombine.[297] This explains the presence of SFs in thin Ge films on Si (001), and their absence in thick films. Alternative mechanisms of SF formation in few-monolayer-thick Ge films have been proposed.[298] It has been found that SFs in thin films disappear after annealing due to recombination of the partial dislocations into a MD.[267,283]

3. Threading dislocations

As a result of the elucidated strain relaxation phenomena, the as-grown Ge epitaxial films on Si(001) present numerous TDs and short segments of MDs at the Ge/Si interface, as shown in Fig. 6(c). In the ideal case, an array of regularly spaced Lomer dislocations with a pitch of ~ 9 nm with no TD is sufficient to fully relax the misfit strain of 4.2%.[274,287] This configuration, however, cannot be achieved through spontaneous strain relaxation during the epitaxial process. At the onset of plastic relaxation, i.e., film thickness $t_f = t_{cr}$, 60° MDs nucleate at stress concentrators, which consist in impurities or surface steps.[288] Their density thus determine the initial TDD, typically of the order of 10^{11}–10^{12} cm^{-2}.[287] As the film grows, the TDs propagate in the new monolayers and, developing mostly in inclined directions with respect to the (001) growth plane, there is an increasingly high probability that they meet a neighboring TD as the film grows.[288] When two TDs with opposite components of $\mathbf{b}$ come within each other's strain field, they can glide/climb under the effect of mutual elastic interactions. They can repel each other, or fuse/annihilate, decreasing the average TDD in the film.[299] As a consequence, it is observed that the thicker the Ge film is grown, the lower its final TDD is.[170] For very large thicknesses of few μm, this geometric effect saturates due to the low TDD and consequent decrease in probability of interaction.[300] To reduce the final TDD without thermal processing, SiGe buffer layers or Si$_{1-x}$Ge$_x$/ Si$_{1-x}$Ge$_x$ superlattice structures may be introduced to act as dislocation filters, causing bending of existing TDs into MDs at the hetero-interfaces.[300,301] Buffer layers also favor nucleation of Lomer MDs over 60° MDs, facilitating a more efficient relaxation of misfit strain with lower MD densities.[287]

During growth of a Ge film, dislocations will tend to diffuse (i.e., glide or climb) under the effect of the resolved shear strain in their slip plane, in an Arrhenius-like thermally activated process.[302] In the case of epitaxial Ge on Si, strain acting on dislocations is induced by the lattice mismatch, and by the interaction with other dislocations, which may be of attractive or repulsive character. TDs glide by thermally activated motion of kinks along the threading segment.[302] TD pairs tend

to move apart under the effect of misfit strain, elongating the associated MD core at the Ge/Si interface. They can remain blocked by the repulsive field of a perpendicular MD,[303,304] or by a parallel TD with opposite **b** that causes cross-slip.[287,305] Dislocations may thus remain pinned by the interactions with other dislocations, or by point defects.[170] Depending on the growth temperature, kinetic barriers of dislocation diffusion may not be overcome, and the Ge film may be left with residual global—i.e., lattice mismatch—and local strains—i.e., dislocation–dislocation interactions—acting on dislocations. Annealing the film at high temperatures, typically $\geq 800\,°C$, activates dislocation diffusion driven by the felt shear stresses. The resulting recombination of dislocations allows to improve the structural and electrical properties of the material, and is thus essential in the absence of different strain engineering strategies. Effective strain relaxation in the film, enabled by high growth temperature or annealing, is recognized by cross-hatch surface roughness patterns, shown in Fig. 6(h). These patterns are associated with surface Ge adatom diffusion driven the strain induced by buried networks of elongated MDs at the Ge/Si interface.[292]

Section VI B is dedicated to explain the dynamics of dislocations in Ge films during annealing.

B. Annealing of Ge buffer

1. Reactions between threading dislocations

As elucidated in Sec. VI A, as-grown epitaxial Ge films on Si(001) contain several segments of MDs with their associated TDs, and possibly residual misfit strain. TDs additionally sense mutual stress fields from neighboring TDs, which can extend with a radius of 50 nm from their dislocation core.[288] Despite the sensed stress, dislocation motion is impeded by the lack of sufficient thermal energy to overcome kinetic diffusion barriers. Upon annealing, TDs glide and climb under the effect of global—i.e., misfit—and local—i.e., neighboring TDs—stress fields, pulling their associated MD segment behind. TD pairs will be pushed apart by the misfit stress, and the associated MDs will be elongated, resulting in the relaxation of misfit strain. As TDs sense the stress field from neighboring TDs, they may repel or attract each other, depending on their relative signs of **b**. TDs can fuse into one TD, or fully annihilate if they have antiparallel **b**. The film TDD will therefore decrease as a result of TD recombination, which can take place in four different modalities,[288] illustrated in Figs. 7(a)–7(d).

(a) Dislocation loop self-annihilation, which can only occur upon reversal of film strain.
(b) TDs on the same slip plane recombine by glide.
(c) TDs on parallel slip planes recombine by glide+cross-slipping, or by climb.
(d) TDs on non-parallel slip planes recombine by glide, climb, or a combination of the two.

Due to the inclined angle of TDs, their interaction probability increases with the film thickness. Wang et al.[171] constructed a simple thermodynamic model considering a balance of the energies involved in reaction (b) to calculate the extent of TDD reduction in function of the Ge layer thickness. Their argument is that in the absence of external stress, which is the case after the misfit stress is fully relaxed, the interaction energy has to be larger than the Peierls barrier—i.e., the energy barrier for dislocation glide—for TDs to glide under the effect of mutual stress fields, independently on their attractive or repulsive interaction. Therefore, in their model, they calculate the *quasi-equilibrium* distance between two interacting TDs dislocations by equating their interaction energy, dependent on the distance between two threading segments, to the TDs Peierls barrier. Their model, presented in Fig. 7(e), was found to describe well the experimental TDD measured in annealed Ge films on Si(001), with the average TDD scaling with the inverse square of the film thickness. They referred to the calculated average TDD as the *quasi-equilibrium TDD*—and not *equilibrium TDD*—as TDs are not equilibrium defects that minimize the free energy of the system. Furthermore, the thermal/processing history of the film can influence the final TDD. For example, micro-patterning of films is beneficial for achieving an improved TDD, as TDs can glide and annihilate at the edges of microstructures: In 10-μm mesas of Ge, Luan et al.[169] have demonstrated an order of magnitude improvement in TDD with respect to equally-thick Ge films. Additionally, also cyclic annealed Ge films are found to achieve lower TDD values than the quasi-equilibrium TDD,[171] as discussed in the following paragraph.

2. Experimental recipes for Ge annealing

In Table V, we summarize the results of a few experimental studies of annealing of Ge epitaxial films on Si(001). Ge is always annealed post-growth at $T \geq 800\,°C$ for a few minutes. Terzieva et al. have
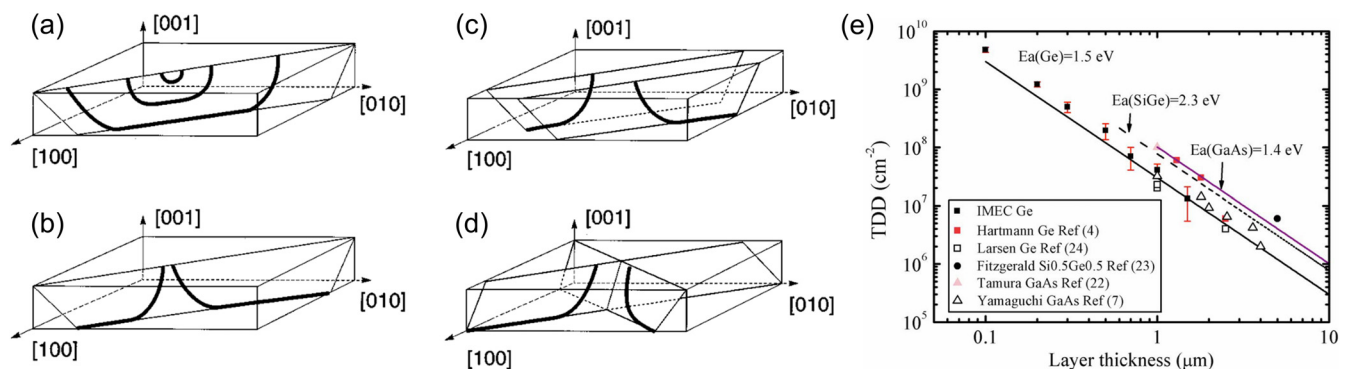
FIG. 7. Modes of TDs recombination: (a) Self-annihilation; (b) On same slip plane by glide; (c) On parallel slip planes by glide+cross-slip or climb; (d) Non-parallel slip planes by glide and/or climb. (e) Prediction of *quasi-equilibrium* TDD according to the model from Ref. 171. Figures (a)–(d) reprinted from Speck et al., J. Appl. Phys. **80**, 3808–3816 (1996), with permission from AIP Publishing.[288] Figure (e) reproduced from Wang et al., Appl. Phys. Lett. **94**, 102115 (2009), with permission from AIP Publishing.[171]

TABLE V. Summary of a few works reporting Ge films annealing processes. Films are annealed after growth unless differently specified. Disclaimer: this table does not report an exhaustive list of all works on Ge annealed films.

Ref.	Growth method	Thick. (μm)	TDD (cm^{-2})		Annealing process	Comments
			As-grown	After anneal.		
Wei et al.[310]	MBE	0.5	$\sim 10^9$	$\sim 8 \times 10^7$	800 °C	Same TDD obtained at 900 °C, but with more Si-Ge intermixing.
Yamamoto et al.[307]	RP-CVD	1	$\cdots$	1.1×10^7	5 cycles: 750, 850 °C	Annealing during growth yields lower TDD.
		5	$\cdots$	2.0×10^6		
		5	$\cdots$	1.3×10^6	850 °C cycles during growth	
Yeh et al.[281]	MS	1	$2.6 \cdot 10^6$	$\sim 10^4$	800 °C (30 min)	Likely error in TDD measurements.
Tan et al.[311]	RP-CVD	0.98	$\cdots$	6×10^6	8 cycles: 825 °C (10 min), 680 °C (10 min)	
Yamamoto et al.[312]	RP-CVD	1	1.6×10^9	6×10^7	800 °C cycles during growth	Cyclic annealing only effective in films with $t > 1\,\mu$m.
				6×10^7	800 °C post-growth	
		4.7	4×10^8	7×10^5	800 °C cycles during growth	
				8×10^6	800 °C post-growth	
Shah et al.[313]	RP-CVD	0.76	2.8×10^8	4.6×10^7	830 °C (10 min) in-situ	
		1.2	1.7×10^8	1.0×10^7		
Choi et al.[314]	CVD	2.5	$\cdots$	5×10^6	Every 500 of film growth: 800 °C (30 min)	Annealing during growth is more effective than same process after growth.
Terzieva et al.[306]	CVD	1.6	1×10^8	2.0×10^7	800 °C (1 min)	Higher annealing temperatures allow to reach quasi-equilibrium TDD faster.
				1.5×10^7	800 °C (3 min)	
				1.2×10^7	800 °C (30 min)	
				1.2×10^7	850 °C (3 min)	
				1.2×10^7	850 °C (20 min)	
Hartmann et al.[274]	RP-CVD	0.73	9×10^8	$< 2 \times 10^8$	10 cycles: 750 °C (10 min), 875 °C (10 min)	
		1.66	$\cdots$	$\cdots$		
Luan et al.[169]	CVD	1	9.5×10^8	2.3×10^7	10 cycles: 900 °C (10 min), 780 °C (10 min)	In 10-μm mesas, obtained TDD is $2.3 \cdot 10^6$ cm^{-2}.

shown that a higher annealing temperature of 850 °C results in the quasi-equilibrium TDD with shorter annealing times.[306] On the other hand, temperature-swing annealing has been found to be a more effective process with respect to single-temperature annealing,[169,307] with the final TDD being potentially lower than the quasi-equilibrium TDD. This is understood as an enhancement of TD diffusion—and probability of interaction—due to cycled compressive-tensile strains developing during cooling and warming owed to the differential TEC of the Ge film and Si substrate.[287,308] However, as clearly visible from Table V, the high and low temperature limits in temperature-swing annealing are chosen arbitrarily, despite respectively having a major influence on the Si-Ge inter-diffusion and dislocation glide velocity. Knowing that the activation energy for TD glide increases linearly with the Si fraction in SiGe,[309] the Si-Ge intermixing occurring at excessively high annealing T may hinder the efficacy of the annealing process in reducing the TDD.[171] A systematic study on the effect of the high and low-temperature limits in cyclic annealing should yield finding the optimal temperatures to employ in the process.

Performing annealing steps during growth has been found to be more effective in reducing the final TDD density with respect to post-growth annealing.[307,314] This is because the annihilated TDs do not thread in the following grown layers, decreasing the density of TD that have to recombine in the post-growth annealing step. This process has been observed to be more effective in Ge films with thickness $> 1\,\mu$m,[312] likely due to the saturation of the geometric effect at the low TDD of thick films.[300] Finally, Nayfeh et al.[315] suggested that the presence of H_2 during annealing enhances Ge adatom mobility, enabling a decrease in surface roughness from 25 to ~ 3 nm. Their as-grown 200-nm-thick Ge films, however, had suboptimal R_{rms} levels. Similarly, annealing in H_2 has been observed to reduce the roughness from 3.5 to 0.7 nm in Ge layers epitaxially overgrown on patterned Si substrates.[316] Furthermore, H_2 annealing was shown to induce monolayer terracing in Ge(001) wafers,[317] and to promote outdiffusion of oxygen impurities.[318] On the other hand, with ~ 1 nm R_{rms} in as-grown 150-nm-thick Ge, annealing in H_2 worsened the R_{rms} at $T > 650$ °C.[319] Hartmann et al.[320] also observed the worsening of R_{rms} with increasing annealing time at 750 °C in smooth 270-nm-thick Ge films on Si(001). In the same study, the authors showed that these annealing conditions had no effect on the roughness of 2.45-μm-thick films, which however considerably roughened with prolonged cyclic annealing between 750 and 890 °C. The data suggests that indeed H_2 enhances surface adatom mobility. This may be detrimental however when the thin films are under strain, e.g., with residual compressive strain in thin Ge epitaxial films, or in strain developed during cyclic annealing

04 January 2025 10:11:00

due to differential TEC, as strain-induced roughening mechanisms may lead to worsening of R_{rms}. Systematic studies of the performance of annealing with/without H_2 in (un)strained films would help clarifying the role of H_2, often employed during Ge annealing.[281,307,311,314]

3. Dislocation arrangement in annealed Ge

After annealing and full strain relaxation of Ge on Si(001), arrays of regularly spaced MDs can be observed at the Ge/Si interface,[281,291,310,314] mainly of 90° character.[287,291,310] This is a consequence of the strain-driven diffusion of TDs, which causes the elongation of MDs segments for efficient misfit strain relaxation. The arrangement in regular spacing of MDs is instead owed to gliding of 60° and vacancy-mediated climbing of 90° MDs due to self-interactions.[321] A regular spacing between 9 and 10 nm is expected to fully release the Ge-Si misfit strain of 4.2%.[274,287,291,310] The MD density will therefore increase as a result of annealing, which should be taken into consideration in case MDs were discovered to be electrically active. Currently, the electrical activity of MDs is not understood, as discussed later in Sec. VII B.

C. Strain relaxation during epitaxial growth of GeSn on Ge buffer

The strain relaxation behavior of GeSn on Ge is similar to that of Ge on Si due to the materials having the same crystal structures. There are, however, some differences attributable to the lower lattice mismatch of GeSn on Ge, and the metastability of GeSn at Sn contents larger than 1 at. %.

The impact of GeSn metastability and the associated Sn out-diffusion on strain relaxation in the material has been discussed in Sec. IV B. In summary, the alteration in alloy composition via Sn out-diffusion has been identified as a possible mechanism for strain relaxation in pseudomorphic GeSn thin films grown on Ge.[174,205] Conversely, bulk Sn clustering has been ruled out to contribute to strain relaxation by APT studies.[322] Sn clustering is only driven by the material metastability upon temperature increase,[322] and it is enhanced in the presence of linear defects.[163,323]

1. Critical thickness for strain relaxation of GeSn on Ge

Wang et al.[156] showed that GeSn relaxes on Ge(001) substrates following People and Bean's (P-B) model for critical thickness,[154,155] in agreement with the critical thickness of strain relaxation (t_{cr}) reported in other studies where GeSn was grown by CVD,[160] MBE,[324] and MS.[46] Slightly lower values of t_{cr} were found in GeSn grown on Ge buffer layers,[325] possibly due to the presence of TDs propagating from the buffer layer that reduce the nucleation energy of MDs in GeSn.[287] One cannot exclude though that it may have been due to different growth parameters (i.e., growth rate and growth T).[156] On the other hand, Cai et al.[326] reported the MBE growth of GeSn on Ge(001) up to 9.7 at. % Sn significantly exceeding the t_{cr} predicted by the P-B model. The authors claimed this originated due to the low growth temperature of 150 °C, though in contrast with the systematic study of Wang et al.,[156] where GeSn films were deposited at the same growth rate and T. The results from Ref. 326 may in fact be affected by Sn-Ge intermixing, clearly visible by the asymmetry of the Bragg-Brentano XRD curves of GeSn films with thickness larger than the t_{cr} predicted by the

P-B model. Intermixing may arise from strain relaxation, and is known to occur in the Si-Ge system.[221,276,327,328] Hence, the mechanism of strain relaxation in Ref. 326 may have been Sn-Ge intermixing rather than nucleation of MDs, explaining the observed t_{cr} exceeding the values predicted by the P-B model. In general, these results support the need to use a strain relaxation model that accurately considers all the kinetic physical processes at play.[153]

2. Strain relaxation mechanisms

Upon relaxation of GeSn on Ge at $t_f = t_{cr}$, 60° half-loops will nucleate on surface,[160,209] gliding to the interface to form a network of MDs. The latter have been observed predominantly to be of 60° character,[159,251] in accordance with predictive models for low-misfit group-IV systems.[287] In contrast with the Ge-on-Si(001) system, after relaxation, SFs along the {111} planes are often observed at the GeSn/Ge interface, extending in short segments across the interface.[128,159,251,329,330] Their origin is associated with two phenomena: (a) splitting of 60° MDs into the more energetically favorable Shockley partials, bound by a SF,[159,329] and (2) SF-bound Frank partial dislocations associated with vacancy complexes.[159,286] The latter may be characteristic of the GeSn material system, where Sn-vacancy complexes are expected to form.[218] In addition, Dou et al.[159] observed the formation of full-edge Lomer dislocations from the reactions between Shockley and Frank partials. Relaxation by strain-induced roughening has also been observed.[160]

In low-temperature growth ($T \sim 150\,°C$), relaxation of GeSn on Ge occurs with slightly different mechanisms due to the limited thermal energy available in the system. In particular, in both MBE[156,242,331] and MS,[260] it has been observed that only the upper part of GeSn films relaxes via the formation of dislocations, while the portion of the film close to the substrate remains fully strained. A model for this phenomenon was proposed by Wan et al.[331] In their model, during growth of GeSn in kinetic roughening regime, surface roughness arises with the typical shape of mounds. Since surface roughness features can give rise to stress concentrators, facilitating dislocation nucleation, at $t = t_{cr}$, MD nucleation is facilitated at the cusps formed between the mounds. Dislocations propagate upwards as the film grows, while the downward propagation is believed to be hindered by the low temperatures,[331] explaining the fully strained bottom region of the film.

Furthermore, the relaxation behavior of GeSn is affected by the layers beneath. For example, nucleation of MDs is facilitated if the Ge buffer has a large TDD.[287,332] In this situation, GeSn films are not expected to follow the P-B model for critical strain relaxation. On the other hand, on graded GeSn buffers, dislocations tend to be confined in the first layers, with limited propagation of TDs to the surface.[159,160,333] This is understood as the result of dislocation bending at the buffers interfaces, with resulting enhanced probability of interaction with dislocations with opposite components of $\mathbf{b}$[287] and due to Hagen-Strunk multiplication mechanisms that induce the nucleation of complementary 60° MD, with resulting formation of Lomer MDs.[159,160] Finally, large amounts of SFs have been found at the interface of GeSn with more than 20 at. % Sn grown directly on Si (001).[113,237] This is unexpected for such large compressive misfits,[297] and it may indicate different relaxation behaviors that remain to be understood to date.

Upon annealing GeSn films, strain relaxation may be activated in pseudomorphic or partially relaxed films. Experimental data suggests

04 January 2025 10:11:00

that MDs elongate during strain relaxation, but that no new MDs are formed.[209] In pseudomorphic films, strain relaxation takes place rather by Sn out-diffusion,[174] although this behavior may be strongly composition-dependent.[205,326] MDs may also nucleate from TDs present in the underlying Ge buffer.[174,218]

D. Point defects in Ge

1. Intrinsic Ge point defects

In pure Ge, theory predicts a formation energy for monovacancy (V) defects of about 2.9 eV,[334] which yields a practically null vacancy concentration at temperatures typically employed for GeSn growth.[335] Self-interstitials have even larger formation energies.[334] At room temperature, these defects are therefore absent in intrinsic Ge.[336]

Vacancies and interstitial defects can arise from irradiation damage,[337,338] out-of-equilibrium growth processes,[248,249,339–342] strain,[201–203] and presence of impurities.[343,344] Experimental studies of neutron-irradiated lightly n-doped Ge ($n_{Sb} \sim 1.5 \times 10^{15}$ cm^{-3}) by positron annihilation spectroscopy (PAS) showed that Ge monovacancies are unstable above 65 K,[345] as they tend to agglomerate into neutral divacancies.[346] Divacancies are stable at room temperature, and tend to agglomerate in larger-sized vacancy clusters after annealing at 200 °C,[344,347] while negatively-charge divacancies are stable up to 400 °C.[337] However, these defects disappear after annealing at 500 °C,[337,348] indicating that after annealing of a Ge buffer for TDD reduction all intrinsic defects are expected to annihilate. Ge self-interstitials caused by irradiation also annihilate at $T > 150$ K.[338] Point defects remaining in the Ge buffer after annealing are due to impurities present in the film, which may typically be H, N, O, C from the base vacuum pressure.

2. Ge-impurity complexes

In germanium, H and O sit in interstitial positions.[348–350] N is often found in the Ge crystal in molecular form (i.e., N$_2$) occupying interstitial sites,[352] while C occupies mainly substitutional sites.[353] Furthermore, N, O, and C form stable complexes with vacancies in the Ge crystal.[354–360] These impurities and defect complexes evolve upon annealing. For example, VO pairs annihilate at 160 °C, forming VO$_2$ complexes, which have different electrical activity,[361] while O interstitials (O$_i$) can cluster into O$_4$ during annealing.[351] The electrical activity of these defects will be reviewed in Sec. VII. Dopant elements, with the exception of B, also tend to form vacancy complexes that are more stable compared to Ge monovacancies.[362] On the other hand, the presence of Ar in the lattice is not expected to yield any electrically-active Ar-specific defect.[363] In additon, surface defects due to Ar implantation are annealed at $T > 250$ °C.[265]

E. Point defects and Sn clustering in GeSn

1. Sn occupies substitutional lattice sites

When adding Sn to the Ge matrix, *ab initio* calculations predict that Sn occupies preferentially substitutional positions in the lattice,[364,365] in agreement with experimental reports.[366] The fraction of Sn atoms occupying substitutional sites can be evaluated with RBS in channeling geometry, comparing the χ_{min}—i.e., ratio of *aligned* to *random* peak height—values of Ge and Sn.[324] It was found that Sn incorporates in substitutional sites for Sn contents up to 14 at. % Sn in CVD,[49,367] MBE,[368,369] and gas-

source molecular beam epitaxy (GS-MBE).[114,206] Su *et al.*[368] measured a decrease in χ_{min} in MBE GeSn with increasing Sn content or decreasing growth temperature, indicating an worsening of crystal quality. A significant improvement in χ_{min} value in CVD-grown Sn-doped Ge films was observed after PDA at 680 °C by Roucka *et al.*[370] Bhargava *et al.*[324] reported substitutional Sn fractions of at least 90% in MBE GeSn with 2.3–14.5 at. % Sn, with a decrease in substitutional fraction with increasing Sn content. Nonetheless, one should note that small deviations from full substitutional Sn occupations measured by RBS may in fact arise from measurement artifacts. In fact, to accommodate the local strain induced by Sn atoms in the Ge matrix, Ge-Sn bonds are distorted.[117,118] This yields a reduced channeling in correspondence with Sn atoms even in a GeSn crystal with full Sn substitutional incorporation.[114]

2. Sn-vacancy complexes

The presence of Sn in the Ge matrix correlates with an increase in point defect concentration, as Sn atoms act as vacancy sinks. Experimental studies of Sn-implanted Ge, backed by *ab initio* computations, demonstrated that Sn-V defects are more stable than isolated vacancies in Ge.[122,197,354,365] Furthermore, due to opposite elastic fields, Sn-V pairs attract neighboring substitutional Sn atoms, favoring phase separation.[371] Intuitively, this can be understood as a vacancy accommodating local lattice strain induced by large Sn atoms in the Ge matrix.[372] The stability of Sn-V defects thus increases when Sn$_n$-V$_m$ complexes are formed.[373] Sn-V pairs arrange in split-configuration – i.e., Sn atom sitting at the bond-centered site—and are stable up to at least 400 °C.[365] Considering the low thermal stability of GeSn alloys,[205–207] this finding suggests that it is not always possible to annihilate Sn-V pairs by annealing GeSn, as Ge-Sn phase separation may occur simultaneously. As we will see in Sec. VII, Sn-V vacancy complexes are electrically active. It is therefore of primary importance to limit the amount of vacancies induced during growth, e.g., by low-temperature growth,[339] excessive growth rate[340] and compressive strain,[201–203] as it may not be possible to eliminate them with post-growth processing. On the other hand, as the processing temperature is increased, the concentration of Sn-V pairs predicted by thermodynamics also increases.[371] This would suggest a trade-off between high-temperature CVD growth methods and low-temperature MBE may be necessary for optimal optoelectronic properties of GeSn. The intermediate temperatures employed in MS GeSn epitaxy may turn out to be favorable in this sense. In this context, an assessment of the electrical properties of MS GeSn is required considering that its carrier concentration, mobility, and lifetime have not been documented before.

Vacancies are difficult to characterize in a material and, for this reason, there exists only a limited amount of studies on vacancy-related defects in epitaxially grown GeSn, which do not allow to draw final conclusions on optimal growth conditions of the material. PAS is the ideal technique to observe vacancy-related defects due to its versatility in measurement conditions and acceptable sensitivity range of 10^{15}–10^{19} cm^{-3}, depending on the charge state of the vacancy.[374] Assali *et al.*[375] studied thoroughly the presence of vacancies in 500–700-nm-thick relaxed GeSn with Sn contents of 6.5–13 at. % grown by low-pressure chemical vapor deposition (CVD) at 330–300 °C on vGe. With room-temperature PAS measurements, they observed the absence of monovacancies, and a predominance for divacancy complexes, with few higher-order vacancy clusters. On the other hand, in the Ge buffer they measured a predominance of vacancy clusters,

04 January 2025 10:11:00

attributed to the diffusion of (di)vacancies and clustering during high-temperature annealing of the material prior to GeSn growth. Interestingly, they also showed a decrease in vacancy clusters and concomitant increase in divacancies with increasing Sn fractions in the film, attributed to capturing of divacancies by the higher concentration of Sn atoms in the lattice. Slotte et al.[376] found somewhat contrasting results in PAS characterization of 400–500 nm GeSn with 6–12.6 at. % Sn (DSR ∼ 70%). In a preliminary study, they observed a predominance of vacancy clusters over mono- or di-vacancies. The difference in claims between the two studies may arise from the growth conditions of the material, unspecified in Ref. 376. Finally, the PAS results from Kamiyama[377] in 200-nm-thick pseudomorphic Ge(Sn) grown at 170 °C by MBE on Ge substrates also hint at a higher vacancy concentration in $Ge_{0.983}Sn_{0.017}$ with respect to pure homoepitaxial Ge. On the other hand, they observed a lower positron lifetime—hence, vacancy concentration—with 0.1 at. % Sn, corroborated by electrical measurements, but they did not provide explanations of this result.

3. Sn clusters

Another type of defect commonly observed in GeSn is few-atom-sized Sn clusters, considered to be the onset of phase separation in metastable GeSn. Atomistic calculations predict a repulsion between Sn substitutional defects in Ge,[122,371] which may explain the SRO recently experimentally observed by Lentz et al.[121] Sn clusters are therefore expected to be stable only in the β-Sn phase. Sn clustering is favored by the presence of vacancies in the film, as Sn-V pairs attract neighboring substitutional Sn atoms,[371] and is also favored by compressive strain.[124] Calculations from Chroneos et al.[373] predict Sn_n-V_m complexes to be more stable with respect to simple Sn-V pairs. Experimentally, Sn clusters have been indirectly detected by APT in AP-CVD GeSn grown at 320 °C with nominal Sn content of 5 at. %,[131] where the authors deduced the presence of Sn_2V, Sn_3V, and Sn_4V_2 complexes. They also observed a higher concentration of these defects in a relaxed film, likely associated with solute segregation at dislocations.[162,163] With successive investigations, the same research group concluded that Sn clustering is not involved in strain relaxation mechanisms, but it is rather driven by the material metastability.[322] Consistent with the tendency of Sn to segregate on surface, Liu et al.[124] found by APT a higher concentration of Sn clusters toward the surface of their CVD $Ge_{0.86}Sn_{0.14}$ films. On the other hand, Rathore et al.[242] employing APT found no evidence of Sn clustering in their MBE-grown $Ge_{0.84}Sn_{0.16}$ films up to thicknesses of 250 nm. This suggests that appropriate growth parameters allow to prevent Sn clustering. On the other hand, one must consider that compositional artifacts may originate from APT characterization.[125] For example, due to the thermal energy deposited in the material, diffusion of Sn may occur during APT sample preparation and measurements, resulting in a change of atomic structure with respect to the as-grown sample. This could potentially lead to the emergence of Sn clusters in the APT sample, which were not present in the as-grown film. Further work is required to shed light on these results.

4. Sn-impurity complexes

The presence of Sn in the GeSn film has also been found to stabilize impurities. Sn-V pairs tend to attract impurities such as C,[354] O,[378] forming complexes that are more stable compared to impurity-V pairs. H/H_2 species have also been reported to interact with Sn-V complexes[379] while, to the best of our knowledge, no study has been reported on the behavior of N impurities in GeSn. Interestingly, substitutional Sn atoms have been found to attract C[380] and repel O impurities.[378] Finally, due to the strong binding energy of Sn with vacancies, Sn-doping of Ge has been proposed as a method to prevent the formation dopant-V pairs that limit dopant activation in Ge.[359,381] However, both As-V[381] and P-V pairs[359,383–385] seem to be more stable than Sn-V pairs.

VII. OPTOELECTRONIC PROPERTIES OF Ge AND GeSn

In this section, we provide an overview of the current understanding of the optoelectronic properties of Ge and GeSn. First, we briefly discuss the optical absorption coefficient of GeSn, focusing on the wavelength of 1.55 μm. We highlight a significant scattering in the data, especially evident in experimental results. Subsequently, we explore the electronic trap states measured in Ge and GeSn, summarizing extensively the data reported in the literature and presenting it in a table format for enhanced clarity. We then undertake a similar process concerning experimental data on unintentional doping levels, carrier lifetime, and mobility in both Ge and GeSn films. For each property, we summarize the main findings to establish a coherent understanding of the subject. Control of these properties is key in achieving optimal performance in GeSn-based devices.[385]

We anticipate that the variations in the reported optoelectronic properties of GeSn thin films reflect a significant influence of the growth technique, parameters, and purity conditions. These aspects are absolutely crucial for controlling the performance of GeSn-based devices.

A. Absorption coefficient of GeSn

The optical properties of GeSn have been extensively investigated with both theory and experiments. Following the bandgap predictions reported in Sec. III, the absorption edge of GeSn shifts toward the infrared for increasing Sn content, as shown in Fig. 8(a) with experimental data plotted from Refs. 234,242, and 386 MWIR wavelengths (∼3–8 μm) can be accessed starting from 15/16 at. % Sn, while by extrapolation of the curves in Fig. 8(a) we can expect the absorption edge to reach the LWIR for $x_{Sn} > 0.3$. Figure 8(b) shows experimental and theoretical values of GeSn absorption coefficient at 1.55 μm, wavelength of interest e.g., for telecommunication and light detection and ranging (LiDAR) applications. The red, dashed line is a fit of theoretical absorption coefficient of unstrained GeSn from Refs. 387 and 388, and serves as a guide to the eye. In spite of the considerable scattering in the data, the absorption coefficient tends to increase with the Sn fraction in the alloy. In Fig. 8(b), we report with a gray, horizontal, dashed line, the absorption coefficient of $In_{0.53}Ga_{0.47}As$, the absorber material employed in commercial III–V technologies. Multiple experimental data suggests that a few at. % Sn in relaxed GeSn are sufficient to surpass the absorption coefficient of $In_{0.53}Ga_{0.47}As$, demonstrating the potential of GeSn for detector applications. On the other hand, in GeSn films the epitaxial compressive strain induces a blue-shift in bandgap energy, and is thus expected to limit the absorption coefficient. This effect however remains hidden by the large scattering in both experimental and computed data in Fig. 8(b). We conclude that a systematic analysis of the material absorption coefficient as a function of strain and material synthesis method is required to resolve the inconsistencies arising from the different experimental and computational methods employed.
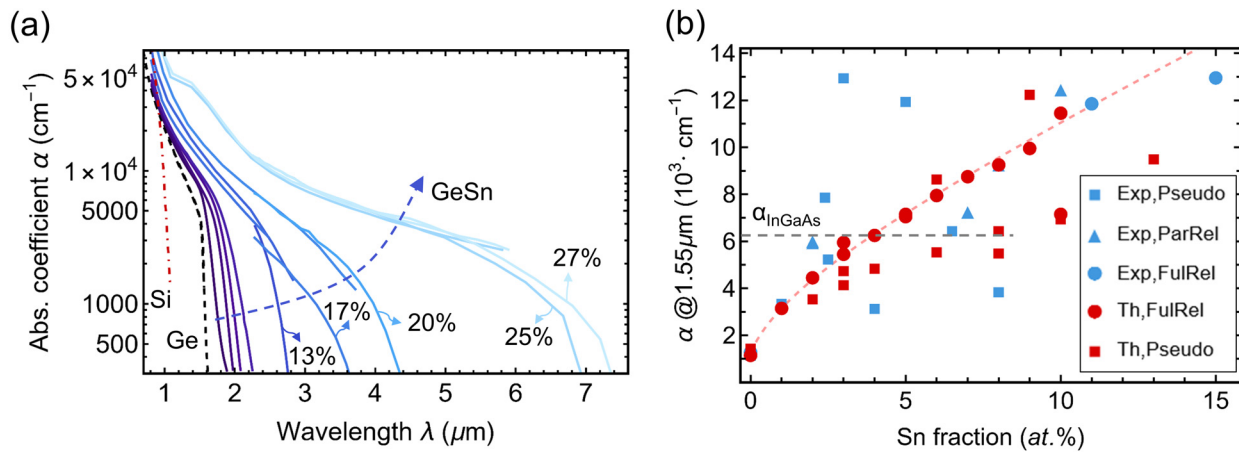
FIG. 8. (a) Shift of absorption edge in GeSn with increasing Sn at. %. Data plotted from Refs. 234,242, and 387. (b) Absorption coefficient of GeSn at 1.55 μm plotted from both theoretical (i.e., *Th.*) and experimental (i.e., *Exp.*) studies.[41,78,389–399] The abbreviations *Pseudo*, *ParRel*, and *FulRel* stand respectively for *pseudomorphic*, *partially relaxed*, *fully relaxed*. The gray, horizontal, dashed line indicates the absorption coefficient of In$_{0.53}$Ga$_{0.47}$As from Ref. 401, while the red, dashed line is a fit for the computed absorption coefficient of Ge$_{1-x}$Sn$_x$ from Ref. 388.

B. Trap states in Ge and GeSn

Trap energy levels in the bandgap of an intrinsic semiconductor determine its electrical properties. Shallow trap levels act as acceptors/donors, releasing free carriers in the material – i.e., unintentional doping concentration – while deep trap levels induce SRH and TAT generation/recombination mechanisms, detrimental for device performance. The SRH recombination rate can be expressed as

$$R_{srh}(T) = \frac{pn - n_i^2}{\tau_{r,p}\left(n + N_C \cdot \exp\left(\dfrac{E_t - E_C}{kT}\right)\right) + \tau_{r,n}\left(p + N_V \cdot \exp\left(-\dfrac{E_t - E_V}{kT}\right)\right)}, \tag{3}$$

where n_i is the intrinsic material concentration, p (n) is the hole (electron) concentration, $\tau_{r,p}$ ($\tau_{r,n}$) is the hole (electron) lifetime, E_V (E_C) is the valence-band (conduction-band) energy, E_f is the Fermi energy, E_t is the trap energy level, k is the Boltzmann constant, and T is the lattice temperature.[149] From Eq. (3), one can deduce that SRH carrier generation has a strong dependence on temperature and on the trap energy level. Traps closer to the middle of the BG will facilitate SRH generation of carriers, as they will ensure the lowest possible rate-determining energetic barrier. TAT mechanisms have an analogous dependence on trap levels.[401] It is thus fundamental to review trap states that may arise from impurities and defects in intrinsic Ge and GeSn. There exist multiple studies reporting electronic levels in both materials, typically measured by deep-level transient spectroscopy (DLTS).

1. Trap states in pure Ge

In Ge, the energy position of electronic levels originating from defects and impurities have been partially reviewed in Refs. 149, 218, 402, and 403. Trap states observed in intrinsic Ge and GeSn are reported in Table VI. Intrinsic point defects in Ge are charged and in principle affect the material electrical properties. However, as discussed in Sec. VI, these defects annihilate at temperatures lower than those employed for Ge annealing.[337,338,348] Consequently, intrinsic Ge point defects are not expected to persist in the annealed Ge buffer layers. Threading dislocations generating from epitaxial strain relaxation are however electrically active. Due to the complexity of the system involved, to date electronic trap states in Ge have not been unambiguously assigned to the different linear defect types. In fact, while mid-gap trap states in Ge are beyond doubt associated with the presence of TDs,[164,166,402,405,407] a reduction in TDD does not always correspond to a proportional reduction in trap concentrations,[408–410] clearly indicating the presence of other sources of deep traps.[404] Deep trap states can be generated by point defects, dislocations, and any combination thereof, substantially complicating the assignment of the measured trap levels to specific defects. A number of different mid-gap levels have been experimentally measured by DLTS, and reported in Table VI. It has been proposed in Ref. 405 that mid-gap traps arise from the interaction of dislocation cores with point-defect clouds,[166,406,410] while clean TDs are expected to generate shallower levels, which may contribute to unintentional doping of the material. This remains however to be verified, since the referred works do not verify if dislocations are clean, or interacting with point defects.[411,412] Studies in which the TDD is reduced by thermal annealing, such as those in Refs. 407 and

TABLE VI. Trap levels generated by defects in Ge and GeSn measured by DLTS, unless differently specified. This table was inspired from that of Ref. 218 and significantly expanded to include data for impurities and extended defects in Ge and GeSn. Additional trap levels for Ge may be found in Ref. 403. Used abbreviations: solid-phase crystallization (SPC), Ge virtual substrate (vGe), PD: point defect, D: dislocation, ED: extended defect (i.e., SF + partial Ds), GB: grain boundary, DB: dangling bonds, BL: band-like states, int.: interface, rlx.: (partially) relaxed, str.: fully strained, Cz: Czochralski, e: electron, p: proton, n:neutron, γ: gamma-ray.

Defects		Activation energy (eV)		Sample condition
		Electron	Hole	
Point defects in Ge	Ge_i	0.11[aa]		e-irradiated Ge
	$V^{-/0}$		0.02[ab]	Anneal+quench Cz-Ge
	$V^{--/-}$		0.26[ab]	Anneal+quench Cz-Ge
	V_2	0.29[ac,ad] 0.31[ae,af]		e-[ac], n-[ac], p-[ad] irradiated, sputter-[ae], e-beam-deposited[af] Ge:Sb
	$V_2^{--/0}$		0.19[ag]	p-irradiated Cz-Ge
	$V_3^{-/0}$		0.08[ag]	e-, p-irradiated Cz-Ge
	Small V cluster	0.1[ac]		n-irradiated Ge:Sb
Linear defects in Ge	Decorated TDs		0.29[ah,ai], 0.25[ai]	vGe
	Clean? D		0.02[aj], 0.10[aj]	D-rich pGe crystal
	Clean? D	0.09[aj]		D-rich nGe crystal
	D-related	0.3?[ak]	0.16[ak], 0.18[ak]	Relaxed Ge:B on Si
	D-V-related	0.28[al]	0.18[al]	Relaxed Ge on grSiGe/Si
	60°/90° partials	0.27[am]	0.07[am], 0.19[am], 0.27[am]	Plastically deformed Ge:Ga
DBs in Ge	DBs	Below VB[an]		DFT calculations
	DBs at GB	0.05–0.10[ao]		SPC poly-Ge[a]
	GB-related	0.32[ah]		poly-Ge
O in Ge	O_{Ge}	0.017, 0.04, 0.2		Unspecified, reported in Ref. 403
	O_i	Neutral[ap]		
	O_4	0.017[ap]		Annealed O-rich Cz-Ge[a]
	$VO^{--/-}$	0.21[aq,ar], 0.27[ad,as]		γ-[aq,ar], p-[ad,as], e-[ad,aq] irradiated Ge
	$VO^{-/0}$		0.27[aq,ar]	γ-[aq,ar], e-[aq] irradiated O-rich Ge
	$VO_2^{--/-}$	0.195[at]		e-irradiated O-rich Ge
	$VO_2^{-/0}$	0.365[at]		e-irradiated O-rich Ge
	O-related	0.14[ad], 0.19[ad]		p-, e-irradiated O-rich n-Ge
	O-, H-related?		0.15[au]	p-irradiated Ge:Sb
	I_{Ge}-O_{2i}	0.06[aa,as], 0.08[aa]		e-[aa], p-[as] irradiated O-rich Ge:Sb[aa], Ge:P[as]
C in Ge	C_{Ge}	Neutral[av,aw]		
	V_2C[ax]	Unknown		
H in Ge	H_i	Shallow acceptor/neutral[ay]		p-irradiated Ge:Sb
	V_2H		0.07[av]	γ-irradiated Ge
	HSi_{Ge}, $H\,C_{Ge}$	Shallow[az,av]		
	HO_i	Shallow[az,av]		
N in Ge	N_{Ge}	Shallow[ba]		DFT calculations
	N_{2i}	Neutral[ba]		DFT calculations
	V_nN_m[bb]	Unknown		DFT calculations
Known defects in GeSn	Clean 60° ED		BL $\leq$ 0.15[bc]	Rlx. $Ge_{0.922}Sn_{0.078}$ on Ge
	TD-related		BL 0.29[bd]	Str. $Ge_{0.93}Sn_{0.07}$ on vGe
	$VSn^{--/-}$		0.19[be], 0.14[as]	e-[be], p-[as] irradiated GeSn
	V_2Sn[bf]	Unknown		e-irradiated Ge:Sn[f]

04 January 2025 10:11:00

TABLE VI. (*Continued.*)

Defects		Activation energy (eV)		Sample condition
		Electron	Hole	
Unidentified defects in GeSn	Unassigned	$0.12-0.14^{as}$	$0.14^{bg}, 0.075^{bg}$ 0.08^{bh}	Rlx. $Ge_{0.9994}Sn_{0.0006}$ on nSi^a p-irr. rlx. $GeSn(x_{Sn} < 0.1)$ on Si Rlx. $Ge_{0.95}Sn_{0.05}$ on vGe^c
	D-related?		$\leq 0.05^{bi}$ $0.085-0.090^{bj}$	Rlx. $Ge_{0.94}Sn_{0.06}$ on pGe^b Rlx. $GeSn(x_{Sn} \leq 0.04)$ on vGe^b
	Sn-related PDs?	$0.23^{bi}, 0.27^{bi}$ $0.14^{bj}, 0.16^{bj}$		Str. $GeSn(x_{Sn} \leq 0.032)$ on nGe Rlx. $Ge_{0.906}Sn_{0.094}$ on vGe^d
	GeSn/Ge int.		$0.20-0.25^{bk}$	Rlx. $Ge_{0.962}Sn_{0.058}$:B on nGe^e

[a]Measured by Hall effect.
[b]Measured by capacitance-voltage (CV).
[c]Extracted from conductivity.
[d]Measured by PC.
[e]Simulated from I-V curves.
[f]Observed with Fourier-transform infrared (FTIR) spectroscopy.
[aa]Ref. 338.
[ab]Ref. 414.
[ac]Ref. 415.
[ad]Ref. 416.
[ae]Ref. 265.
[af]Ref. 417.
[ag]Ref. 347.
[ah]Ref. 405.
[ai]Ref. 418.
[aj]Ref. 411.
[ak]Ref. 409.
[al]Ref. 410.
[am]Ref. 419.
[an]Ref. 334.
[ao]Ref. 148.
[ap]Ref. 351.
[aq]Ref. 357.
[ar]Ref. 420.
[as]Ref. 421.
[at]Ref. 361.
[au]Ref. 422.
[av]Ref. 423.
[aw]Ref. 424.
[ax]Ref. 354.
[ay]Ref. 425.
[az]Ref. 426.
[ba]Ref. 427.
[bb]Ref. 356.
[bc]Ref. 329.
[bd]Ref. 428.
[be]Ref. 382.
[bf]Ref. 429.
[bg]Ref. 430.
[bh]Ref. 431.
[bi]Ref. 432.
[bj]Ref. 165.
[bk]Ref. 433.

408, may thus be influenced by the diffusion and clustering of point defects, which may explain the sub-proportional reduction in trap states with TDDs. The elongation of MDs upon annealing may additionally play a role in changing the electrical properties of annealed Ge.

However, to the best of our knowledge, there has been no investigation into the electrical activity of isolated MDs in epitaxial Ge on Si. The only study addressing the influence of MDs in Ge(Sn) is that of Elbaz *et al.,*[68] which examines the lasing of GeSn microdisks. The authors

observed a one-order-of-magnitude decrease in the lasing threshold by etching a dense array of misfit dislocations at the microdisk laser edges. This suggests the likely presence of trap recombination centers in MDs, but further studies are needed to confirm this. Finally, electronic states in the bandgap arise also from the interaction between dislocations[413] and from dangling bonds at grain boundaries.[148,405] From the presented literature, it is clear that further systematic studies backed by computational works are required to discern among trap states induced by TDs, 60° MDs, 90° MDs, SFs, and partial dislocations.

2. Impurity-related traps in Ge

Additional sources of trap states in the bandagap are spurious impurities introduced in the films during growth. Impurities originating from background pressure in the growth chamber correspond to O, C, N, and H. In the following, we summarize the known trap states that they can induce in pure Ge growth:

- **Oxygen impurity**: O occupies interstitial positions, but is electrically inactive.[351] On the other hand, upon annealing of O-rich Ge, O_4 clusters can form and lead to n-type doping of the material.[351] O also acts as vacancy sink, and O-V complexes have been found to induce both acceptor and donor deep levels in Ge.[357,416]

- **Carbon impurity**: C occupies neutral substitutional positions[426] and, due to its small size, the C_{Ge} defect has a structure similar to a Ge monovacancy.[424] It only weakly binds to vacancies, but it is stabilized by double vacancies.[354] It also tends to bind to and neutralize dopant-vacancy complexes, inactivating dopants.[353] Despite its large contamination levels during epitaxy,[434] trap levels induced by C complexes are seldom studied,[336] and, to the best of our knowledge, there exists no information on the resulting trap states. However, knowing that C is universally present in the base pressure, often due to the use of graphite heaters, it may be assumed that its contributions to the trap concentration in Ge are not dominant, since they have not been observed in experimental DLTS studies.

- **Hydrogen impurity**: Supported by experimental findings,[425] first-principle calculations predict interstitial H^- impurities to behave as acceptors with shallow traps resonant or very close to the valence band (VB).[334,349,350] In Ge, atomic H has been observed to induce shallow acceptor levels by forming complexes with isoelectric Si and C, and donor levels with O.[426] V_2H complexes instead induce shallow acceptor levels in pure Ge.[423] Contrary to Si, H does not passivate completely dangling bonds in Ge, with at best only 60% of the surface dangling bonds passivated upon annealing in H_2.[435] On the other hand, it has been experimentally verified that atomic H species introduced from a H_2 plasma can passivate dislocations reducing their electrical activity in Ge.[436] The same effect was not observed in He plasma or simple annealing in H_2 atmosphere, demonstrating that the passivation effect is induced by atomic H species generated by the plasma process diffusing into in the material. Dislocations act as sinks for vacancies and excess H,[423] and therefore in vGe we can expect H impurities to be attracted by dislocations and passivate defects at dislocation cores. VH_n complexes with $n \leq 3$ have also been theoretically predicted, and were found to possess acceptor levels within 0.35 eV of the VB, and donor levels close

to the VB.[437] The effect of atomic hydrogen in sputtered Ge should thus be accurately evaluated to see if it is negative or positive in terms of electrical properties.

- **Argon impurity**: The effect of Ar plasma or implantation was studied in Ge, and no Ar-specific trap levels were found.[363,438,439] All trap levels were induced by non-Ar-specific ion bombardment. This indicates that, as expected, Ar does not electrically interact with the material.

- **Nitrogen impurity**: Being from group-V in the periodic table of elements, N is expected to be a n-type dopant for Ge. However, N is a poor dopant[352] because it tends to form electrically inactive N interstitial pairs.[427] When in substitutional positions, N gives a shallow level close to the CB,[427] although it has been suggested that it also gives rise to deep traps due to lattice distortions.[352]

3. Trap states in GeSn

In low-Sn-content GeSn alloys, we can typically find the same trap levels of pure Ge.[440] The lower processing temperatures of GeSn, however, lead to the presence of additional defects that are absent in Ge. For example, intrinsic Ge point defects that are expected to annihilate during high-temperature annealing of the Ge buffer may instead be observed in GeSn due to its low growth temperature. This is the case of Ge divacancies, which have been reported to show mid-gap trap levels.[265,347,415] These defects are expected to be stable up to $400\,°C$,[337] well above typical GeSn growth temperatures in PVD methods. Hence, these divacancies forming in the film during growth are not expected to be annihilated, and will likely affect the film electrical properties. The growth temperatures should therefore be maintained as high as possible to limit the formation of vacancies.

In addition to the Ge-related traps, in GeSn alloys there will be trap states induced by the presence of Sn in the material, which we summarize in the following. There exists several studies of defect levels arising in GeSn, but rarely the observed traps are unambiguously assigned to specific defects. Table VI reports the measured trap levels induced by the presence of Sn in the GeSn alloy. These are generally independent of the alloy composition.[329,421,432] Concerning point defects in GeSn, Markevich et al.[382] measured by DLTS hole trap levels 0.19 eV in electron-irradiated GeSn and assigned them to Sn-V complexes. Similar traps were measured in proton-irradiated GeSn.[421] As seen in Sec. VI E, monovacancy complexes were not observed in as-grown epitaxial GeSn; PAS characterization rather evidenced significant concentrations of divacancy complexes and larger vacancy clusters.[375,376] Hence, we can deduce Sn-V complexes are annihilated at the temperatures employed for epitaxial growth. Sn-divacancies complexes have been observed in irradiated Sn-doped Ge,[429,441] but, to the best of our knowledge, their electrical levels have never been reported. In analogy with the SnV_2 defect in Si,[442] we can expect SnV_2 complexes to introduce a deep level in Ge.

Dislocations present in GeSn will also affect its electrical properties. In addition to the electronic levels known to be induced in pure Ge, there have been reports of electronic trap states induced by dislocations in GeSn. Gupta et al.[329] studied by DLTS the trap levels in a $Ge_{0.922}Sn_{0.078}$ film grown by CVD on a n+Ge substrate. They observed band-like shallow acceptor defects with energies ≤ 0.15 eV, and attributed them to clean extended defects (EDs) observed in proximity of the GeSn/Ge interface. These defects, consisting in SFs bound by

Shockley partials, showed trap states similar to Shockley partials in pure Ge.[419] Despite the low activation energy of these EDs, the authors ruled out their role as acceptor dopants due to their small capture cross sections, implying these defects act as donor-like repulsive centers. They further demonstrated that the EDs determined the SRH minority electron generation rate in GeSn, by analyzing the Arrhenius behavior of a pGeSn/nGe diode, where the GeSn was p-doped unintentionally. The presence of defects at the GeSn/Ge interface determining the dark currents of pGeSn/nGe diodes had already been supposed through simulations and fittings of the dark currents in an earlier work by the same authors, though the simulated trap levels yielded defects of 0.20–0.25 eV above the VB.[433] Kondratenko et al.[165] fitted photoconductivity (PC) curves to find activation energies of 85–90 meV above the VB, which they attributed to the large dislocation density in their CVD-grown relaxed GeSn ($x_{Sn} \leq 0.04$) films on vGe. On the other hand, in GeSn films with better structural properties—as measured by XRD—and larger Sn contents ($x_{Sn} > 0.04$) they found that dominant traps were placed at 0.14–0.16 meV above the VB. They suggested these traps were not related to dislocations, and tentatively associated them to SnV complexes.[382,421] The latter trap level was also observed by Ryu et al.[430] with Hall measurements of CVD-grown relaxed Ge$_{0.9994}$Sn$_{0.0006}$ on nSi substrates. Furthermore, the authors reported the appearance of a p-type degenerate conductive layer at the GeSn/Si interface, attributing to the arrays of 90° MDs generated due to epitaxial strain relaxation. This result is in agreement with the decrease in lasing threshold observed when removing MDs in the active region of GeSn microdisks lasers.[68]

In conclusion, the few studies reporting trap states of GeSn are mostly speculative, with often ambiguous assignment of trap states to specific defects. The investigation of trap states in GeSn is still at its infancy, and more systematic studies are required to evaluate the influence of the epitaxial technique of choice, and of the employed growth parameters, which will ultimately determine the film electrical properties.

Finally, it is important to mention possible defects arising from the atomic impingement of species from the plasma in plasma-based growth techniques, such as MS and plasma-enchanced chemical vapor deposition (CVD). DLTS investigations of bulk Ge:Sb exposed to Ar plasma during sputtering have evidenced the absence of hole traps.[266] On the other hand, several electron traps were observed down to the first 400 nm of the nGe crystal, mostly associated with Sb and Ge interstitial induced by Ar impingement. They reported only one intrinsic trap level—at 0.31 eV below the CB—tentatively attributed to Ge divacancies. All observed sputtering-induced defects were annihilated above 250 °C,[265,266] suggesting the growth temperature should be above this value to prevent plasma-induced defects.

C. Unintentional doping concentration

Epitaxial GeSn alloys, including pure Ge, always show carrier concentration levels higher than the intrinsic values at room temperature, despite being nominally intrinsic. This charge carrier concentration is therefore termed *unintentional*, and originates from the presence of defects and impurities in the material. High levels of unintentional doping can be detrimental for the operation of diode devices. For example, they can increase the junction capacitance and decrease the frequency bandwidth of PDs,[76] or induce breakdown in the GeSn absorber of eventual GeSn-on-Si SPADs.[96] Representative studies reporting unintentional doping levels in Ge and GeSn thin films are

listed in Table VII. Carrier concentrations refer to majority holes at 300 K (p_{300K}) unless differently specified with the symbol "$n =$" inserted before the concentration values. In most cases, GeSn thin films show unintentional doping of type p, while pure Ge is reported possessing both n- and p-type unintentional doping.

1. Potential sources of unintentional doping in Ge

In pure Ge films, unintentional doping concentrations in the 10^{16} cm^3 range can be achieved.[247,281,310,396,421,443] To the best of our knowledge, a concentration in the 10^{15} cm^3 range was measured only by Roucka et al.,[396] who reported $p_{300K} = 7 \cdot 10^{15}$ cm^3 in Ge grown by gas-source molecular beam epitaxy (MBE). Unintentional doping in pure Ge is often attributed to the presence of multi-level vacancy complexes[218] or divacancies.[375] Considering the trap levels reported in the literature, summarized in Table VI, divacancies and vacancy clusters may effectively yield both n- and p-type doping. However, DLTS analysis of neutron- and proton-irradiated Ge[337,348] showed that intrinsic vacancy defects in Ge annihilate completely at temperatures above 500 °C. Hence, intrinsic Ge vacancies—or vacancy complexes—are not expected to be present in annealed Ge films and are unlikely to be the source of unintentional doping in the material. We thus discuss other possible sources of shallow traps that may lead to unintentional doping.

Clean dislocations have also been proposed as source of residual doping in Ge.[405] This may be in accordance with observations made in Ref. 281, by Yeh et al., who measured the dependence of unintentional doping concentration on Ge film thickness, reported in Fig. 9(a). They observed a decrease in p with Ge film thickness, explained as a reduction in defect concentration. We believe there are two possible explanations for this behavior: (1) On the one hand, if we consider solely the film defects, the TDD is well known to decrease with film thickness as a consequence of enhanced TD interaction due to the geometric effect.[170] On the other hand, there is no reason why the point defect concentration should change with film thickness if the growth conditions are kept constant. Hence, the results from Fig. 9(a) would point at TDs contributing to unintentional p-type doping at room temperature. Table VI shows various trap levels measured in Ge and associated with the presence of TDs. (2) The decrease in apparent concentration with thickness can also be explained due to a fixed concentration of traps at the interface, e.g., MDs or impurities adsorbed on the substrate prior to film growth, whose contribution to the total amount of carriers in the film decreases with thickness, leading to an apparent decrease in film carrier concentration.

2. Influence of Ge annealing on unintentional doping

Annealing of Ge films has been reported to be beneficial for the material electrical properties. In particular, a reduction of unintentional doping and an improvement in mobility have been observed as a consequence of a decrease in defect concentration during annealing.[281,310] Nevertheless, Hall measurements from 300 K to cryogenic temperatures revealed that the unintentional doping concentration does not decrease over the whole temperature range after annealing. Two examples are shown in Figs. 9(b) and 9(c). After annealing in vacuum a MBE Ge film, Wei et al.[310] measured a reduced carrier concentration across the entire temperature measurement range, shown in (b). However, a thermal treatment of 600 °C allowed to obtain a lower

04 January 2025 10:11:00

TABLE VII. Unintentional doping concentrations in $Ge_{1-x}Sn_x$ thin films reported in the literature. Concentrations refer to holes (p), unless differently specified (n). Acronyms: amrp.: amorphous, solid-phase crystallization (SPC), capacitance-voltage (CV) and electrochemical capacitance-voltage (CV) measurements, Van der Pauw (VdP), post-deposition annealing (PDA), silicon-on-insulator (SOI), germanium-on-insulator (GOI), and resistance (R).

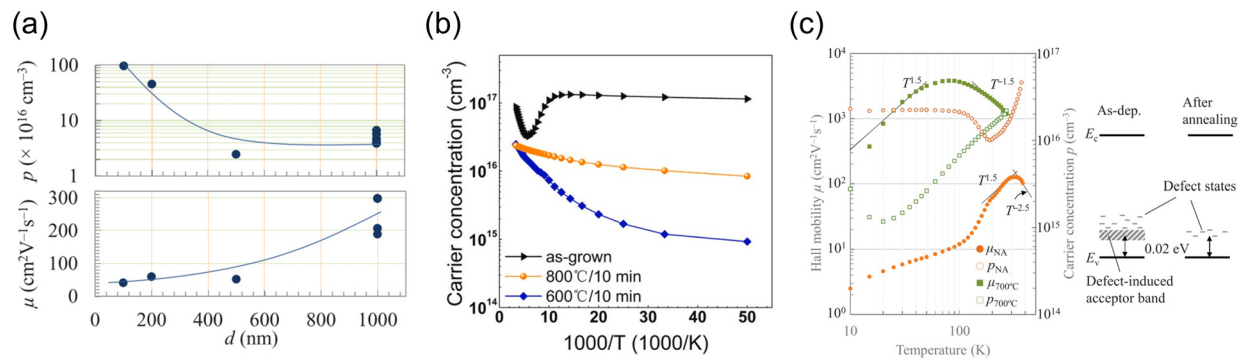| Ref.	Comp. Sn at. %	Substrate	Growth method	Gr. T (°C)	Thick. (nm)	p_{300K} (cm^{-3})	Meas. method	Comments
Mizoguchi et al.[444]	1.2–4.0	SiO$_2$	MBE amrp. + PDA + SPC	*	150	$> 5 \times 10^{17}$	Hall VdP	*: 500–700 °C PDA for 2 h. Then SPC in N$_2$ at 400–650 °C for 40 h gave poly-GeSn.
Atalla et al.[247]	0–17	Ge/Si(001)	LP-CVD	⋯	120–160	Pure Ge: 7×10^{16} $x_{Sn} \geq 10.5\%$: 1–5×10^{17}	CV	Increase in dark current in GeSn PD with larger Sn at. %.
Hogsed et al.[421]	0–9.4	Si(001)	CVD	⋯	300–800	Pure Ge: $n = 5 \times 10^{16}$ $x_{Sn} = 2\%$: 2×10^{16} $x_{Sn} = 9.4\%$: 2×10^{17}	CV DLTS	Measured in *pin* devices. p increases with at. % Sn.
Tao et al.[399]	0–14	Ge(001)	MBE	200	30	Pure Ge: $n = 5.8 \times 10^{17}$ $x_{Sn} = 4\%$: $n = 3.9 \times 10^{17}$ $x_{Sn} = 8\%$: $n = 5.2 \times 10^{17}$ $x_{Sn} = 14\%$: $n = 5.4 \times 10^{17}$	Hall	Films reported partially relaxed, but MBE 30-nm-thick GeSn with $x_{Sn} \leq 8$ at. % is expected to be pseudomorphic on Ge[156]. **Carriers are *n*-type also in GeSn.**
Wei et al.[310]	0	Si(001)	MBE	200	500	As-grown Ge: 9×10^{16} PDA ≥ 500 °C: $\sim 2 \times 10^{16}$	Hall	$p_{<300K}$ is higher with PDA of 800 °C compared to 600 °C.
Julsgaard et al.[445]	12.5	Ge/Si(001)	CVD	⋯	350	9×10^{17}	e-CV	
Scajev et al.[431]	5	Ge/SiGe//Si(001)	MBE	150	200	1.1×10^{17} $p_{200K} = 6 \times 10^{16}$	R	TDD $\sim 3 \cdot 10^6$ cm^{-2}. Hole activation energy of 80 ± 10 meV.
Gupta et al.[329]	7.8	Ge(001)	CVD	320	315	2×10^{16}	CV	GeSn is partially relaxed.
Schulte-Braucks et al.[446]	0–12.5	Ge/Si(001)	CVD	350	2500 768 835 414	Pure Ge: 4×10^{17} $x_{Sn} = 8.5\%$: 5×10^{17} $x_{Sn} = 10\%$: 1.5×10^{18} $x_{Sn} = 12.5\%$: 4×10^{18}	Hall	Cooling down, p_{200K} lower by 1 order of magnitude in GeSn, and by 2.5 in Ge.
Asano et al.[268]	5	Ge(001)	MBE	150	55–70	8×10^{17} no H$_2$ 1×10^{17} with H$_2$	CV	Growth in partial pressure of H$_2$. Pseudomorphic films.
Kamiyama et al.[377]	0–1.7	GOI(001)	MBE	170	200	Pure Ge: 1.7×10^{17} $x_{Sn} = 0.1\%$: 2.4×10^{16} $x_{Sn} = 1.7\%$: 5.5×10^{17}	Hall	**Carrier type unspecified.** PAS used to measured vacancy concentration in films, which matched p (n).
Oehme et al.[443]	0–4.2	Ge/Si(001)	MBE	160	300	Pure Ge: $\sim 1 \times 10^{16}$ $x_{Sn} = 2\%$: $\sim 1 \times 10^{16}$ $x_{Sn} = 4.2\%$: $\sim 1 \times 10^{17}$	CV	**Carrier type unspecified.** Indirect measurements of conc. in *pGe-iGeSn-nGe* PD.
Yeh et al.[281]	0	Si(001)	MS	< 360	1000	As-grown Ge: 5×10^{16} PDA 700 °C: 1.3×10^{16}	Hall	p_{200K} is higher in film annealed at 700 °C.
Nakatsuka et al.[379]	0–2	SOI(001)	MBE	200	⋯	Pure Ge: $\sim 1 \times 10^{18}$ $x_{Sn} = 0.01, 2\%$: $\sim 1 \times 10^{18}$ $x_{Sn} = 0.1\%$: $\sim 1 \times 10^{17}$	Hall	Anneal in H$_2$ decreases p by one order of magnitude.
Ryu et al.[430]	0.06	Si(001)	UHV CVD	390 + RTA 680 °C	800	1.4×10^{16}	Hall VdP	Degenerate *p*-type conductive layer at GeSn/Si interface due to MDs.
Roucka et al.[396]	0	Si(001)	GS-MBE	390	350 900	Pure Ge $n = 7 \times 10^{15}$–5×10^{16}	Hall	
Nakatsuka et al.[447]	0–5.8	SOI(001)	MBE	200	160–170	$> 7 \times 10^{17}$ as-grown 3×10^{17} after PDA	Hall VdP	Anneal in N$_2$ at 500 °C for 60 min decreases p. Slight increase in p with Sn at. %.
Soref et al.[29]	2	⋯	CVD	⋯	⋯	5.6×10^{16}	Hall	PDA improved mobility and decreased p.

04 January 2025 10:11:00

FIG. 9. Hall measurements of Ge films from (a) and (c) Ref. 282 and (b).[310] More details of these studies are reported in Table VII. In both cases Ge is unintentionally doped *p*-type. Figures (a) and (c) reproduced from Yeh *et al.*,[281] ECS J. Solid State Sci. Technol. **3**, Q195–Q199 (2014). Copyright authors, licensed under a Creative Commons Attribution (CC BY) license. Figure (b) reprinted with permission from Wei *et al.*, J. Cryst. Growth. **548**, 125838 (2020). Copyright 2020 Elsevier.[310]

unintentional doping levels compared to 800 °C, except for room-temperature measurements, where *p* was equal. This suggests that shallow trap levels formed at higher processing temperatures, despite an overall reduction in defect concentration. On the same line, Yeh *et al.*,[281] in (c), compared Hall measurements of MS Ge with and without thermal treatment (30 min at 700 °C in N_2+3.8%H_2). They observed a higher unintentional doping level after Ge annealing at 700 °C between 300 and ~150 K. On the other hand, at lower temperatures, the carrier concentration was strongly reduced with annealing. Hence, in this study, it was observed that deeper trap levels, which contribute to unintentional doping at 300 K, were created as a consequence of the annealing process. Conversely, shallower trap levels were eliminated during the thermal processing, leading to a reduction in unintentional doping at lower temperatures. The formation of deep trap levels after annealing cannot be associated with intrinsic point defects, nor TDs, since their concentration decreases with thermal processing. On the other hand, MDs elongate during annealing, and may be a source of deep traps. This could explain also the results in Fig. 7(b), where a higher density of MDs is expected following annealing at 800 °C. Alternatively, the increase in unintentional doping observed with annealing could also be associated with the evolution during annealing of defect complexes involving impurities. It is important to note that the role of impurities is mostly overlooked when trying to individuate the origin of the material unintentional doping. However, intrinsic defects in Ge, being V, V_2, or larger clusters, may form complexes with impurities that are stable at higher temperatures[382,383] or may form during the annealing process through diffusion and recombination. In particular, Table VI shows that O- and H-related defects can be source of doping (*n*-type: $I_{Ge} - O_{2i}$, O_{Ge}, O_4, HO_i. *p*-type: H_i, V_2H, HSi_{Ge}, HC_{Ge}). Trap levels associated with C and N complexes are unknown, but cannot be discarded *a priori* as source of doping. In addition, precise data on the thermal stability of these complexes is often lacking, complicating unambiguous individuation of the source of shallow traps. The different impurity levels, growth techniques and thermal processes of the grown Ge films can therefore explain the apparent inconsistencies found in the literature.

3. Unintentional doping behavior with temperature

On a side note, it is interesting to observe the analogous temperature-dependence of *p* in as-grown MS and MBE Ge films in

Figs. 7(b) and 7(c); as the films are cooled down from 300 K, the carrier concentration first decreases and, round 150 K *p* starts increasing again. It then saturates around 100 K, remaining unchanged as the film is further cooled down to *T* < 20 K. Yeh *et al.* explained the saturation behavior at low temperatures with the presence of an impurity band formed due to defects at energies approximately 20 meV above the VB, schematized in Fig. 7(c). This impurity band disappears upon annealing as a consequence of the reduction in defect concentration. From Table VI, plausible defects with trap energy of 20 meV are dislocations.[411] This is in line with the strong decrease in TDD occurring upon annealing. Monovacancies ($V^{-/0}$) also show the same trap level, but they are not expected to be stable above 65 K,[345] and are thus to be excluded as possible source of this behavior.[448]

4. Potential sources of unintentional doping in GeSn

In contrast to Ge, whose unintentional doping type is equally reported to be *n*- or *p*-type, GeSn alloys are predominantly reported to be *p*-type, as shown in Table VII. Typical room-temperature carrier concentrations are on the order of 10^{16}–10^{17} cm^{-3}. Concentrations on the order of 10^{15} cm^{-3} have never been reported to the best of our knowledge. The fact that GeSn is consistently reported to be *p*-type, with generally increasing *p* for higher Sn contents,[247,399,421,443,446,447] could suggest that there exists a Sn-related dominant acceptor trap that overshadows any other defect. This is often associated with Sn-vacancy complexes.[247,329,443] In agreement with this hypothesis, Kamiyama *et al.*[377] have observed a proportionality between vacancy concentration measured by PAS and hole doping in Ge and GeSn. However, the exact nature of this defect remains unknown: Sn-V pairs are expected to induce hole trap levels between 140 and 190 meV, as shown in Table VI, but PAS characterization of epitaxial GeSn revealed a predominance of divacancies and vacancy clusters.[375,376] Sn_2-V[429] and higher order Sn_nV_m complexes[373] are thus more likely candidates, though their trap energies remain unknown to date. Alternatively, acceptor defects in GeSn may also arise from dislocations,[165,432] or their interaction with Sn, since most studies are performed on relaxed GeSn films. A systematic comparison of pseudomorphic and relaxed GeSn would shed light on the role of dislocations, though Asano *et al.*[268] reported high concentrations of *p*-type dopants in pseudomorphic GeSn, suggesting dislocations are not the source of *p*-type doping.

Ultimately, the growth conditions and impurity levels govern the electronic trap states in the material and thus its unintentional doping concentration. The consistency in p-type doping in GeSn, as opposed to the inconsistency in majority carrier type observed in Ge, may also arise from the lower deposition temperature employed for the alloy. Higher growth temperatures have been reported to be beneficial to reduce the concentration of point defects in the film,[248,249] and thus in principle the unintentional doping. Nevertheless, a systematic study of the effect of temperature on p has not been performed to the best of our knowledge. It has been reported that the presence of H_2 gas in the MBE growth atmosphere has a positive effect in reducing p by almost one order of magnitude, possibly due to point defect passivation from dissociated H species.[268] Post-deposition annealing (PDA) of Ge at 500–700 °C was also seen to be beneficial in reducing p,[29,447] especially when performed in H_2 ambient.[379] However, this approach is constrained when dealing with metastable GeSn alloys due to their limited thermal stability, as discussed in Sec. IV B. To circumvent this limitation, subsecond annealing methods,[449] namely, laser and flash annealing, may prove beneficial. These processes have the potential to reduce defect density responsible for unintentional doping, all the while preventing excessive Sn diffusion and segregation thanks to the limited employed thermal budget.

D. Carrier lifetime

The free carrier lifetime is a key figure of merit for the quality of semiconductor materials in view of their employment in optoelectronic devices. It determines the device performance, affecting its noise and efficiency.[70,96,128,431,450] The term *lifetime* can refer to both carrier generation and recombination phenomena, and the relative importance depends on the type of optoelectronic device. For example, in optical detectors, the *generation* lifetime determines the rate at which free carriers are generated in the reverse-biased depletion region in the dark conditions. These *dark* carriers induce currents that affect the noise performance of the device.[96,450] In this case, Eq. (3) can be used to calculate the device dark currents, assuming the carrier generation in the depletion region is governed by SRH processes. In the presented form, Eq. (3) is expressed in function of the recombination lifetimes (i.e., τ_r). It can however be expressed in function of the generation lifetime (τ_g) in the form of $G \sim n_i/\tau_g$,[407] considering that $n_i^2 \gg pn$ in the depletion region of the device. The recombination and generation lifetimes are thus not equal, but are related via material's parameters.[451] For example, in the depletion region of a p-n junction in reverse bias, if the hole and electron capture cross sections (σ_p, σ_n) do not differ by more than 2 orders of magnitude, the generation and recombination lifetimes are related via

$$\tau_g \simeq 2\tau_r \sqrt{\sigma_n/\sigma_p} \cosh\left[(E_t - E_g/2)/kT\right], \quad (4)$$

where E_t and E_g are respectively the trap energy and the bandgap energy.[451]

The carrier lifetime is highly sensitive to the electronic trap states in a semiconductor, and can thus be employed to assess its crystal quality. The recombination lifetime τ_r can be measured by injecting carriers in a material and monitoring their decay time with time-resolved measurements. In this setup, τ_r depends non-linearly on the excess carrier density (Δn), and can be decomposed in three contributions[451]

$$1/\tau_r = 1/\tau_{SRH} + 1/\tau_{rad} + 1/\tau_{Auger} = A + B(\Delta n) + C(\Delta n)^2, \quad (5)$$

where A, B, C are material constants, and τ_{SRH}, τ_{rad}, τ_{Auger} are the SRH, radiative and Auger lifetimes, respectively. The latter becomes important only at high injection regimes, generally avoided when assessing carrier lifetime in thin films. In a highly-defective material, $\tau_{SRH} \ll \tau_{rad}$, and thus $\tau_r \sim \tau_{SRH}$.

1. Carrier lifetimes in Ge

Table VIII summarizes carrier lifetimes reported for Ge and GeSn films in the literature. In Ge crystals, bulk recombination lifetimes ($\tau_{r,B}$) have been measured to be between 100 and 5000 μs.[452,453] These values are however far from the reported carrier lifetimes in Ge films grown on Si substrates, which are of only a few ns.[455–457] This is attributed to the large density of dislocations generated by epitaxial relaxation phenomena, and to the presence of a surface and an interface in the vicinity of injected carriers.[457] In thin films, carriers can in fact diffuse and recombine at surface traps with a non-negligible contribution to the overall carrier recombination time. The measured effective carrier lifetime can thus be decomposed in two separate contributions[452]

$$\tau_r = \left[\frac{1}{\tau_{r,B}} + \frac{1}{\tau_{r,S} + \tau_D}\right]^{-1}, \quad (6)$$

where $\tau_{r,S} = d_{eff}/v_{r,S}$ is the surface recombination lifetime and $\tau_D = d_{eff}/(\pi^2 D)$ is the carrier diffusion time. $v_{r,S}$ is the surface recombination velocity, D the carrier diffusion coefficient, and d_{eff} the effective probed depth of the material. τ_D takes into account the loss of carriers due to diffusion out of the probed region, and can be mostly neglected with the low $\tau_{r,B}$ measured in epitaxial Ge and GeSn thin films. $\tau_{r,B}$ is a proper figure of merit of material quality, while $\tau_{r,S}$ is indicative of the presence of trap states at the film surface or at the film/substrate interface. $\tau_{r,S}$ is also sensitive to surface roughness.[458] In configurations where $\tau_{r,S}$ is comparable to $\tau_{r,B}$, the resulting measurements of τ_r are strongly affected by the film thickness, as carriers can diffuse and recombine at the interfaces. Thicker films will be less sensitive to $\tau_{r,S}$, yielding longer recombination lifetimes. This situation is typical of few-μm-thick Ge films grown and annealed on Si substrates, as dislocations remain confined near the interface after a PDA process.[170] To properly account for the effect of this defective interface on τ_r, Eq. (6) can be fitted over τ_r measured at different film thicknesses – i.e., d_{eff} –.[455] This yields an effective $\tau_{r,S}$ that describes the recombination rate at the defective epitaxial interface or film surface.[459] Doing so, Ge bulk lifetimes ($\tau_{r,B}$) from few ns[454] up to 11 ns[455] were reported, with recombination velocities ($v_{r,S}$) of tens of m/s at the Si/Ge interface. An exceptional $\tau_{r,B} = 91$ ns was measured by Kako et al.,[459] possibly due to a low TDD in the film owed to its large thickness (>3 μm).

2. Carrier lifetimes in GeSn

For GeSn thin films, recombination lifetimes are even lower than in Ge films. Measurements of τ_r in GeSn have been reported in a handful of studies, summarized in Table VIII. Direct measurements of carrier lifetime in pseudomorphic GeSn on vGe substrates yielded values of $\tau_{r,300K}$ between a few hundreds of ps[4,431,445,462,464] to 1–2 ns.[461–463] These recombination lifetimes are significantly shorter than the room-

04 January 2025 10:11:00

TABLE VIII. Carrier lifetimes reported in the literature. Introduced acronyms: surface recombination velocity ($v_{r,S}$), bulk and surface recombination lifetimes ($\tau_{r,B}$, $\tau_{r,S}$), plasma-enhanced chemical vapor deposition (PECVD), light-induced transient grating (LITG), electroluminesce (EL), microwave photoconductance decay (μW-PCD), time-resolved differential reflectivity (TRDR), time-resolved photoluminescence spectroscopy (TRPLS), infrared (IR), broadband pump-probe differential transmission measurements [$\Delta T/T(t)$], inductive-coupled photoconductance decay (IC-PCD).

Ref.	Comp. Sn at. %	Substrate	Growth method	Gr. T (°C)	Thick. (nm)	τ_r (ns)	τ meas. method	Comments
Daligou et al.[460]	17	GeSn/Ge//Si(001)	LP-CVD	280	160	@10–300 K: $\tau_{rad} \sim 3.2$–22.2	Indirect	τ_{rad} is the radiative carrier lifetime, extracted from rigorous modeling of PL spectra. Reported dependence of τ_{rad} with T.
Hudait et al.[458]	0–6	III-V buf.//GaAs	MBE	175––250	50–600	@300 K: 90–470	μW-PCD	GeSn lattice matched or pseudomorphic. $\tau_r = \tau_{SRH}$, increased with higher gr. T or lower R_{rms}. $\tau_{r,S}$ not properly considered.
Rogowicz et al.[461]	6–12	Ge/Si(001)	RP-CVD	$\cdots$	36–60	$\tau_{r,B}$@300 K: $x_{Sn} = 6\%$: 1.5 $x_{Sn} = 11\%$: 1.2 $\tau_{r,S}$@300 K: 0.7–0.5	TRPLS TRDR	Pseudomorphic GeSn. Slightly longer lifetimes with less Sn. Report T-dependence of $\tau_{r,B}$ and $\tau_{r,S}$.
Julsgaard et al.[445]	12.5	Ge/Si(001)	CVD	$\cdots$	350	0.22 @20 K Same @300 K	TRPLS	Claim $\tau_r = \tau_{SRH}$. Modest variation with measurement T.
Scajev et al.[431]	5	Ge/SiGe//Si(001)	MBE	150	200	0.05–0.15 @ 50–350 K	LITG	Pseudomorphic GeSn, with TDD $\sim 3\times10^6$ cm^{-2} inherited from buffers. At 300 K, $\tau_h \gg \tau_e$. Measured diffusion length of 450 nm.
Vitiello et al.[462]	2–10	Ge/Si(001)	RP-CVD	200––300	150 45 35 70 40 40	@10 K: $x_{Sn} = 2\%$: 0.70 $x_{Sn} = 3\%$: 0.75 $x_{Sn} = 4\%$: 0.90 $x_{Sn} = 6\%$: 2.5 $x_{Sn} = 8\%$: 0.65 $x_{Sn} = 10\%$: 0.4	Hanle effect	GeSn pseudomorphic on 600-nm-thick Ge buffer. Claim $\tau_r = \tau_{SRH}$. Not a clear trend on alloy composition, justified with different growth conditions. Observed a proportional decrease in τ_r with TDD.
De Cesari et al.[463]	5	Ge/Si(001)	RP-CVD	280	70	1.1 @300 K 0.9 @210 K	TRPLS	GeSn pseudomorphic on 650-nm-thick Ge buffer. Traps at 13 meV and 17 meV above Fermi level.
Geiger et al.[464]	0–12.5	Ge/Si(001)	RP-CVD	350––390	2700 800 560	@300 K: Pure Ge buffer: 2.6 8.5%: 0.47 (0.43@20 K) 12.5%: 0.26 (0.17@25 K)	IR $\Delta T/T(t)$	Ge buffer underwent PDA. τ_r slightly decreases at $\sim$ 20 K compared to 300 K. Pure Ge shows 10-fold longer τ_r compared to GeSn.
Wirths et al.[4]	8–13	Ge/Si(001)	RP-CVD	350––390	200–560	0.35 @300 K 2.1 @15 K	Indirect	τ_r extracted from PL measurements. Fit SRH temperature behavior of τ_r and obtain $E_t - E_F = 19$ meV.

04 January 2025 10:11:00

TABLE VIII. (*Continued.*)

Ref.	Comp. Sn at. %	Substrate	Growth method	Gr. T (°C)	Thick. (nm)	τ_r (ns)	τ meas. method	Comments
Gallagher et al.[128]	0–11	Ge(001)	UHV CVD	285–−320	400–700	@300 K Rlxd. 400 nm: 30 Rlxd. 700 nm: 95 Psdmrp.: 100–300	Indirect	τ_r extracted from EL measurements in *pin* diodes. Strong reduction of τ_r in presence of interface relaxation defects.
Kako et al.[459]	0	Si(001)	CVD	· · ·	230–3150	Pure Ge @300 K: $\tau_{r,B} \sim 91$ ns $v_{r,S} \sim 130$ m/s	TRPLS	Surface recombination dominated by defective Ge/Si interface. Demonstrate fitting PL decay time with bulk and surface components.
Srinivasan et al.[465]	0	SOI	· · ·	· · ·	350	Pure Ge @300 K: 1.6 $v_{r,S} < 200$ m/s	TRPLS	τ_r measured in Ge waveguides. $v_{r,S}$ at Ge/Si interface.
Saito et al.[454]	0	Si(001)	CVD -PDA	500		Pure Ge @300 K: 2 $\tau_{r,B} = 3.5$ ns $v_{r,S} < 55$ m/s	TRPLS	They consider τ_r is equal to twice the PL decay time. Growth T and PDA conditions unspecified.
Geiger et al.[456]	0	Si(001) GOI	PECVD	500+ PDA	1700 2600	Pure Ge @300 K: 2.0 ($v_{r,S} \sim 850$ m/s) 5.3 ($v_{r,S} \sim 490$ m/s)	IR $\Delta T/T(t)$	6-cycle PDA between 800 and 600 °C. Report $\tau_r = \tau_{r,S}$, assuming recombination occurs only at defective interface with substrate.
Conley et al.[466]	10	Ge/Si(001)	RP-CVD	< 450	95	120–1000 @ 77 K	Indirect	τ_r extracted from optical responsivity at 1.55 μm. They however used an unrealistic abs. coeff. of 19 200 cm^{-1} for Ge$_{0.093}$Sn$_{0.07}$. Mesa diameter determines τ_r, indicating an unaccounted contribution of $\tau_{r,S}$.
Sheng et al.[455]	0	Si(001)	MBE	· · ·	3500	Pure Ge @300 K: 7 TDD $\sim 3.3 \times 10^7$ cm^{-2}: $\tau_{r,B} = 8.2$ ns TDD $\sim 1.6 \times 10^7$ cm^{-2}: $\tau_{r,B} = 11$ ns	μW-PCD	Strong decrease in τ_r near Ge/Si interface. $\tau_{r,B}$ reflects TDD.
Gonzalez et al.[407]	0	Si(001)	CVD	450	330	Bulk Ge @300 K: TDD $\sim 1.6 \times 10^{10}$ cm^{-2}: $\tau_g = 0.5$ ns TDD $\sim 4.2 \times 10^8$ cm^{-2}: $\tau_g = 6.8$ ns	Indirect	PDA (850 °C, 3 min, in N$_2$) decreased TDD 40-fold, but τ_g increased only 14-fold. τ_g was extracted from dark currents in Ge pFET, and found to be governed by SRH and TAT generation.
Gaubas et al.[452]	0	None	Cz, FZ	· · ·	· · ·	Bulk Ge @300 K: $1 - 5 \times 10^5$	μW-PCD	Study on Ge Czochralski (Cz) or float-zone (FZ) bulk Ge crystals.
Derhacobian et al.[453]	0	None	· · ·	· · ·	· · ·	Bulk Ge @300 K: $\tau_{r,B} = 5 \times 10^6$ ns $v_{r,S} = 13$ m/s	IC-PCD	Study on bulk Ge crystal, with nominal doping $< 10^{10}$ cm^{-3}.

04 January 2025 10:11:00

temperature radiative lifetime of 22 ns extracted from PL measurements in $Ge_{0.83}Sn_{0.17}$ grown on step-graded GeSn/vGe substrates.[460] This signifies that a significant portion of free carriers would undergo non-radiative recombination in an emissive device, thereby reducing its performance. Considerably larger $\tau_{r,300K}$ of tens of ns was measured by microwave photoconductance decay (μW-PCD) in a study by Hudait *et al.*[458] on GeSn grown pseudomorphically or lattice-matched[467] on III-V-buffered GaAs substrates. The high values of $\tau_{r,300K}$ measured in this study were possibly due to the absence of dislocations in the GeSn films. However, comparing τ_r in GeSn to pure Ge films, one must consider that in studies concerning pure Ge films the surface and bulk recombination rates are often discerned by fitting Eq. (6) to measurements in films of varying thickness. This is not the case for GeSn, as typically only the effective τ_r is reported. This value is thus dependent on the film thickness in few-hundred-nm-thick GeSn films, as confirmed in Refs.128 and 458. In addition, Rogowicz *et al.*[461] showed that measured PL lifetimes of a few hundred of ps are consistent with surface-recombination phenomena, rather than the film bulk properties. With time-resolved differential reflectivity (TRDR) measurements of various GeSn films with different compositions, they consistently observed two different decay lifetimes, attributed to surface and SRH bulk recombination processes. time-resolved photoluminescence spectroscopy (PL) measurements of the same samples yielded PL lifetimes matching almost perfectly the fast TRDR decay owed to surface processes. Their work highlighted the importance to decompose the bulk and surface lifetimes to accurately evaluate material performance.

3. Takeaways from τ measurements in the literature

From the measurements of carrier lifetime in Ge and GeSn thin films, we can draw a few conclusions. A clear correlation between the TDD and τ_r has been observed in multiple works.[128,407,455,458,462] Vitiello *et al.*[462] measured τ_r in $Ge_{0.92}Sn_{0.08}$ films grown on vGe substrates with constant composition and different TDD. They observed a linearly proportional decrease in τ_r, and could estimate a recombination velocity at TD lines of $(1.77\pm0.03) \times 10^5$ cm/s, which is 2- to 10-fold higher than $v_{r,S}$ at Si/Ge interfaces. We highlight that the authors of this study tuned the TDD in GeSn films solely by controlling their thickness, and thus the film DSR, which is directly correlated with the TDD. On the other hand, when the TDD is tuned through thermal processes, the varying temperatures employed to obtain different TDDs also result in differing point defect concentrations, which also affect measurements of τ_r. For example, Gonzalez *et al.*[407] found that a decrease in TDD obtained through high-temperature PDA processing of Ge films led to a subproportional increase in lifetime. This suggests that at high-temperature processing of the material, besides the known reactions occurring among dislocations (see Sec. VI B), additional reactions involving different types of defects occurred—e.g., formation of point defect complexes—affecting the trap concentration in the material and thus its carrier lifetime. This is in line with the investigations of unintentional doping concentrations in annealed films discussed in Sec. VII C.

The GeSn alloy composition has also been found to influence the carrier recombination lifetimes. A few studies reported that τ_r decreases with increasing Sn content in the alloy.[461,462,464] In particular, a large difference in carrier lifetime was observed between pure Ge and GeSn alloy films. A 10-fold decrease in τ_r was

measured between a Ge buffer layer and a pseudomorphic GeSn film grown on the buffer itself.[464] Since the TDD should be the same in the two materials, one can speculate the resulting lower τ_r in GeSn is owed to the increased concentration of vacancies that induce mid-gap traps, enhancing SRH recombination processes. As elucidated in Secs. VI D and VI E, vacancies are expected in considerably lower concentrations in pure Ge as a consequence of the higher growth temperature and PDA processes of Ge films. Lowering the growth temperature has been demonstrated to decrease the lifetime in GeSn.[458] Furthermore, the concentration of vacancies is known to increase with increasing Sn content,[375,377] explaining the observed trends in τ_r with alloy composition.

To conclude, the measured recombination lifetimes in GeSn films are always attributed to SRH or surface recombination phenomena. In GeSn, τ_r measures a few ns in the best cases, which is considerably smaller than its computed radiative recombination lifetimes.[468] From Ref. 468, τ_r in GeSn is computed to decrease with Sn content, but still remains above 100 ns up to 18 at. % Sn; this computed lifetime is two order of magnitudes higher than any experimental carrier lifetime measured in GeSn on (Ge-buffered) Si substrates. Hence, the reviewed experimental results elucidate the difficulty in achieving efficient room-temperature emission and lasing. More systematic studies are required to understand the material defects in depth, and find effective passivation techniques for linear and point defects in order to increase the non-radiative lifetimes in GeSn. For example, H species have been observed to passivate point defects in GeSn.[379]

E. Mobility

The carrier mobility (μ) of a semiconductor is affected by multiple scattering phenomena in the material. For epitaxial Ge and GeSn films, the main scattering mechanisms involve phonon scattering, neutral and ionized point defect (ND, ID) scattering, dislocation scattering, and alloy scattering. Their contributions can be discerned thanks to their different temperature dependences, via the use of Matthiesen's rule,[149]

$$\frac{1}{\mu} = \sum_i \frac{1}{\mu_i} \simeq \frac{1}{\mu_{ph}} + \frac{1}{\mu_{ND}} + \frac{1}{\mu_{ID}} + \frac{1}{\mu_{disl}} + \frac{1}{\mu_{alloy}} + \cdots. \quad (7)$$

Carrier mobility values reported in the literature for Ge and GeSn films are summarized in Table IX. In the following, we will focus mainly on discussing the hole mobility, as it is the majority carrier type most frequently observed as a result of unintentional doping in the GeSn alloy (see Sec. VII C).

1. Mobility in Ge

For pure bulk Ge, the theoretical room-temperature hole mobility (μ_h) is 1800 cm^2/V s.[15] Experimental values of μ_h in as-grown Ge films are however significantly lower, between 100 and 500 cm^2/Vs[281,310,446,447] due to carrier scattering from point defects and dislocations present in the material. In a systematic study of Ge hole mobility in function of dislocation density, Ghosh *et al.*[469] have demonstrated a clear inverse relation between TDD and μ_h. In particular, they observed a drop in μ_h for TDD $> 2 \times 10^7$ cm^{-2}, as dislocation scattering became the predominant carrier scattering mechanism in the material. In this regime of TDD, the Ge film thickness is another factor indirectly influencing μ_h, as the average TDD decreases with

TABLE IX. Carrier mobility in intrinsic $Ge_{1-x}Sn_x$ thin films reported in the literature. We report the hole mobility (μ_h), unless differently specified. Acronyms: optical pump-THz probe spectroscopy (OPTP), solid-phase crystallization (SPC), post-deposition annealing (PDA), flashlamp annealing (FLA), capacitance–voltage (CV), current–voltage (IV), and metal-oxide-semiconductor field-effect transistor (MOSFET).

Ref.	Comp. Sn at. %	Substrate	Growth method	Gr. T (°C)	Thick. (nm)	μ_h @ 300 K (cm²/Vs)	μ meas. method	Comments
Liu et al.[470]	1.5	Ge(001)	MS	300	350	$\mu = 80 - 210$	OPTP	**Carrier type unspecified.** Mobility decreases with large pump fluences due to carrier–carrier scattering phenomena.
Tao et al.[399]	0–14	Ge(001)	MBE	200	30	Pure Ge: $\mu_e = 1113$ $x_{Sn} = 4\%$: $\mu_e = 1210$ $x_{Sn} = 8\%$: $\mu_e = 1123$ $x_{Sn} = 14\%$: $\mu_e = 1007$	Hall	Films reported partially relaxed, but MBE 30-nm-thick GeSn with $x_{Sn} \leq 8$ at. % is expected to be pseudomorphic on Ge[156]. **Carriers are *n*-type also in GeSn.**
Wei et al.[310]	0	Si(001)	MBE	200	500	As-grown Ge: 343 PDA 900 °C: 1252	Hall	Monotonic increase in μ_h with increasing annealing T. Improvements with higher annealing T across the entire T range of 20–300 K.
Scajev et al.[431]	5	Ge/SiGe/ /Si(001)	MBE	150	200	490	⋯	Carrier scattering from ionized and neutral impurities dominant across the 70–300 K temperature range.
Imajo et al.[473]	0	GeO₂/SiO₂	aGeSn MBE + SPC	*	500	Pure Ge: 440 After PDA: 620	Hall VdP	*: SPC at 450 °C for 5 h + 375 °C for 150 h (+ PDA at 500 °C for 5 h), resulting in **polycrystalline Ge.** Improvement in μ_h with increase in grain size.
Prucnal et al.[471]	5	Si(001)	MBE	160 + PDA	300	155	Hall VdP	PDA: FLA with no pre-heating and a pulse of 3 ms and 65 J/cm².
Huang et al.[18]	10	Ge/Si(001)	CVD	⋯	9	509	CV + IV in MOSFET	GeSn capped with 1 nm Ge to reduce surface scattering. Material underwent thermal processing at 400 °C prior μ_h measurements. GeSn MOSFET outperforms Ge MOSFET in terms of μ_h.
Schulte-Braucks et al.[446]	0–12.5	Ge/Si(001)	CVD	350	2500 768 835 414	Pure Ge: ~ 350 $x_{Sn} = 8.5\%$: ~ 400 $x_{Sn} = 10\%$: ~ 350 $x_{Sn} = 12.5\%$: ~ 300	Hall	While at room T μ_h is comparable in GeSn and Ge, for $T < 250$ K, $\mu_h, Ge \gg \mu_h, GeSn$.
Yeh et al.[281]	0	Si(001)	MS	< 360	200 1000 1000	Pure Ge: ~ 60 ~ 200–300 After PDA: 1180	Hall	Progressive increase in μ_h with film thickness. In 1 μm Ge, they observed a 4-fold improvement in μ_h after PDA at 700 °C.

04 January 2025 10:11:00

TABLE IX. (*Continued.*)

Ref.	Comp. Sn at. %	Substrate	Growth method	Gr. T (°C)	Thick. (nm)	μ_h @ 300 K (cm²/Vs)	μ meas. method	Comments
Ghosh et al.[469]	0	Si(001)	MBE	600 + PDA 800 °C	100 1000 1000 1000	Pure Ge: ~ 950 TDD = 2×10^7 cm⁻²: 1020 TDD = 5×10^7 cm⁻²: ~ 600 TDD = 7×10^7 cm⁻²: ~ 360	Hall VdP	Found two scattering regimes, dominated by (1) impurities and (2) dislocations. Clear drop in μ_h for TDD > 2×10^7 cm⁻². μ_h slightly increases with Ge film thickness.
Ryu et al.[430]	0.06	Si(001)	UHV CVD	390 + RTA 680 °C	800	~ 370	Hall VdP	Degenerate p-type conductive layer at GeSn/Si interface due to MDs. μ_h measured down to 4 K. $\mu_h, max = 638$ cm²/Vs at ~ 130 K.
Roucka et al.[370]	0–0.1	Si(001)	CVD	390 + RTA 680 °C	500 800 1100	Pure Ge: 700–800 $x_{Sn} = 0.06\%$: 345–390 $x_{Sn} = 0.1\%$: 270–360	Hall	They show alloy scattering causes halvening of Hall mobility with respect to pure Ge.
Vincent et al.[62]	8	Ge/Si(001)	AP-CVD	320	40	~ 600	micro-Hall	GeSn *in-situ* doped with B to $p = 2 \times 10^{17}$ cm⁻³.
Nakatsuka et al.[447]	0–5.8	SOI	MBE	200	160–170	Before/After PDA: Pure Ge: ~ 90/~ 150 $x_{Sn} = 2.0\%$: ~ 170/~ 290 $x_{Sn} = 4.0\%$: ~ 120/~ 260 $x_{Sn} = 5.8\%$: ~ 110/~ 150	Hall VdP	PDA: 500 °C for 1 h in N₂. Clear improvement in μ_h after PDA. Impurity band induces parallel conduction. Authors present also higher μ_h values removing the contribution of the parallel conduction layer.

increasing Ge film thickness.[170] As a consequence, the hole mobility has been found to increase with film thickness,[281,469] as shown in Fig. 9(a), reprinted from Ref. 281. High-temperature processing of Ge films has also been proven to be beneficial in terms of hole mobility, thanks to the associated reduction of defect density in the material. Upon annealing, a significant increase in Ge μ_h beyond 1000 cm²/Vs was observed.[281,310,469] A record $\mu_h = 1252$ cm²/Vs, not far from the material bulk mobility, was measured at room temperature in annealed 500-nm-thick MBE Ge by Wei et al.[310]

The temperature dependence of μ_h in Ge has been investigated in a few studies.[281,310,446] An example of such behavior is reported in Fig. 9(c), reprinted from Ref. 281, where μ_h in as-grown Ge is plotted with filled, orange dots. All Ge films investigated in the literature showed a similar temperature dependence. As the measurement temperature was decreased from 300 K, μ_h initially increased due to the reduction of phonon scattering, but below a threshold T μ_h started decreasing as a consequence of stronger ionized defect scattering.[281] The threshold T reported in the cited studies varied between 80 and 300 K and was dependent on the material quality. In particular, it was found to decrease after PDA of Ge,[281,310] as visible in Fig. 9(c), suggesting a decrease in ionized defects after annealing, possibly associated with the reduction in TDD.

2. Mobility in GeSn

For the GeSn alloy, the electron mobility (μ_e) is predicted to be higher than that of pure Ge. This is a consequence of an increase in carrier population of the Γ valley in the CB of GeSn. Conversely, when solely considering the band structures, no significant change in μ_h is anticipated.[15] Nevertheless, alloy scattering is expected to contribute to a decrease in μ_h compared to Ge.[15,370] In the literature, the reported values of room-temperature μ_h in GeSn span from 100 to 600 cm²/Vs,[18,62,370,430,431,446,447,470,471] similarly to as-grown Ge. The influence of GeSn alloy composition on experimental values of μ_h is still unclear. Two studies, by Schulte-Braucks et al.[446] and Nakatsuka et al.,[447] measured μ_h in function of alloy composition in GeSn films grown keeping all other growth parameters constant. However, these reports present somewhat contrasting results. In Ref. 447, the room-temperature μ_h decreased with higher Sn content (Sn at. %: 2.0–5.8), but did not follow a clear trend at cryogenic temperatures. In this study, the Ge μ_h was lower than for GeSn from room T down to cryogenic temperatures. On the other hand, in Ref. 446, μ_h decreased with higher Sn content (Sn at. %: 8.5–12.5) across a large temperature window from room T down to 80 K. The Ge μ_h was comparable to GeSn at room T, but considerably higher at cryogenic temperatures. These results may suggest that larger Sn contents lead to enhanced impurity

04 January 2025 10:11:00

and defect scattering, similarly to what is found with carrier lifetime measurements described in Sec. VII D. Additional studies are required to support this hypothesis. Furthermore, an accurate determination of the contribution of alloy scattering to μ_h in GeSn is yet to be achieved.

To improve the GeSn mobility, a few techniques have been reported in the literature. Nakatsuka *et al.*[447] obtained a noticeable increase in μ_h by a PDA process for GeSn with Sn content 0–5.8 at. %. An annealing of $500\,^\circ$C for 1 h in N_2 led to an almost twofold improvement in mobility across the range of studied compositions, likely due to a reduction in the material defect density. For thin GeSn films, of the order of a few nm to a few tens of nm, surface passivation by a 1-nm-thick Ge layer has been proven effective in enhancing the film μ_h.[18] The Ge layer confines charge carriers within the GeSn film, reducing carrier surface scattering. Alternatively, a Si passivation layer has also be employed for improved carrier confinement[472] at the expenses of a more complex epitaxial growth.

Finally, concerning the dependency of GeSn μ_h on temperature, a behavior analogous to Ge has been reported in the literature.[430,446,447] As the measurement T is decreased from 300 K down to a threshold T, μ_h increases as a result of reduced phonon scattering. The threshold T has been most frequently measured to be between 100 and 200 K and is dependent on the growth conditions and composition of the GeSn film. Below this T, ionized defect scattering starts dominating, causing a decrease in μ_h with decreasing T, as shown in the Hall measurements of a Ge film shown in Fig. 9(c).

VIII. CONCLUSION

Over the last 15 years, GeSn has showcased its potential across a range of optoelectronic devices including photodetectors, LEDs and lasers, showing its promise for applications in the SWIR and MWIR domains. However, despite significant performance improvements, no GeSn-based device has yet made it to commercialization. The current bottleneck in device performance lies in the incomplete understanding of material defects and their associated trap states. This deficiency ultimately results in a lack of precise control over device properties. With this review, we provided a perspective and critical view on how the material defects impact the optoelectronic properties, ranging from light absorption to electronic transport and unintentional doping.

The electrical properties of GeSn depend on the microstructure and order at the atomic scale, and, in particular, on the material defects. Typical defects in the GeSn crystal structure are dislocations and point defects. Dislocations originate from the lattice mismatch with the substrate, while point defects form due to impurities and low-temperature, out-of-equilibrium growth. The defect density is determined by the epitaxial growth conditions and post-deposition thermal treatments. Dislocations and point defects in Ge and GeSn are predominantly electrically active, as they are source of shallow and deep traps in the bandgap. Additional traps are induced by impurities. These traps affect the material carrier lifetime, mobility, and unintentional doping concentration. Consequently, pinpointing the origin of each trap is pivotal for controlling electrical properties. However, this task is complex due to the simultaneous presence of multiple defects in the material. For instance, to the best of our knowledge, there has been no investigation differentiating the trap states associated with threading or misfit dislocations. This distinction is crucial for managing the electrical properties of annealed Ge, where the density of threading dislocations is reduced while that of misfit dislocations is increased. To precisely identify the defect responsible for the most common traps, it

is imperative to utilize the purest materials available, and work in a synergy between computations and experiments.

The literature evidenced a general lack of agreement regarding the source of shallow trap states responsible for the high unintentional doping concentrations in Ge and GeSn. Ge films have been reported to show both *n*-type and *p*-type unintentional doping, while GeSn is predominantly *p*-type. Given the latter, shallow traps responsible for *p*-type unintentional doping in GeSn are likely to be associated with the presence of Sn or to the lower growth temperatures employed with respect to Ge. While shallow traps are generally attributed to vacancy complexes, in fact, threading dislocations have also been reported to induce shallow trap levels. A systematic study of unintentional doping concentrations in pseudomorphic GeSn—i.e., free of dislocations—grown on Ge(001) may allow to rule out the latter. On a different line, thermal treatment of Ge films has evidenced a non-linear variation in unintentional doping, which led in some cases to an increase in unintentional doping upon annealing. This phenomenon is presently not understood and may be owed to point defect evolution and/or formation of misfit dislocations.

Threading dislocations have been demonstrated to affect negatively the Ge/GeSn carrier lifetime, through SRH recombination mechanisms associated with deep traps. Similarly, increasing Sn composition has also been associated with reduced carrier lifetimes. We speculate this is owed to an increase in vacancy complexes associated with the larger Sn contents. However, this hypothesis remains to be proven.

In conclusion, it is important to emphasize that both point defects and dislocations have been linked to the formation of shallow and deep traps, consequently impacting the material's carrier lifetime and unintentional doping concentrations. While trap levels in Ge have been relatively well examined in the past, defects and traps specific to GeSn remain largely unexplored. A deeper understanding of these aspects could facilitate a greater degree of control of the material's electrical properties, thereby enabling the integration of GeSn into commercial devices.

Overall, this review provides the base to understand the state-of-the-art and challenges of GeSn as an optoelectronically grade semiconductor. It also provides a critical view on where the field may evolve so that the semiconductor reaches the optoelectronics market.

AUTHOR DECLARATIONS
Conflict of Interest

The authors have no conflicts to disclose.

Author Contributions

Andrea Giunto: Conceptualization (lead); Writing – original draft (lead); Writing – review & editing (lead). **Anna Fontcuberta i Morral:** Funding acquisition (lead); Writing – original draft (supporting); Writing – review & editing (supporting).

04 January 2025 10:11:00

DATA AVAILABILITY

Data sharing is not applicable to this article as no new data were created or analyzed in this study.

REFERENCES

[1]O. Moutanabbir, S. Assali, X. Gong, E. O'Reilly, C. A. Broderick, B. Marzban, J. Witzens, W. Du, S.-Q. Yu, A. Chelnokov, D. Buca, and D. Nam, "Monolithic infrared silicon photonics: The rise of (Si)GeSn semiconductors," Appl. Phys. Lett. **118**, 110502 (2021).

[2]S. A. Ghetmiri, W. Du, J. Margetis, A. Mosleh, L. Cousar, B. R. Conley, L. Domulevicz, A. Nazzal, G. Sun, R. A. Soref, J. Tolle, B. Li, H. A. Naseem, and S. Q. Yu, "Direct-bandgap GeSn grown silicon with 2230 nm photoluminescence," Appl. Phys. Lett. **105**, 151109 (2014).

[3]J. D. Gallagher, C. L. Senaratne, J. Kouvetakis, and J. Menéndez, "Compositional dependence of the bowing parameter for the direct and indirect band gaps in Ge$_{1-y}$Sn$_y$ alloys," Appl. Phys. Lett. **105**, 142102 (2014).

[4]S. Wirths, R. Geiger, N. von den Driesch, G. Mussler, T. Stoica, S. Mantl, Z. Ikonic, M. Luysberg, S. Chiussi, J. M. Hartmann, H. Sigg, J. Faist, D. Buca, and D. Grützmacher, "Lasing in direct-bandgap GeSn alloy grown on Si," Nat. Photonics **9**, 88 (2015).

[5]M. R. Atalla, C. Lemieux-Leduc, S. Assali, S. Koelling, P. Daoust, and O. Moutanabbir, "Extended short-wave infrared high-speed all-GeSn PIN photodetectors on silicon," APL Photonics **9**, 056103 (2024).

[6]E. Talamas Simola, V. Kiyek, A. Ballabio, V. Schlykow, J. Frigerio, C. Zucchetti, A. De Iacovo, L. Colace, Y. Yamamoto, G. Capellini, D. Grützmacher, D. Buca, and G. Isella, "CMOS-compatible bias-tunable dual-band detector based on GeSn/Ge/Si coupled photodiodes," ACS Photonics **8**, 2166 (2021).

[7]H. Tran, T. Pham, J. Margetis, Y. Zhou, W. Dou, P. C. Grant, J. M. Grant, S. Al-Kabi, G. Sun, R. A. Soref, J. Tolle, Y.-H. Zhang, W. Du, B. Li, M. Mortazavi, and S.-Q. Yu, "Si-based GeSn photodetectors toward mid-infrared imaging applications," ACS Photonics **6**, 2807 (2019).

[8]D. Zhang, X. Hu, D. Liu, X. Lin, W. Wang, Z. Ding, Z. Wang, B. Cheng, and C. Xue, "GeSn on Si avalanche photodiodes for short wave infrared detection," Proc. SPIE **10846**, 108461B (2018).

[9]Y. Kim, S. Assali, D. Burt, Y. Jung, H.-J. Joo, M. Chen, Z. Ikonic, O. Moutanabbir, and D. Nam, "Improved GeSn microdisk lasers directly sitting on Si," Proc. SPIE **12006**, 120060M (2022).

[10]S. Ojo, Y. Zhou, S. Acharya, N. Saunders, S. Amoah, Y.-T. Jheng, H. Tran, W. Du, G.-E. Chang, B. Li, and S.-Q. Yu, "Silicon-based electrically injected GeSn lasers," Proc. SPIE **11995**, 119950B (2022).

[11]B. Marzban, L. Seidel, T. Liu, K. Wu, V. Kiyek, M. H. Zoellner, Z. Ikonic, J. Schulze, D. Grützmacher, G. Capellini, M. Oehme, J. Witzens, and D. Buca, "Strain engineered electrically pumped SiGeSn microring lasers on Si," ACS Photonics **10**, 217 (2023).

[12]C. Cardoux, L. Casiez, N. Pauc, V. Calvo, N. Coudurier, P. Rodriguez, J. Richy, P. Barritault, O. Lartigue, C. Constancias, M. Frauenrath, J.-M. Hartmann, A. Chelnokov, O. Gravrand, and V. Reboud, "Room temperature spectral characterization of direct band gap Ge$_{0.85}$Sn$_{0.15}$ LEDs and photodiodes," Proc. SPIE **12006**, 120060A (2022).

[13]B.-J. Huang, C.-Y. Chang, Y.-D. Hsieh, R. A. Soref, G. Sun, H.-H. Cheng, and G.-E. Chang, "Electrically injected GeSn vertical-cavity surface emitters on silicon-on-insulator platforms," ACS Photonics **6**, 1931 (2019).

[14]C. Chang, T. Chang, H. Li, H. H. Cheng, R. Soref, G. Sun, and J. R. Hendrickson, "Room-temperature 2-μm GeSn P-I-N homojunction light-emitting diode for inplane coupling to group-IV waveguides," Appl. Phys. Lett. **111**, 141105 (2017).

[15]J. D. Sau and M. L. Cohen, "Possibility of increased mobility in Ge-Sn alloy system," Phys. Rev. B **75**, 045208 (2007).

[16]S. Mukhopadhyay, B. Mukhopadhyay, G. Sen, and P. K. Basu, "Maximum theoretical electron mobility in n-type Ge$_{1-x}$Sn$_x$ due to minimum doping requirement set by intrinsic carrier density," J. Comput. Electron. **20**, 274 (2021).

[17]M. Liu, K. Mertens, N. von den Driesch, V. Schlykow, T. Grap, F. Lentz, S. Trellenkamp, J. Hartmann, J. Knoch, D. Buca, and Q. Zhao, "Vertical heterojunction Ge$_{0.92}$Sn$_{0.08}$/Ge gate-all-around nanowire pMOSFETs with NiGeSn contact," Solid-State Electron. **168**, 107716 (2020).

[18]Y.-S. Huang, Y. Tsou, C.-H. Huang, C.-H. Huang, H. Lan, C. W. Liu, Y.-C. Huang, H. Chung, C.-P. Chang, S. S. Chu, and S. Kuppurao, "High-mobility CVD-grown Ge/strained Ge$_{0.9}$Sn$_{0.1}$/Ge quantum-well pMOSFETs on Si by optimizing Ge cap thickness," IEEE Trans. Electron Devices **64**, 2498 (2017).

[19]W. Wang, D. Lei, Y.-C. Huang, K. H. Lee, W.-K. Loke, Y. Dong, S. Xu, C. S. Tan, H. Wang, S.-F. Yoon, X. Gong, and Y.-C. Yeo, "High-performance GeSn photodetector and fin field-effect transistor (FinFET) on an advanced GeSn-on-insulator platform," Opt. Express **26**, 10305 (2018).

[20]A. Portavoce, H. Khelidj, N. Oueldna, S. Amhil, M. Bertoglio, D. Mangelinck, L. Essaleh, and K. Hoummada, "Thermoelectric power factor of Ge$_{1-x}$Sn$_x$ thin films," Materialia **14**, 100873 (2020).

[21]D. Spirito, N. von den Driesch, C. L. Manganelli, M. H. Zoellner, A. A. Corley-Wiciak, Z. Ikonic, T. Stoica, D. Grützmacher, D. Buca, and G. Capellini, "Thermoelectric efficiency of epitaxial GeSn alloys for integrated Si-based applications: Assessing the lattice thermal conductivity by raman thermometry," ACS Appl. Energy Mater. **4**, 7385 (2021).

[22]C. Goodman, "Direct-gap group IV semiconductors based on tin," IEE Proc. I **129**, 189 (1982).

[23]F. A. Trumbore, "Solid solubilities and electrical properties of tin in germanium single crystals," J. Electrochem. Soc. **103**, 597 (1956).

[24]R. W. Olesinski and G. J. Abbaschian, "The Ge-Sn (Germanium-Tin) system," Bull. Alloy Phase Diagrams **5**, 265 (1984).

[25]S. Oguz, W. Paul, T. F. Deutsch, B. Tsaur, and D. V. Murphy, "Synthesis of metastable, semiconducting Ge–Sn alloys by pulsed UV laser crystallization," Appl. Phys. Lett. **43**, 848 (1983).

[26]S. Shah, J. Greene, L. Abels, Q. Yao, and P. Raccah, "Growth of single-crystal metastable Ge$_{1-x}$Sn$_x$ alloys on Ge(100) and GaAs(100) substrates," J. Cryst. Growth **83**, 3 (1987).

[27]Scopus Analytics (2024), http://www.scopus.com (last accessed April 2024).

[28]G. He and H. A. Atwater, "Synthesis of epitaxial Sn$_x$Ge$_{1-x}$ alloy films by ion-assisted molecular beam epitaxy," Nucl. Instrum. Methods Phys. Res. Sect. B **106**, 126 (1995).

[29]R. Soref, J. Kouvetakis, and J. Menendez, "Advances in SiGeSn/Ge technology," MRS Proc. **958**, 108 (2006).

[30]J. Mathews, R. Roucka, J. Xie, S.-Q. Yu, J. Menéndez, and J. Kouvetakis, "Extended performance GeSn/Si(100) p-i-n photodetectors for full spectral range telecommunication applications," Appl. Phys. Lett. **95**, 133506 (2009).

[31]P. R. Pukite, A. Harwit, and S. S. Iyer, "Molecular beam epitaxy of metastable, diamond structure Sn$_x$Ge$_{1-x}$ alloys," Appl. Phys. Lett. **54**, 2142 (1989).

[32]H. Gossmann, "Determination of critical layer thicknesses in IV–IV-alloy systems using reflection high energy electron diffraction intensity oscillations: Ge (100)/Ge$_x$Sn$_{1-x}$," J. Appl. Phys. **68**, 2791 (1990).

[33]A. Harwit, P. R. Pukite, J. Angilello, and S. S. Iyer, "Properties of diamond structure SnGe films grown by molecular beam epitaxy," Thin Solid Films **184**, 395 (1990).

[34]W. Wegscheider, J. Olajos, U. Menczigar, W. Dondl, and G. Abstreiter, "Fabrication and properties of epitaxially stabilized Ge/α-Sn heterostructures on Ge(001)," J. Cryst. Growth **123**, 75 (1992).

[35]P. Desjardins, T. Spila, O. Gürdal, N. Taylor, and J. E. Greene, "Hybrid surface roughening modes during low-temperature heteroepitaxy: Growth of fully-strained metastable Ge$_{1-x}$Sn$_x$ alloys on Ge(001)2 × 1," Phys. Rev. B **60**, 15993 (1999).

[36]O. Gurdal, M. A. Hasan, M. R. Sardela, J. E. Greene, H. H. Radamson, J. E. Sundgren, and G. V. Hansson, "Growth of metastable Ge$_{1-x}$Sn$_x$/Ge strained layer superlattices on Ge(001)2 × 1 by temperature-modulated molecular beam epitaxy," Appl. Phys. Lett. **67**, 956 (1995).

[37]O. Gurdal, P. Desjardins, J. R. Carlsson, N. Taylor, H. H. Radamson, J. E. Sundgren, and J. E. Greene, "Low-temperature growth and critical epitaxial thicknesses of fully strained metastable Ge$_{1-x}$Sn$_x$(x ≤ 0.26) alloys on Ge(001) 2 × 1," J. Appl. Phys. **83**, 162 (1998).

[38]K. A. Bratland, Y. L. Foo, T. Spila, H.-S. Seo, R. T. Haasch, P. Desjardins, and J. E. Greene, "Sn-mediated Ge/Ge(001) growth by low-temperature molecular-beam epitaxy: Surface smoothening and enhanced epitaxial thickness," J. Appl. Phys. **97**, 044904 (2005).

[39]G. He and H. A. Atwater, "Synthesis of epitaxial Sn$_x$Ge$_{1-x}$ alloy films by ion-assisted molecular beam epitaxy," Appl. Phys. Lett. **68**, 664 (1996).

04 January 2025 10:11:00

[40]R. Ragan and H. A. Atwater, "Measurement of the direct energy gap of coherently strained Sn$_x$Ge$_{1-x}$/Ge(001) heterostructures," Appl. Phys. Lett. **77**, 3418 (2000).

[41]G. He and H. A. Atwater, "Interband transitions in Sn$_x$Ge$_{1-x}$ Alloys," Phys. Rev. Lett. **79**, 1937 (1997).

[42]D. W. Jenkins and J. D. Dow, "Electronic properties of metastable GeSn alloys," Phys. Rev. B **36**, 7994 (1987).

[43]Y. Chibane, B. Bouhafs, and M. Ferhat, "Unusual structural and electronic properties of Sn$_x$Ge$_{1-x}$ alloys," Phys. Status Solidi B **240**, 116 (2003).

[44]V. R. D'Costa, C. S. Cook, A. G. Birdwell, C. L. Littler, M. Canonico, S. Zollner, J. Kouvetakis, and J. Menéndez, "Optical critical points of thin-film Ge$_{1-y}$Sn$_y$ alloys: A comparative Ge$_{1-y}$Sn$_y$/Ge$_{1-x}$Si$_x$ study," Phys. Rev. B **73**, 125207 (2006).

[45]W. J. Yin, X. G. Gong, and S. H. Wei, "Origin of the unusually large band-gap bowing and the breakdown of the band-edge distribution rule in the Sn$_x$Ge$_{1-x}$ alloys," Phys. Rev. B **78**, 161203 (2008).

[46]H. P. Perez Ladron de Guevara, A. G. Rodr iiguez, H. Navarro-Contreras, and M. A. Vidal, "Ge$_{1-x}$Sn$_x$ alloys pseudomorphically grown on Ge(001)," Appl. Phys. Lett. **83**, 4942 (2003).

[47]H. P. Ladron de Guevara, A. G. Rodr iiguez, H. Navarro-Contreras, and M. A. Vidal, "Determination of the optical energy gap of Ge$_{1-x}$Sn$_x$ alloys with 0<x<0.14," Appl. Phys. Lett. **84**, 4532 (2004).

[48]J. Taraci, S. Zollner, M. R. McCartney, J. Menendez, M. A. Santana-Aranda, D. J. Smith, A. Haaland, A. V. Tutukin, G. Gundersen, G. Wolf, and J. Kouvetakis, "Synthesis of silicon-based infrared semiconductors in the Ge-Sn system using molecular chemistry methods," J. Am. Chem. Soc. **123**, 10980 (2001).

[49]M. Bauer, J. Taraci, J. Tolle, A. V. Chizmeshya, S. Zollner, D. J. Smith, J. Menendez, C. Hu, and J. Kouvetakis, "Ge-Sn semiconductors for band-gap and lattice engineering," Appl. Phys. Lett. **81**, 2992 (2002).

[50]M. R. Bauer, C. S. Cook, P. Aella, J. Tolle, J. Kouvetakis, P. A. Crozier, A. V. Chizmeshya, D. J. Smith, and S. Zollner, "SnGe superstructure materials for Si-based infrared optoelectronics," Appl. Phys. Lett. **83**, 3489 (2003).

[51]M. Bauer, C. Ritter, P. A. Crozier, J. Ren, J. Menendez, G. Wolf, and J. Kouvetakis, "Synthesis of ternary SiGeSn semiconductors on Si(100) via Sn$_x$Ge$_{1-x}$ buffer layers," Appl. Phys. Lett. **83**, 2163 (2003).

[52]S. Wirths, D. Buca, and S. Mantl, "Si–Ge–Sn alloys: From growth to applications," Prog. Cryst. Growth Charact. Mater. **62**(1), 1–39 (2016).

[53]M. Yamazaki, S. Takeuchi, O. Nakatsuka, A. Sakai, M. Ogawa, and S. Zaima, "Scanning tunneling microscopy observation of initial growth of Sn and Ge$_{1-x}$Sn$_x$ layers on Ge(0 0 1) substrates," Appl. Surf. Sci. **254**, 6048 (2008).

[54]S. Takeuchi, Y. Shimura, O. Nakatsuka, S. Zaima, M. Ogawa, and A. Sakai, "Growth of highly strain-relaxed Ge$_{1-x}$Sn$_x$/virtual Ge by a Sn precipitation controlled compositionally step-graded method," Appl. Phys. Lett. **92**, 231916 (2008).

[55]S. Gupta, B. Magyari-Köpe, Y. Nishi, and K. C. Saraswat, "Achieving direct band gap in germanium through integration of Sn alloying and external strain," J. Appl. Phys. **113**, 073707 (2013).

[56]A. V. G. Chizmeshya, C. Ritter, J. Tolle, C. Cook, J. Menéndez, and J. Kouvetakis, "Fundamental Studies of P(GeH$_3$)$_3$, As(GeH$_3$)$_3$, and Sb(GeH$_3$)$_3$: Practical n-dopants for new group IV semiconductors," Chem. Mater. **18**, 6266 (2006).

[57]S. Su, B. Cheng, C. Xue, W. Wang, Q. Cao, H. Xue, W. Hu, G. Zhang, Y. Zuo, and Q. Wang, "GeSn p-i-n photodetector for all telecommunication bands detection," Opt. Express **19**, 6400 (2011).

[58]G. Han, S. Su, C. Zhan, Q. Zhou, Y. Yang, L. Wang, P. Guo, W. Wei, C. P. Wong, Z. X. Shen, B. Cheng, and Y. C. Yeo, "High-mobility germanium-tin (GeSn) P-channel MOSFETs featuring metallic source/drain and sub-370 °C process modules," in *Technical Digest - International Electron Devices Meeting (IEDM)* (IEEE, 2011), p. 402.

[59]S. Gupta, R. Chen, B. Magyari-Kope, H. Lin, B. Yang, A. Nainani, Y. Nishi, J. S. Harris, and K. C. Saraswat, "GeSn technology: Extending the Ge electronics roadmap," in *International Electron Devices Meeting* (IEEE, 2011), pp. 16.6.1–16.6.4.

[60]M. Oehme, J. Werner, M. Gollhofer, M. Schmid, M. Kaschel, E. Kasper, and J. Schulze, "Room-temperature electroluminescence from GeSn light-emitting pin diodes on Si," IEEE Photonics Technol. Lett. **23**, 1751 (2011).

[61]R. Roucka, J. Mathews, R. T. Beeler, J. Tolle, J. Kouvetakis, and J. Menéndez, "Direct gap electroluminescence from Si/Ge$_{1-y}$Sn$_y$ p-i-n heterostructure diodes," Appl. Phys. Lett. **98**, 061109 (2011).

[62]B. Vincent, F. Gencarelli, H. Bender, C. Merckling, B. Douhard, D. H. Petersen, O. Hansen, H. H. Henrichsen, J. Meersschaut, W. Vandervorst, M. Heyns, R. Loo, and M. Caymax, "Undoped and in-situ B doped GeSn epitaxial growth on Ge by atmospheric pressure-chemical vapor deposition," Appl. Phys. Lett. **99**, 152103 (2011).

[63]S. Wirths, D. Buca, A. T. Tiedemann, B. Hollander, P. Bernardy, T. Stoica, D. Grutzmacher, and S. Mantl, "Epitaxial growth of Ge$_{1-x}$Sn$_x$ by reduced pressure CVD using SnCl$_4$ and Ge$_2$H$_6$," ECS Trans. **50**, 885 (2013).

[64]R. Soref, "Mid-infrared photonics in silicon and germanium," Nat. Photonics **4**, 495 (2010).

[65]Y. Zhou, Y. Miao, S. Ojo, H. Tran, G. Abernathy, J. M. Grant, S. Amoah, G. Salamo, W. Du, J. Liu, J. Margetis, J. Tolle, Y. Zhang, G. Sun, R. A. Soref, B. Li, and S.-Q. Yu, "Electrically injected GeSn lasers on Si operating up to 100 K," Optica **7**, 924 (2020).

[66]D. Buca, A. Bjelajac, D. Spirito, O. Concepción, M. Gromovyi, E. Sakat, X. Lafosse, L. Ferlazzo, N. von den Driesch, Z. Ikonic, D. Grützmacher, G. Capellini, and M. El Kurdi, "Room temperature lasing in GeSn microdisks enabled by strain engineering," Adv. Opt. Mater. **10**, 2201024 (2022).

[67]B. Marzban, L. Seidel, V. Kiyek, T. Liu, M. Zöllner, Z. Ikonic, G. Capellini, D. Buca, J. Schulze, M. Oehme, and J. Witzens, "Modeling and design of an electrically pumped SiGeSn microring laser," Proc. SPIE **12006**, 120060K (2022).

[68]A. Elbaz, R. Arefin, E. Sakat, B. Wang, E. Herth, G. Patriarche, A. Foti, R. Ossikovski, S. Sauvage, X. Checoury, K. Pantzas, I. Sagnes, J. Chrétien, L. Casiez, M. Bertrand, V. Calvo, N. Pauc, A. Chelnokov, P. Boucaud, F. Boeuf, V. Reboud, J.-M. Hartmann, and M. El Kurdi, "Reduced lasing thresholds in GeSn microdisk cavities with defect management of the optically active region," ACS Photonics **7**, 2713 (2020).

[69]Q. M. Thai, N. Pauc, J. Aubin, M. Bertrand, J. Chrétien, V. Delaye, A. Chelnokov, J.-M. Hartmann, V. Reboud, and V. Calvo, "GeSn heterostructure micro-disk laser operating at 230 K," Opt. Express **26**, 32500 (2018).

[70]B. Marzban, D. Stange, D. Rainko, Z. Ikonic, D. Buca, and J. Witzens, "Modeling of a SiGeSn quantum well laser," Photonics Res. **9**, 1234 (2021).

[71]Y. Dong, W. Wang, D. Lei, X. Gong, Q. Zhou, S. Y. Lee, W. K. Loke, S.-F. Yoon, E. S. Tok, G. Liang, and Y.-C. Yeo, "Suppression of dark current in germanium-tin on silicon p-i-n photodiode by a silicon surface passivation technique," Opt. Express **23**, 18611 (2015).

[72]S. Gupta, E. Simoen, R. Loo, O. Madia, D. Lin, C. Merckling, Y. Shimura, T. Conard, J. Lauwaert, H. Vrielinck, and M. Heyns, "Density and capture cross-section of interface traps in GeSnO$_2$ and GeO$_2$ grown on heteroepitaxial GeSn," ACS Appl. Mater. Interfaces **8**, 13181 (2016).

[73]M. Morea, C. E. Brendel, K. Zang, J. Suh, C. S. Fenrich, Y. C. Huang, H. Chung, Y. Huo, T. I. Kamins, K. C. Saraswat, and J. S. Harris, "Passivation of multiple-quantum-well Ge$_{0.97}$Sn$_{0.03}$/Ge p-i-n photodetectors," Appl. Phys. Lett. **110**, 091109 (2017).

[74]D. Stange, N. von den Driesch, T. Zabel, F. Armand-Pilon, D. Rainko, B. Marzban, P. Zaumseil, J.-M. Hartmann, Z. Ikonic, G. Capellini, S. Mantl, H. Sigg, J. Witzens, D. Grützmacher, and D. Buca, "GeSn/SiGeSn heterostructure and multi quantum well lasers," ACS Photonics **5**, 4628 (2018).

[75]Q. Chen, J. Jung, H. Zhou, S. Wu, X. Gong, Y. Huang, K. H. Lee, L. Zhang, D. Nam, J. Liu, J. Luo, W. Fan, and C. S. Tan, "GeSn/Ge multiquantum-well vertical-cavity surface-emitting p-i-n structures and diode emitters on a 200 mm Ge-on-insulator platform," ACS Photonics **10**, 1716 (2023).

[76]S. Xu, W. Wang, Y.-C. Huang, Y. Dong, S. Masudy-Panah, H. Wang, X. Gong, and Y.-C. Yeo, "High-speed photo detection at two-micron-wavelength: Technology enablement by GeSn/Ge multiple-quantum-well photodiode on 300 mm Si substrate," Opt. Express **27**, 5798 (2019).

[77]M. R. M. Atalla, S. Assali, S. Koelling, A. Attiaoui, and O. Moutanabbir, "High-bandwidth extended-SWIR GeSn photodetectors on silicon achieving ultrafast broadband spectroscopic response," ACS Photonics **9**, 1425 (2022).

[78]Y. Dong, W. Wang, S. Y. Lee, D. Lei, X. Gong, W. K. Loke, S.-F. Yoon, G. Liang, and Y.-C. Yeo, "Germanium-tin multiple quantum well on silicon avalanche photodiode for photodetection at two micron wavelength," Semicond. Sci. Technol. **31**, 095001 (2016).

04 January 2025 10:11:00

[79]M. Wanitzek, M. Oehme, C. Spieth, D. Schwarz, L. Seidel, and J. Schulze, "GeSn-on-Si avalanche photodiodes for short-wave infrared detection," in *IEEE 48th European Solid State Circuits Conference (ESSCIRC)* (IEEE, 2022), pp. 169–172.

[80]J. Zheng, L. Li, T. Zhou, Y. Zuo, C. Li, B. Cheng, and Q. Wang, "Growth of crystalline Ge$_{1-x}$Sn$_x$ films on Si (100) by magnetron sputtering," ECS Solid State Lett. **3**, P111 (2014).

[81]G. Chen, Y. Yu, Y. Shi, N. Li, W. Luo, L. Cao, A. J. Danner, A. Liu, and X. Zhang, "High–speed photodetectors on silicon photonics platform for optical interconnect," Laser Photonics Rev. **16**, 2200117 (2022).

[82]H. Zhou, S. Xu, Y. Lin, Y.-C. Huang, B. Son, Q. Chen, X. Guo, K. H. Lee, S. C.-K. Goh, X. Gong, and C. S. Tan, "High-efficiency GeSn/Ge multiple-quantum-well photodetectors with photon-trapping microstructures operating at 2 μm," Opt. Express **28**, 10280 (2020).

[83]H. Wang, J. Zhang, G. Zhang, Y. Chen, Y.-C. Huang, and X. Gong, "High-speed and high-responsivity p-i-n waveguide photodetector at a 2 μm wavelength with a Ge$_{0.92}$Sn$_{0.08}$/Ge multiple-quantum-well active layer," Opt. Lett. **46**, 2099 (2021).

[84]X. Li, L. Peng, Z. Liu, Z. Zhou, J. Zheng, C. Xue, Y. Zuo, B. Chen, and B. Cheng, "30 GHz GeSn photodetector on SOI substrate for 2 μm wavelength application," Photonics Res. **9**, 494 (2021).

[85]C.-H. Tsai, B.-J. Huang, R. A. Soref, G. Sun, H. H. Cheng, and G.-E. Chang, "GeSn resonant-cavity-enhanced photodetectors for efficient photodetection at the μm wavelength band," Opt. Lett. **45**, 1463 (2020).

[86]Y.-H. Huang, G.-E. Chang, H. Li, and H. H. Cheng, "Sn-based waveguide p-i-n photodetector with strained GeSn/Ge multiple-quantum-well active layer," Opt. Lett. **42**, 1652 (2017).

[87]M. R. M. Atalla, S. Assali, S. Koelling, A. Attiaoui, and O. Moutanabbir, "Dark current in monolithic extended-SWIR GeSn PIN photodetectors," Appl. Phys. Lett. **122**, 031103 (2023).

[88]G.-E. Chang, S.-Q. Yu, J. Liu, H.-H. Cheng, R. A. Soref, and G. Sun, "Achievable performance of uncooled homojunction GeSn mid-infrared photodetectors," IEEE J. Select. Top. Quantum Electron. **28**, 3800611 (2022).

[89]L. Luo, M. R. M. Atalla, S. Assali, S. Koelling, G. Daligou, and O. Moutanabbir, "Mid-infrared imaging using strain-relaxed Ge$_{1-x}$Sn$_x$ alloys grown on 20 nm Ge nanowires," Nano Lett. **24**, 4979 (2024).

[90]S. Ghosh, R. Bansal, G. Sun, R. A. Soref, H.-H. Cheng, and G.-E. Chang, "Design and optimization of GeSn waveguide photodetectors for 2-μm band silicon photonics," Sensors **22**, 3978 (2022).

[91]C.-H. Liu, R. Bansal, C.-W. Wu, Y.-T. Jheng, and G.-E. Chang, "GeSn waveguide photodetectors with vertical p–i–n heterostructure for integrated photonics in the 2 μm wavelength band," Adv. Photonics Res. **3**, 2100330 (2022).

[92]C.-H. Tsai, K.-C. Lin, C.-Y. Cheng, K.-C. Lee, H. H. Cheng, and G.-E. Chang, "GeSn lateral p-i-n waveguide photodetectors for mid-infrared integrated photonics," Opt. Lett. **46**, 864 (2021).

[93]C. Li, X. Gao, K. Guan, W. Li, Z. Ma, G. Xu, Z. Li, S. Yang, N. Wang, and C. Xue, "Influence of photonic crystals on the performance parameters of GeSn vertical-structure photodiodes," Opt. Laser Technol. **163**, 109375 (2023).

[94]J. Rudie, S. Amoah, X. Wang, R. Kumar, G. Abernathy, S. Akwabli, P. C. Grant, J. Liu, B. Li, W. Du, and S.-Q. Yu, "Monolithic germanium tin on Si avalanche photodiodes," arXiv:2405.13761 (2024).

[95]R. A. Soref, F. De Leonardis, and V. M. Passaro, "Simulations of nanoscale room temperature waveguide-coupled single-photon avalanche detectors for silicon photonic sensing and quantum applications," ACS Appl. Nano Mater. **2**, 7503 (2019).

[96]Q. Chen, S. Wu, L. Zhang, W. Fan, and C. S. Tan, "Simulation of high-efficiency resonant-cavity-enhanced GeSn single-photon avalanche photodiodes for sensing and optical quantum applications," IEEE Sens. J. **21**, 14789 (2021).

[97]A. Giunto, "GeSn as next-generation material for short-wave infrared single-photon detection," Ph.D. thesis (EPFL, 2023).

[98]M. Wanitzek, M. Hack, D. Schwarz, J. Schulze, and M. Oehme, "Low-temperature performance of GeSn-on-Si avalanche photodiodes toward single-photon detection," Mater. Sci. Semicond. Process. **176**, 108303 (2024).

[99]V. Reboud, D. Buca, H. Sigg, J. M. Hartmann, N. Pauc, V. Calvo, P. Rodriguez, and A. Chelnokov, "Lasing in group-IV materials," in *Topics in Applied Physics*, edited by D. Lockwood and L. Pavesi (Springer, Cham, 2021), Vol. 139, pp. 105–195.

[100]L. Casiez, M. Bertrand, J. Chretien, A. Quintero, Q. M. Thai, M. Frauenrath, O. Lartigue, P. Barritault, N. Bernier, P. Rodriguez, A. Chelnokov, J. M. Hartmann, N. Pauc, V. Calvo, and V. Reboud, "GeSn heterostructures LEDs for gas detection," in *IEEE Photonics Conference (IPC 2020)* (IEEE, 2020).

[101]D. Stange, N. von den Driesch, D. Rainko, S. Roesgaard, I. Povstugar, J.-M. Hartmann, T. Stoica, Z. Ikonic, S. Mantl, D. Grützmacher, and D. Buca, "Short-wave infrared LEDs from GeSn/SiGeSn multiple quantum wells," Optica **4**, 185 (2017).

[102]R. Bansal, Y.-T. Jheng, K.-C. Lee, H. H. Cheng, and G.-E. Chang, "GeSn vertical heterostructure p-i-n waveguide light emitting diode for 2μm band silicon photonics," IEEE Electron Device Lett. **44**, 364 (2023).

[103]L. Peng, X. Li, J. Zheng, X. Liu, M. Li, Z. Liu, C. Xue, Y. Zuo, and B. Cheng, "Room-temperature direct-bandgap electroluminescence from type-I GeSn/SiGeSn multiple quantum wells for 2 μm LEDs," J. Lumin. **228**, 117539 (2020).

[104]M. R. Atalla, S. Assali, G. Daligou, A. Attiaoui, S. Koelling, P. Daoust, and O. Moutanabbir, "Continuous-wave GeSn light-emitting diodes on silicon with 2.5 μm room-temperature emission," ACS Photonics **11**, 1335 (2024).

[105]V. Reboud, O. Concepción, W. Du, M. El Kurdi, J. Hartmann, Z. Ikonic, S. Assali, N. Pauc, V. Calvo, C. Cardoux, E. Kroemer, N. Coudurier, P. Rodriguez, S.-Q. Yu, D. Buca, and A. Chelnokov, "Advances in GeSn alloys for MIR applications," Photonics Nanostruct. Fundam. Appl. **58**, 101233 (2024).

[106]M. Liu, Y. Junk, Y. Han, D. Yang, J. H. Bae, M. Frauenrath, J.-M. Hartmann, Z. Ikonic, F. Bärwolf, A. Mai, D. Grützmacher, J. Knoch, D. Buca, and Q.-T. Zhao, "Vertical GeSn nanowire MOSFETs for CMOS beyond silicon," Commun. Eng. **2**, 7 (2023).

[107]J. Doherty, S. Biswas, E. Galluccio, C. A. Broderick, A. Garcia-Gil, R. Duffy, E. P. O'Reilly, and J. D. Holmes, "Progress on Germanium-Tin nanoscale alloys," Chem. Mater. **32**, 4383 (2020).

[108]B. M. Ferrari, F. Marcantonio, F. Murphy-Armando, M. Virgilio, and F. Pezzoli, "Quantum spin Hall phase in GeSn heterostructures on silicon," Phys. Rev. Res. **5**, L022035 (2023).

[109]W. Chen, C.-W. Chang, and S.-H. Yang, "Group IV THz large area emitter based on GeSn alloy," Opt. Lett. **47**, 4411 (2022).

[110]K. Momma and F. Izumi, "VESTA 3 for three-dimensional visualization of crystal, volumetric and morphology data," J. Appl. Crystallogr. **44**, 1272 (2011).

[111]B. Predel, "Ge-Sn (Germanium-Tin)," in *Ga-Gd – Hf-Zr*, edited by O. Madelung (Springer-Verlag, Berlin/Heidelberg, 1996), pp. 1–4.

[112]M. P. Polak, P. Scharoch, and R. Kudrawiec, "The electronic band structure of Ge$_{1-x}$Sn$_x$ in the full composition range: Indirect, direct, and inverted gaps regimes, band offsets, and the Burstein–Moss effect," J. Phys. D **50**, 195103 (2017).

[113]C. Xu, D. Ringwala, D. Wang, L. Liu, C. D. Poweleit, S. L. Chang, H. L. Zhuang, J. Menéndez, and J. Kouvetakis, "Synthesis and fundamental studies of Si-compatible (Si)GeSn and GeSn Mid-IR systems with ultrahigh Sn contents," Chem. Mater. **31**, 9831 (2019).

[114]C. Xu, C. L. Senaratne, R. J. Culbertson, J. Kouvetakis, and J. Menéndez, "Deviations from Vegard's law in semiconductor thin films measured with X-ray diffraction and Rutherford backscattering: The Ge$_{1-y}$Sn$_y$ and Ge$_{1-x}$Si$_x$ cases," J. Appl. Phys. **122**, 125702 (2017).

[115]S. Magalhaes, M. Dias, B. Nunes, F. Oliveira, M. F. Cerqueira, and E. Alves, "Confronting Vegard's rule in Ge$_{1-x}$Sn$_x$ epilayers: From fundamentals to the effect of defects," J. Phys. D **55**, 295301 (2022).

[116]J. Shen, J. Zi, X. Xie, and P. Jiang, "Ab initio calculation of the structure of the random alloys," Phys. Rev. B **56**, 12084 (1997).

[117]F. Gencarelli, D. Grandjean, Y. Shimura, B. Vincent, D. Banerjee, A. Vantomme, W. Vandervorst, R. Loo, M. Heyns, and K. Temst, "Extended X-ray absorption fine structure investigation of Sn local environment in strained and relaxed epitaxial Ge$_{1-x}$Sn$_x$ films," J. Appl. Phys. **117**, 095702 (2015).

[118]R. Beeler, R. Roucka, A. V. G. Chizmeshya, J. Kouvetakis, and J. Menéndez, "Nonlinear structure-composition relationships in the Ge$_{1-y}$Sn$_y$/Si(100) (y <0.15) system," Phys. Rev. B **84**, 035204 (2011).

[119]S. Assali, J. Nicolas, S. Mukherjee, A. Dijkstra, and O. Moutanabbir, "Atomically uniform Sn-rich GeSn semiconductors with 3.0–3.5 μm room-temperature optical emission," Appl. Phys. Lett. **112**, 251903 (2018).

[120]B. Cao, S. Chen, X. Jin, J. Liu, and T. Li, "Short-range order in GeSn alloy," ACS Appl. Mater. Interfaces **12**, 57245 (2020).

[121]J. Z. Lentz, J. C. Woicik, M. Bergschneider, R. Davis, A. Mehta, K. Cho, and P. C. McIntyre, "Local ordering in Ge/Ge-Sn semiconductor alloy core/shell nanowires revealed by extended x-ray absorption fine structure (EXAFS)," Appl. Phys. Lett. **122**, 062103 (2023).

[122]J. D. Fuhr, C. I. Ventura, and R. A. Barrio, "Formation of non-substitutional β-Sn defects in $Ge_{1-x}Sn_x$ alloys," J. Appl. Phys. **114**, 193508 (2013).

[123]W. Windl and S.-C. Chien, "Free–energy parameterization and thermodynamics in Si-Ge-Sn alloys," Phys. Status Solidi B **259**, 2100590 (2022).

[124]S. Liu, A. C. Covian, X. Wang, C. T. Cline, A. Akey, W. Dong, S. Yu, and J. Liu, "3D nanoscale mapping of short–range order in GeSn alloys," Small Methods **6**, 2200029 (2022).

[125]M. Müller, G. D. W. Smith, B. Gault, and C. R. M. Grovenor, "Compositional nonuniformities in pulsed laser atom probe tomography analysis of compound semiconductors," J. Appl. Phys. **111**, 064908 (2012).

[126]Z. Song, W. Fan, C. S. Tan, Q. Wang, D. Nam, D. H. Zhang, and G. Sun, "Corrigendum: Band structure of $Ge_{1-x}Sn_x$ alloy: A full-zone 30-band $k \cdot p$ model," New J. Phys. **22**, 019502 (2020).

[127]H.-S. Lan, S. T. Chang, and C. W. Liu, "Semiconductor, topological semimetal, indirect semimetal, and topological Dirac semimetal phases of GeSn alloys," Phys. Rev. B **95**, 201201 (2017).

[128]J. D. Gallagher, C. L. Senaratne, C. Xu, P. Sims, T. Aoki, D. J. Smith, J. Menéndez, and J. Kouvetakis, "Non-radiative recombination in $Ge_{1-y}Sn_y$ light emitting diodes: The role of strain relaxation in tuned heterostructure designs," J. Appl. Phys. **117**, 245704 (2015).

[129]Y. Chibane and M. Ferhat, "Electronic structure of Sn_xGe_{1-x} alloys for small Sn compositions: Unusual structural and electronic properties," J. Appl. Phys. **107**, 053512 (2010).

[130]P. Moontragoon, R. A. Soref, and Z. Ikonic, "The direct and indirect bandgaps of unstrained $Si_xGe_{1-x-y}Sn_y$ and their photonic device applications," J. Appl. Phys. **112**, 073106 (2012).

[131]A. Kumar, M. P. Komalan, H. Lenka, A. K. Kambham, M. Gilbert, F. Gencarelli, B. Vincent, and W. Vandervorst, "Atomic insight into $Ge_{1-x}Sn_x$ using atom probe tomography," Ultramicroscopy **132**, 171 (2013).

[132]Z. Song, W. Fan, C. S. Tan, Q. Wang, D. Nam, D. H. Zhang, and G. Sun, "Band structure of strained $Ge_{1-} \sim Sn_x$ alloy: A full-zone 30-band $k \cdot p$ model," IEEE J. Quantum Electron. **56**, 7100208 (2020).

[133]G.-E. Chang, S. Chang, and S. L. Chuang, "Strain-balanced $Ge_zSn_{1-z} - Si_xGe_ySn_{1-x-y}$ multiple-quantum-well lasers," IEEE J. Quantum Electron. **46**, 1813 (2010).

[134]J. Michel, J. Liu, and L. C. Kimerling, "High-performance Ge-on-Si photodetectors," Nat. Photonics **4**, 527 (2010).

[135]C. Eckhardt, K. Hummer, and G. Kresse, "Indirect-to-direct gap transition in strained and unstrained Sn_xGe_{1-x} alloys," Phys. Rev. B **89**, 165201 (2014).

[136]V. R. D'Costa, W. Wang, and Y.-C. Yeo, "Near-bandgap optical properties of pseudomorphic GeSn alloys grown by molecular beam epitaxy," J. Appl. Phys. **120**, 063104 (2016).

[137]N. S. Fernando, R. A. Carrasco, R. Hickey, J. Hart, R. Hazbun, S. Schoeche, J. N. Hilfiker, J. Kolodzey, and S. Zollner, "Band gap and strain engineering of pseudomorphic $Ge_{1-x-y}Si_xSn_y$ alloys on Ge and GaAs for photonic applications," J. Vac. Sci. Technol. B **36**, 021202 (2018).

[138]K. Zelazna, M. P. Polak, P. Scharoch, J. Serafinczuk, M. Gladysiewicz, J. Misiewicz, J. Dekoster, and R. Kudrawiec, "Electronic band structure of compressively strained $Ge_{1-x}Sn_x$ with x < 0.11 studied by contactless electroreflectance," Appl. Phys. Lett. **106**, 142102 (2015).

[139]L. Jiang, J. D. Gallagher, C. L. Senaratne, T. Aoki, J. Mathews, J. Kouvetakis, and J. Menéndez, "Compositional dependence of the direct and indirect band gaps in $Ge_{1-y}Sn_y$ alloys from room temperature photoluminescence: Implications for the indirect to direct gap crossover in intrinsic and n-type materials," Semicond. Sci. Technol. **29**, 115028 (2014).

[140]H. Lin, R. Chen, W. Lu, Y. Huo, T. I. Kamins, and J. S. Harris, "Investigation of the direct band gaps in $Ge_{1-x}Sn_x$ alloys with strain control by photoreflectance spectroscopy," Appl. Phys. Lett. **100**, 102109 (2012).

[141]H. Perez Ladron de Guevara, A. G. Rodriguez, H. Navarro-Contreras, and M. A. Vidal, "Nonlinear behavior of the energy gap in $Ge_{1-x}Sn_x$ alloys at 4K," Appl. Phys. Lett. **91**, 161909 (2007).

[142]S.-Q. Liu and S.-T. Yen, "Extraction of eight-band k · p parameters from empirical pseudopotentials for GeSn," J. Appl. Phys. **125**, 245701 (2019).

[143]T. D. Eales, I. P. Marko, S. Schulz, E. O'Halloran, S. Ghetmiri, W. Du, Y. Zhou, S. Q. Yu, J. Margetis, J. Tolle, E. P. O'Reilly, and S. J. Sweeney, "$Ge_{1-x}Sn_x$ alloys: Consequences of band mixing effects for the evolution of the band gap Γ-character with Sn concentration," Sci. Rep. **9**(1), 14077 (2019).

[144]E. J. O'Halloran, C. A. Broderick, D. S. P. Tanner, S. Schulz, and E. P. O'Reilly, "Comparison of first principles and semi-empirical models of the structural and electronic properties of $Ge_{1-x}Sn_x$ alloys," Opt. Quantum Electron. **51**, 314 (2019).

[145]G. Landwehr and S. Uchida, "The germanium grain boundary: A disordered two-dimensional electronic system," in *Localization and Metal-Insulator Transitions* (Springer, Boston, MA, 1985), pp. 379–391.

[146]I. Vladimirov, M. Kühn, T. Geßner, F. May, and R. T. Weitz, "Energy barriers at grain boundaries dominate charge carrier transport in an electron-conductive organic semiconductor," Sci. Rep. **8**(1), 14868 (2018).

[147]S. Tsurekawa, K. Kido, S. Hamada, T. Watanabe, and T. Sekiguchi, "Electrical activity of grain boundaries in polycrystalline silicon - influences of grain boundary structure, chemistry and temperature," Int. J. Mater. Res. **96**, 197–206 (2005).

[148]T. Imajo, T. Ishiyama, K. Nozawa, T. Suemasu, and K. Toko, "Acceptor defects in polycrystalline Ge layers evaluated using linear regression analysis," Sci. Rep. **12**, 14941 (2022).

[149]M. Grundmann, *The Physics of Semiconductors*, Graduate Texts in Physics (Springer, Berlin, Heidelberg, 2010), p. 744.

[150]W. A. Jesser and J. Kui, "Misfit dislocation generation mechanisms in heterostructures," in *Fundamental Aspects of Dislocation Interactions* (Elsevier, 1993), pp. 101–110.

[151]J. Matthews and A. Blakeslee, "Defects in epitaxial multilayers," J. Cryst. Growth **27**, 118 (1974).

[152]W. D. Nix, "Mechanical properties of thin films," Metall. Trans. A **20**, 2217 (1989).

[153]D. C. Houghton, "Strain relaxation kinetics in $Si_{1-x}Ge_x$/Si heterostructures," J. Appl. Phys. **70**, 2136 (1991).

[154]R. People and J. C. Bean, "Calculation of critical layer thickness versus lattice mismatch for Ge_xSi_{1-x}/Si strained-layer heterostructures," Appl. Phys. Lett. **47**, 322 (1985).

[155]R. People and J. C. Bean, "Erratum: Calculation of critical layer thickness versus lattice mismatch for Ge_xSi_{1-x}/Si strained–layer heterostructures [Appl. Phys. Lett. **47**, 322 (1985)]," Appl. Phys. Lett. **49**, 229 (1986).

[156]W. Wang, Q. Zhou, Y. Dong, E. S. Tok, and Y.-C. Yeo, "Critical thickness for strain relaxation of $Ge_{1-x}Sn_x$ (x ≤ 0.17) grown by molecular beam epitaxy on Ge(001)," Appl. Phys. Lett. **106**, 232106 (2015).

[157]H. V. Stanchu, A. V. Kuchuk, Y. I. Mazur, J. Margetis, J. Tolle, S.-Q. Yu, and G. J. Salamo, "Strain suppressed Sn incorporation in GeSn epitaxially grown on Ge/Si(001) substrate," Appl. Phys. Lett. **116**, 232101 (2020).

[158]J. Margetis, S. Al-Kabi, W. Du, W. Dou, Y. Zhou, T. Pham, P. Grant, S. Ghetmiri, A. Mosleh, B. Li, J. Liu, G. Sun, R. Soref, J. Tolle, M. Mortazavi, and S. Q. Yu, "Si-based GeSn lasers with wavelength coverage of 2–3 μm and operating temperatures up to 180 K," ACS Photonics **5**, 827 (2018).

[159]W. Dou, M. Benamara, A. Mosleh, J. Margetis, P. Grant, Y. Zhou, S. Al-Kabi, W. Du, J. Tolle, B. Li, M. Mortazavi, and S.-Q. Yu, "Investigation of GeSn strain relaxation and spontaneous composition gradient for low-defect and high-Sn alloy growth," Sci. Rep. **8**, 5640 (2018).

[160]S. Assali, J. Nicolas, and O. Moutanabbir, "Enhanced Sn incorporation in GeSn epitaxial semiconductors via strain relaxation," J. Appl. Phys. **125**, 025304 (2019).

[161]J. Aubin, J. M. Hartmann, A. Gassenq, J. L. Rouviere, E. Robin, V. Delaye, D. Cooper, N. Mollard, V. Reboud, and V. Calvo, "Growth and structural properties of step-graded, high Sn content GeSn layers on Ge," Semicond. Sci. Technol. **32**, 094006 (2017).

[162]J. Nicolas, S. Assali, S. Mukherjee, A. Lotnyk, and O. Moutanabbir, "Dislocation pipe diffusion and solute segregation during the growth of metastable GeSn," Cryst. Growth Des. **20**, 3493 (2020).

[163]S. Mukherjee, S. Assali, and O. Moutanabbir, "Atomic pathways of solute segregation in the vicinity of nanoscale defects," Nano Lett. **21**, 9882 (2021).

[164]L. M. Giovane, H.-C. Luan, A. M. Agarwal, and L. C. Kimerling, "Correlation between leakage current density and threading dislocation density in SiGe p-i-n diodes grown on relaxed graded buffer layers," Appl. Phys. Lett. **78**, 541 (2001).

[165]S. V. Kondratenko, S. S. Derenko, Y. I. Mazur, H. Stanchu, A. V. Kuchuk, V. S. Lysenko, P. M. Lytvyn, S.-Q. Yu, and G. J. Salamo, "Impact of defects on photoexcited carrier relaxation dynamics in GeSn thin films," J. Phys: Condens. Matter **33**, 065702 (2020).

[166]H. Tetzner, I. A. Fischer, O. Skibitzki, M. M. Mirza, C. L. Manganelli, G. Luongo, D. Spirito, D. J. Paul, M. De Seta, and G. Capellini, "Current leakage mechanisms related to threading dislocations in Ge-rich SiGe heterostructures grown on Si(001)," Appl. Phys. Lett. **119**, 153504 (2021).

[167]S. Sze and K. K. Ng, *America*, Environmental Science and Engineering, Vol. 10, edited by V. K. Jain and A. Verma (John Wiley & Sons, Inc., Hoboken, NJ, 2006), pp. 739–751.

[168]J. S. Park, J. Bai, M. Curtin, B. Adekore, M. Carroll, and A. Lochtefeld, "Defect reduction of selective Ge epitaxy in trenches on Si(001) substrates using aspect ratio trapping," Appl. Phys. Lett. **90**, 052113 (2007).

[169]H. C. Luan, D. R. Lim, K. K. Lee, K. M. Chen, J. G. Sandland, K. Wada, and L. C. Kimerling, "High-quality Ge epilayers on Si with low threading-dislocation densities," Appl. Phys. Lett. **75**, 2909 (1999).

[170]R. Loo, G. Wang, L. Souriau, J. Lin, S. Takeuchi, G. Brammertz, and M. Caymax, "Epitaxial Ge on standard STI patterned Si wafers: High quality virtual substrates for Ge pMOS and III/V nMOS," ECS Trans. **25**, 335 (2009).

[171]G. Wang, R. Loo, E. Simoen, L. Souriau, M. Caymax, M. M. Heyns, and B. Blanpain, "A model of threading dislocation density in strain-relaxed Ge and GaAs epitaxial films on Si (100)," Appl. Phys. Lett. **94**, 102115 (2009).

[172]O. Olorunsola, A. Said, S. Ojo, H. Stanchu, G. Abernathy, S. Amoah, S. Saha, E. Wangila, J. Grant, S. Acharya, L. Miller, K. Rosler, Y.-T. Jheng, G.-E. Chang, B. Li, G. J. Salamo, S.-Q. F. Yu, and W. Du, "SiGeSn quantum well for photonics integrated circuits on Si photonics platform: A review," J. Phys. D **55**, 443001 (2022).

[173]J. Xie, A. V. G. Chizmeshya, J. Tolle, V. R. D'Costa, J. Menendez, and J. Kouvetakis, "Synthesis, stability range, and fundamental properties of Si-Ge-Sn semiconductors grown directly on Si(100) and Ge(100) platforms," Chem. Mater. **22**, 3779 (2010).

[174]N. von den Driesch, S. Wirths, R. Troitsch, G. Mussler, U. Breuer, O. Moutanabbir, D. Grützmacher, and D. Buca, "Thermally activated diffusion and lattice relaxation in (Si)GeSn materials," Phys. Rev. Mater. **4**, 033604 (2020).

[175]D. Grützmacher, O. Concepción, Q.-T. Zhao, and D. Buca, "Si-Ge-Sn alloys grown by chemical vapour deposition: A versatile material for photonics, electronics, and thermoelectrics," Appl. Phys. A **129**, 235 (2023).

[176]X. Yuan, D. Pan, Y. Zhou, X. Zhang, K. Peng, B. Zhao, M. Deng, J. He, H. H. Tan, and C. Jagadish, "Selective area epitaxy of III-V nanostructure arrays and networks: Growth, applications, and future directions," Appl. Phys. Rev. **8**, 021302 (2021).

[177]L. Güniat, P. Caroff, and A. Fontcuberta i Morral, "Vapor phase growth of semiconductor nanowires: Key developments and open questions," Chem. Rev. **119**, 8958 (2019).

[178]P. McIntyre and A. Fontcuberta i Morral, "Semiconductor nanowires: To grow or not to grow?," Mater. Today Nano **9**, 100058 (2020).

[179]C. Thelander, P. Agarwal, S. Brongersma, J. Eymery, L. Feiner, A. Forchel, M. Scheffler, W. Riess, B. Ohlsson, U. Gösele, and L. Samuelson, "Nanowire-based one-dimensional electronics," Mater. Today **9**, 28 (2006).

[180]F. Glas, "Critical dimensions for the plastic relaxation of strained axial heterostructures in free-standing nanowires," Phys. Rev. B **74**, 121302 (2006).

[181]R. S. Wagner and W. C. Ellis, "Vapor-liquid-solid mechanism of single crystal growth," Appl. Phys. Lett. **4**, 89 (1964).

[182]J. Doherty, S. Biswas, D. McNulty, C. Downing, S. Raha, C. O'Regan, A. Singha, C. O'Dwyer, and J. D. Holmes, "One-step fabrication of GeSn branched nanowires," Chem. Mater. **31**, 4016 (2019).

[183]T. Haffner, M. Zeghouane, F. Bassani, P. Gentile, A. Gassenq, F. Chouchane, N. Pauc, E. Martinez, E. Robin, S. David, T. Baron, and B. Salem, "Growth of Ge$_{1-x}$Sn$_x$ nanowires by chemical vapor deposition via vapor-liquid-solid mechanism using GeH$_4$ and SnCl$_4$," Phys. Status Solidi A **215**, 1700743 (2017).

[184]A. C. Meng, C. S. Fenrich, M. R. Braun, J. P. McVittie, A. F. Marshall, J. S. Harris, and P. C. McIntyre, "Core-shell germanium/germanium–tin nanowires exhibiting room-temperature direct- and indirect-gap photoluminescence," Nano Lett. **16**, 7521 (2016).

[185]S. Assali, A. Dijkstra, A. Li, S. Koelling, M. A. Verheijen, L. Gagliano, N. von den Driesch, D. Buca, P. M. Koenraad, J. E. M. Haverkort, and E. P. A. M. Bakkers, "Growth and optical properties of direct band gap Ge/Ge$_{0.87}$Sn$_{0.13}$ core/shell nanowire arrays," Nano Lett. **17**, 1538 (2017).

[186]M. Albani, S. Assali, M. A. Verheijen, S. Koelling, R. Bergamaschini, F. Pezzoli, E. P. A. M. Bakkers, and L. Miglio, "Critical strain for Sn incorporation into spontaneously graded Ge/GeSn core/shell nanowires," Nanoscale **10**, 7250 (2018).

[187]A. Meng, A. Braun, Y. Wang, C. Fenrich, M. Xue, D. Diercks, B. Gorman, M.-I. Richard, A. Marshall, W. Cai, J. Harris, and P. McIntyre, "Coupling of coherent misfit strain and composition distributions in core–shell Ge/Ge$_{1-x}$Sn$_x$ nanowire light emitters," Mater. Today Nano **5**, 100026 (2019).

[188]A. C. Meng, M. R. Braun, Y. Wang, S. Peng, W. Tan, J. Z. Lentz, M. Xue, A. Pakzad, A. F. Marshall, J. S. Harris, W. Cai, and P. C. McIntyre, "Growth mode control for direct-gap core/shell Ge/GeSn nanowire light emission," Mater. Today **40**, 101 (2020).

[189]Y. Kang, S. Xu, K. Han, E. Y.-J. Kong, Z. Song, S. Luo, A. Kumar, C. Wang, W. Fan, G. Liang, and X. Gong, "Ge$_{0.95}$Sn$_{0.05}$ gate-all-around p-channel metal-oxide-semiconductor field-effect transistors with sub-3 nm nanowire width," Nano Lett. **21**, 5555 (2021).

[190]M. S. Seifner, A. Dijkstra, J. Bernardi, A. Steiger-Thirsfeld, M. Sistani, A. Lugstein, J. E. M. Haverkort, and S. Barth, "Epitaxial Ge$_{0.81}$Sn$_{0.19}$ nanowires for nanoscale mid-infrared emitters," ACS Nano **13**, 8047 (2019).

[191]Y. Shen, W. Chen, and B. Sun, "Research progress of out-of-plane GeSn nanowires," Nanotechnology **35**, 242002 (2024).

[192]H. Li, Y. X. Cui, K. Y. Wu, W. K. Tseng, H. H. Cheng, and H. Chen, "Strain relaxation and Sn segregation in GeSn epilayers under thermal treatment," Appl. Phys. Lett. **102**, 251907 (2013).

[193]H. Groiss, M. Glaser, M. Schatzl, M. Brehm, D. Gerthsen, D. Roth, P. Bauer, and F. Schäffler, "Free-running Sn precipitates: An efficient phase separation mechanism for metastable Ge$_{1-x}$Sn$_x$ epilayers," Sci. Rep. **7**, 16114 (2017).

[194]A. Kuchuk, P. Lytvyn, Y. Mazur, H. Stanchu, S. Kondratenko, F. de Oliveira, S. Malyuta, M. Teodoro, M. Benamara, S.-Q. Yu, and G. Salamo, "Sn-guided self-grown Ge stripes banded by GeSn Nanowires: Formation mechanism and electric-field-induced switching from p- to n-type conduction," Appl. Surf. Sci. **604**, 154443 (2022).

[195]S. Wu, L. Zhang, B. Son, Q. Chen, H. Zhou, and C. S. Tan, "Insights into the origins of guided microtrenches and microholes/rings from Sn segregation in germanium-tin epilayers," J. Phys. Chem. C **124**, 20035 (2020).

[196]C. Schulte-Braucks, E. Hofmann, S. Glass, N. von den Driesch, G. Mussler, U. Breuer, J. Hartmann, P. Zaumseil, T. Schröder, Q. Zhao, S. Mantl, and D. Buca, "Schottky barrier tuning via dopant segregation in NiGeSn-GeSn contacts," J. Appl. Phys. **121**, 205705 (2017).

[197]I. Riihimaki, A. Virtanen, S. Rinta-Anttila, P. Pusa, J. Raisanen, and T. ISOLDE Collaboration, "Vacancy-impurity complexes and diffusion of Ga and Sn in intrinsic and p-doped germanium," Appl. Phys. Lett. **91**, 091922 (2007).

[198]P. Kringhoj and R. G. Elliman, "Diffusion of ion implanted Sn in Si, Si$_{1-x}$ Ge$_x$, and Ge," Appl. Phys. Lett. **65**, 324 (1994).

[199]M. Friesel, U. Sodervall, and W. Gust, "Diffusion of tin in germanium studied by secondary ion mass spectrometry," J. Appl. Phys. **78**, 5351 (1995).

[200]Y. Panayiotatos, V. Saltas, A. Chroneos, and F. Vallianatos, "Tin diffusion in germanium: A thermodynamic approach," J. Mater. Sci: Mater. Electron. **28**, 9936 (2017).

[201]A. Antonelli and J. Bernholc, "Pressure effects on self-diffusion in silicon," Phys. Rev. B **40**, 10643 (1989).

[202]M. J. Aziz, "Thermodynamics of diffusion under pressure and stress: Relation to point defect mechanisms," Appl. Phys. Lett. **70**, 2810 (1997).

[203]J.-H. Choi, K.-D. Na, S.-C. Lee, and C. S. Hwang, "First-principles study on the formation of a vacancy in Ge under biaxial compressive strain," Thin Solid Films **518**, 6373 (2010).

[204]The atomic diffusion coefficient follows the Arrhenius-type law $D = D_0 \exp(-E_a/kT)$, where E_a is the activation energy for diffusion.

04 January 2025 10:11:00

[205]P. Zaumseil, Y. Hou, M. A. Schubert, N. von den Driesch, D. Stange, D. Rainko, M. Virgilio, D. Buca, and G. Capellini, "The thermal stability of epitaxial GeSn layers," APL Mater. **6**, 076108 (2018).

[206]C. Xu, T. Hu, A. Zhang, D. A. Ringwala, J. Menéndez, and J. Kouvetakis, "Synthesis of short-wave infrared $Ge_{1-x}Sn_y$ semiconductors directly on Si(100) via ultralow temperature molecular routes for monolithic integration applications," J. Vac. Sci. Technol. A **40**, 063405 (2022).

[207]B. R. Conley, A. Mosleh, S. A. Ghetmiri, W. Du, G. Sun, R. Soref, J. Margetis, J. Tolle, H. A. Naseem, and S.-Q. Yu, "Stability of pseudomorphic and compressively strained $Ge_{1-x}Sn_x$ thin films under rapid thermal annealing," ECS Trans. **64**, 881 (2014).

[208]H. Stanchu, A. Said, O. Olorunsola, S. Acharya, S. Amoah, M. Zamani-Alavijeh, F. M. de Oliveira, S. K. Chhetri, J. Hu, Y. I. Mazur, S.-Q. Yu, and G. Salamo, "Role of dislocations on Sn diffusion during low temperature annealing of GeSn layers," J. Vac. Sci. Technol. B **41**, 052208 (2023).

[209]H. V. Stanchu, A. V. Kuchuk, Y. I. Mazur, K. Pandey, F. M. de Oliveira, M. Benamara, M. D. Teodoro, S.-Q. Yu, and G. J. Salamo, "Quantitative correlation study of dislocation generation, strain relief, and Sn outdiffusion in thermally annealed GeSn epilayers," Cryst. Growth Des. **21**, 1666 (2021).

[210]V. Bonino, N. Pauc, V. Calvo, M. Frauenrath, J.-M. Hartmann, A. Chelnokov, V. Reboud, M. Rosenthal, and J. Segura-Ruiz, "Microstructuring to improve the thermal stability of GeSn layers," ACS Appl. Mater. Interfaces **14**, 22270 (2022).

[211]M. R. Braun, J. Z. Lentz, I. Bishnoi, A. C. Meng, L. Casalena, H. Cheng, and P. C. McIntyre, "Oxide decomposition and Sn surface segregation on core/shell Ge/GeSn nanowires," ACS Appl. Electron. Mater. **4**, 5406 (2022).

[212]E. Azrak, W. Chen, S. Moldovan, S. Gao, S. Duguay, P. Pareige, and P. Roca i Cabarrocas, "Growth of in-plane $Ge_{1-x}Sn_x$ nanowires with 22 at. % Sn using a solid–liquid–solid mechanism," J. Phys. Chem. C **122**, 26236 (2018).

[213]C. M. Comrie, C. B. Mtshali, P. T. Sechogela, N. M. Santos, K. van Stiphout, R. Loo, W. Vandervorst, and A. Vantomme, "Interplay between relaxation and Sn segregation during thermal annealing of GeSn strained layers," J. Appl. Phys. **120**, 145303 (2016).

[214]H. Jia, P. Jurczak, J. Yang, M. Tang, K. Li, H. Deng, M. Dang, S. Chen, and H. Liu, "Impact of ex-situ annealing on strain and composition of MBE grown GeSn," J. Phys. D **53**, 485104 (2020).

[215]T. Tsukamoto, N. Hirose, A. Kasamatsu, T. Mimura, T. Matsui, and Y. Suda, "Investigation of Sn surface segregation during GeSn epitaxial growth by Auger electron spectroscopy and energy dispersive x-ray spectroscopy," Appl. Phys. Lett. **106**, 052103 (2015).

[216]N. Taoka, G. Capellini, N. von den Driesch, D. Buca, P. Zaumseil, M. A. Schubert, W. M. Klesse, M. Montanari, and T. Schroeder, "Sn migration control at high temperature due to high deposition speed for forming high-quality GeSn layer," Appl. Phys. Express **9**, 031201 (2016).

[217]A. Giunto, L. E. Webb, T. Hagger, and A. Fontcuberta i Morral, "Surfactant behavior and limited incorporation of indium during in situ doping of GeSn grown by molecular beam epitaxy," Phys. Rev. Mater. **7**, 074605 (2023).

[218]S. Zaima, O. Nakatsuka, N. Taoka, M. Kurosawa, W. Takeuchi, and M. Sakashita, "Growth and applications of GeSn-related group-IV semiconductor materials," Sci. Technol. Adv. Mater **16**, 43502 (2015).

[219]J. Zheng, Z. Liu, C. Xue, C. Li, Y. Zuo, B. Cheng, and Q. Wang, "Recent progress in GeSn growth and GeSn-based photonic devices," J. Semicond. **39**, 061006 (2018).

[220]Y. Miao, G. Wang, Z. Kong, B. Xu, X. Zhao, X. Luo, H. Lin, Y. Dong, B. Lu, L. Dong, J. Zhou, J. Liu, and H. H. Radamson, "Review of Si-based GeSn CVD growth and optoelectronic applications," Nanomaterials **11**, 2556 (2021).

[221]T. Tsukamoto, N. Hirose, A. Kasamatsu, T. Mimura, T. Matsui, and Y. Suda, "Formation of GeSn layers on Si (001) substrates at high growth temperature and high deposition rate by sputter epitaxy method," J. Mater. Sci. **50**, 4366 (2015).

[222]Y. Miao, Y. Wang, H. Hu, X. Liu, H. Su, J. Zhang, J. Yang, Z. Tang, X. Wu, J. Song, R. Xuan, and H. Zhang, "Characterization of crystalline GeSn layer on tensile-strained Ge buffer deposited by magnetron sputtering," Mater. Sci. Semicond. Process. **85**, 134 (2018).

[223]I. Dascalescu, N. C. Zoita, A. Slav, E. Matei, S. Iftimie, F. Comanescu, A.-M. Lepadatu, C. Palade, S. Lazanu, D. Buca, V. S. Teodorescu, M. L. Ciurea, M. Braic, and T. Stoica, "Epitaxial GeSn obtained by high power impulse magnetron sputtering and the heterojunction with embedded GeSn nanocrystals for shortwave infrared detection," ACS Appl. Mater. Interfaces **12**, 33879 (2020).

[224]H. Huang, D. Zhao, C. Qi, J. Huang, Z. Zeng, B. Zhang, and S. Lu, "Effect of growth temperature on crystallization of $Ge_{1-x}Sn_x$ films by magnetron sputtering," Crystals **12**, 1810 (2022).

[225]R. R. Lieten, J. W. Seo, S. Decoster, A. Vantomme, S. Peters, K. C. Bustillo, E. E. Haller, M. Menghini, and J.-P. Locquet, "Tensile strained GeSn on Si by solid phase epitaxy," Appl. Phys. Lett. **102**, 052106 (2013).

[226]T. Sadoh, A. Ooato, J.-H. Park, and M. Miyao, "High Sn-concentration (~8%) GeSn by low-temperature (~ 150°C) solid-phase epitaxy of a-GeSn/c-Ge," Thin Solid Films **602**, 20 (2016).

[227]K. Moto, T. Sugino, R. Matsumura, H. Ikenoue, M. Miyao, and T. Sadoh, "Low-temperature (<200C) solid-phase crystallization of high substitutional Sn concentration (~10%) GeSn on insulator enhanced by weak laser irradiation," AIP Adv. **7**, 075204 (2017).

[228]S. Dev, K. R Khiangte, and S. Lodha, "Wafer-scale mono-crystalline GeSn alloy on Ge by sputtering and solid phase epitaxy," J. Phys. D **53**, 21LT01 (2020).

[229]K. Gao, S. Prucnal, R. Huebner, C. Baehtz, I. Skorupa, Y. Wang, W. Skorupa, M. Helm, and S. Zhou, "$Ge_{1-x}Sn_x$ alloys synthesized by ion implantation and pulsed laser melting," Appl. Phys. Lett. **105**, 042107 (2014).

[230]K. Inenaga, R. Motomura, M. Ishimaru, R. Nakamura, and H. Yasuda, "Liquid-mediated crystallization of amorphous GeSn under electron beam irradiation," J. Appl. Phys. **127**, 205304 (2020).

[231]S. Prucnal, Y. Berencen, M. Wang, L. Rebohle, R. Kudrawiec, M. Polak, V. Zviagin, R. Schmidt-Grund, M. Grundmann, J. Grenzer, M. Turek, A. Droździel, K. Pyszniak, J. Zuk, M. Helm, W. Skorupa, and S. Zhou, "Band gap renormalization in n-type GeSn alloys made by ion implantation and flash lamp annealing," J. Appl. Phys. **125**, 203105 (2019).

[232]J. Zheng, Z. Liu, Y. Zhang, Y. Zuo, C. Li, and C. Xue, "Growth of high-Sn content (28%) GeSn alloy films by sputtering epitaxy," J. Cryst. Growth **492**, 29 (2018).

[233]D. Imbrenda, R. Hickey, R. A. Carrasco, N. S. Fernando, J. VanDerslice, S. Zollner, and J. Kolodzey, "Infrared dielectric response, index of refraction, and absorption of germanium-tin alloys with tin contents up to 27% deposited by molecular beam epitaxy," Appl. Phys. Lett. **113**, 122104 (2018).

[234]M. Oehme, K. Kostecki, M. Schmid, F. Oliveira, E. Kasper, and J. Schulze, "Epitaxial growth of strained and unstrained GeSn alloys up to 25% Sn," Thin Solid Films **557**, 169 (2014).

[235]R. Hickey, N. Fernando, S. Zollner, J. Hart, R. Hazbun, and J. Kolodzey, "Properties of pseudomorphic and relaxed germanium $_{1-x}$ tin$_x$ alloys (x < 0.185) grown by MBE," J. Vac. Sci. Technol. B **35**, 021205 (2017).

[236]E. Kasper, M. Kittler, M. Oehme, and T. Arguirov, "Germanium tin: Silicon photonics toward the mid-infrared [Invited]," Photonics Res. **1**, 69 (2013).

[237]M. A. Mircovich, C. Xu, D. A. Ringwala, C. D. Poweleit, J. Menéndez, and J. Kouvetakis, "Extended compositional range for the synthesis of SWIR and LWIR $Ge_{1-y}Sn_y$ alloys and device structures via CVD of SnH_4 and Ge_3H_8," ACS Appl. Electron. Mater. **3**, 3451 (2021).

[238]G. Ehrlich, "Atomic events at lattice steps and clusters: A direct view of crystal growth processes," Surf. Sci. **331–333**, 865 (1995).

[239]M. Nerding, L. Oberbeck, T. A. Wagner, R. B. Bergmann, and H. P. Strunk, "Single to polycrystalline transition in silicon growth by ion-assisted deposition at low temperatures," J. Appl. Phys. **93**, 2570 (2003).

[240]A. Cullis, "Strain-induced modulations in the surface morphology of heteroepitaxial layers," MRS Bull. **21**, 21 (1996).

[241]C. Xu, P. M. Wallace, D. A. Ringwala, S. L. Chang, C. D. Poweleit, J. Kouvetakis, and J. Menéndez, "Mid-infrared (3–8 um) $Ge_{1-y}Sn_y$ alloys (0.15 < y < 0.30): Synthesis, structural, and optical properties," Appl. Phys. Lett. **114**, 212104 (2019).

[242]J. Rathore, A. Nanwani, S. Mukherjee, S. Das, O. Moutanabbir, and S. Mahapatra, "Composition uniformity and large degree of strain relaxation in MBE-grown thick GeSn epitaxial layers, containing 16% Sn," J. Phys. D **54**, 185105 (2021).

[243]J. Aubin, J. M. Hartmann, A. Gassenq, L. Milord, N. Pauc, V. Reboud, and V. Calvo, "Impact of thickness on the structural properties of high tin content GeSn layers," J. Cryst. Growth **473**, 20 (2017).

[244]C. L. Senaratne, P. M. Wallace, J. D. Gallagher, P. E. Sims, J. Kouvetakis, and J. Menéndez, "Direct gap Ge$_{1-y}$Sn$_y$ alloys: Fabrication and design of mid-IR photodiodes," J. Appl. Phys. **120**, 025701 (2016).

[245]W. Dou, Y. Zhou, J. Margetis, S. A. Ghetmiri, S. Al-Kabi, W. Du, J. Liu, G. Sun, R. A. Soref, J. Tolle, B. Li, M. Mortazavi, and S.-Q. Yu, "Optically pumped lasing at 3 um from compositionally graded GeSn with tin up to 23%," Opt. Lett. **43**, 4558 (2018).

[246]A. Attiaoui and O. Moutanabbir, "Indirect-to-direct band gap transition in relaxed and strained Ge$_{1-x-y}$Si$_x$Sn$_y$ ternary alloys," J. Appl. Phys. **116**, 063712 (2014).

[247]M. R. M. Atalla, S. Assali, A. Attiaoui, C. Lemieux–Leduc, A. Kumar, S. Abdi, and O. Moutanabbir, "All–Group IV transferable membrane mid–infrared photodetectors," Adv. Funct. Mater. **31**, 2006329 (2021).

[248]T. Ueno, T. Irisawa, Y. Shiraki, A. Uedono, and S. Tanigawa, "Low temperature buffer growth for modulation doped SiGe/Ge/SiGe heterostructures with high hole mobility," Thin Solid Films **369**, 320 (2000).

[249]A. P. Knights, R. M. Gwilliam, B. J. Sealy, T. J. Grasby, C. P. Parry, D. J. F. Fulgoni, P. J. Phillips, T. E. Whall, E. H. C. Parker, and P. G. Coleman, "Growth temperature dependence for the formation of vacancy clusters in Si/Si$_{0.64}$Ge$_{0.36}$/Si structures," J. Appl. Phys. **89**, 76 (2001).

[250]L. Qian, J. Tong, W. Fan, J. S. Pan, and D. H. Zhang, "Growth of direct bandgap Ge$_{1-x}$Sn$_x$ alloys by modified magnetron sputtering," IEEE J. Quantum Electron. **56**(1), 7100104 (2020).

[251]G. Lin, K. Qian, H. Ding, J. Qian, J. Xu, J. Wang, S. Ke, W. Huang, S. Chen, and C. Li, "Effective strain relaxation of GeSn single crystal with Sn content of 16.5% on Ge grown by high-temperature sputtering," Appl. Surf. Sci. **623**, 157086 (2023).

[252]A. Giunto, N. Humblot, L. Burnier, A. Krammer, A. Schüler, and A. Fontcuberta i Morral, "Co-sputtered monocrystalline GeSn for infrared photodetection," in *IEEE Photonics Society Summer Topical Meeting Series (SUM 2020)* (IEEE, 2020).

[253]G. Lin, J. Qian, H. Ding, S. Wu, C. Li, J. Wang, J. Xu, W. Huang, and S. Chen, "Harvesting strong photoluminescence of physical vapor deposited GeSn with record high deposition temperature," J. Phys. D **56**, 355104 (2023).

[254]J. Zheng, S. Wang, Z. Liu, H. Cong, C. Xue, C. Li, Y. Zuo, B. Cheng, and Q. Wang, "GeSn p-i-n photodetectors with GeSn layer grown by magnetron sputtering epitaxy," Appl. Phys. Lett. **108**, 033503 (2016).

[255]Y. Zhu, T. Yang, H. Ding, G. Lin, C. Li, W. Huang, S. Chen, J. Wang, and J. Xu, "Sputtering-grown undoped GeSn/Ge multiple quantum wells on n-Ge for low-cost visible/shortwave infrared dual-band photodetection," Appl. Surf. Sci. **656**, 159673 (2024).

[256]T. Tsukamoto, K. Ikeno, N. Hirose, A. Kasamatsu, T. Matsui, and Y. Suda, "Sn distribution in Ge/GeSn heterostructures formed by sputter epitaxy method," J. Cryst. Growth **604**, 127045 (2023).

[257]H. Khelidj, A. Portavoce, M. Bertoglio, M. Descoins, L. Patout, K. Hoummada, A. Hallén, A. Charaï, M. Benoudia, and D. Mangelinck, "Ge(Sn) growth on Si (001) by magnetron sputtering," Mater. Today Commun. **26**, 101915 (2021).

[258]T. Tsukamoto, N. Hirose, A. Kasamatsu, T. Matsui, and Y. Suda, "Effects of low-temperature GeSn buffer layers on Sn surface segregation during GeSn epitaxial growth," Electron. Mater. Lett. **16**, 9 (2020).

[259]J. Yang, H. Hu, Y. Miao, L. Dong, B. Wang, W. Wang, H. Su, R. Xuan, and H. Zhang, "High-quality GeSn layer with Sn composition up to 7% grown by low-temperature magnetron sputtering for optoelectronic application," Materials **12**, 2662 (2019).

[260]J. Zheng, W. Huang, Z. Liu, C. Xue, C. Li, Y. Zuo, B. Cheng, and Q. Wang, "Influence of H$_2$ on strain evolution of high-Sn-content Ge$_{1-x}$Sn$_x$ alloys," J. Mater. Sci. **52**, 431 (2017).

[261]E. Napolitani and G. Impellizzeri, "Ion implantation defects and shallow junctions in Si and Ge," in *Semiconductors and Semimetals*, edited by L. Romano, V. Privitera, and C. Jagadish (Elsevier, 2015), Chap. 3, Vol. 91, pp. 93–122.

[262]T. Drüsedau, M. Löhmann, F. Klabunde, and T.-M. John, "Investigations on energy fluxes in magnetron sputter-deposition: Implications for texturing and nanoporosity of metals," Surf. Coat. Technol. **133–134**, 126 (2000).

[263]J. T. Gudmundsson, "Physics and technology of magnetron sputtering discharges," Plasma Sources Sci. Technol. **29**, 113001 (2020).

[264]T. Takagi, "Ion–surface interactions during thin film deposition," J. Vac. Sci. Technol. A **2**, 382 (1984).

[265]F. Auret, S. Coelho, W. Meyer, C. Nyamhere, M. Hayes, and J. Nel, "Electrical characterization of defects introduced during sputter deposition of Schottky contacts on n-type Ge," J. Elec. Mater. **36**, 1604 (2007).

[266]F. D. Auret, S. M. Coelho, G. Myburg, P. J. van Rensburg, and W. E. Meyer, "Defect introduction in Ge during inductively coupled plasma etching and Schottky barrier diode fabrication processes," Thin Solid Films **518**, 2485 (2010).

[267]A. Sakai and T. Tatsumi, "Ge growth on Si using atomic hydrogen as a surfactant," Appl. Phys. Lett. **64**, 52 (1994).

[268]T. Asano, N. Taoka, K. Hozaki, W. Takeuchi, M. Sakashita, O. Nakatsuka, and S. Zaima, "Impact of hydrogen surfactant on crystallinity of Ge$_{1-x}$Sn$_x$ epitaxial layers," Jpn. J. Appl. Phys., Part 1 **54**, 04DH15 (2015).

[269]H. Johll, M. Samuel, R. Y. Koo, H. C. Kang, Y.-C. Yeo, and E. S. Tok, "Influence of hydrogen surface passivation on Sn segregation, aggregation, and distribution in GeSn/Ge(001) materials," J. Appl. Phys. **117**, 205302 (2015).

[270]H. Ye and J. Yu, "Germanium epitaxy on silicon," Sci. Technol. Adv. Mater. **15**, 024601 (2014).

[271]B. Cunningham, J. O. Chu, and S. Akbar, "Heteroepitaxial growth of Ge on (100) Si by ultrahigh vacuum, chemical vapor deposition," Appl. Phys. Lett. **59**, 3574 (1991).

[272]L. Colace, G. Masini, F. Galluzzi, G. Assanto, G. Capellini, L. D. Gaspare, E. Palange, and F. Evangelisti, "Metal-semiconductor-metal near-infrared light detector based on epitaxial Ge/Si," Appl. Phys. Lett. **72**, 3175 (1998).

[273]D. D. Cannon, J. Liu, Y. Ishikawa, K. Wada, D. T. Danielson, S. Jongthammanurak, J. Michel, and L. C. Kimerling, "Tensile strained epitaxial Ge films on Si(100) substrates with potential application in L-band telecommunications," Appl. Phys. Lett. **84**, 906 (2004).

[274]J. M. Hartmann, A. Abbadie, A. M. Papon, P. Holliger, G. Rolland, T. Billon, J. M. Fedeli, M. Rouviere, L. Vivien, and S. Laval, "Reduced pressure-chemical vapor deposition of Ge thick layers on Si(001) for 1.3–1.55-μm photodetection," J. Appl. Phys. **95**, 5905 (2004).

[275]T. K. P. Luong, M. T. Dau, M. A. Zrir, M. Stoffel, V. Le Thanh, M. Petit, A. Ghrib, M. El Kurdi, P. Boucaud, H. Rinnert, and J. Murota, "Control of tensile strain and interdiffusion in Ge/Si(001) epilayers grown by molecular-beam epitaxy," J. Appl. Phys. **114**, 083504 (2013).

[276]H. Hanafusa, N. Hirose, A. Kasamatsu, T. Mimura, T. Matsui, and Y. Suda, "Ge flat layer growth on heavily phosphorus-doped Si(001) by sputter epitaxy," Jpn. J. Appl. Phys. **51**(2), 055502 (2012).

[277]T. Tsukamoto, N. Hirose, A. Kasamatsu, T. Mimura, T. Matsui, and Y. Suda, "Effects of boron dopants of Si (001) substrates on formation of Ge layers by sputter epitaxy method," Appl. Phys. Lett. **103**, 172103 (2013).

[278]T. Tsukamoto, N. Hirose, A. Kasamatsu, T. Mimura, T. Matsui, and Y. Suda, "Control of surface flatness of Ge layers directly grown on Si (001) substrates by DC sputter epitaxy method," Thin Solid Films **592**, 34 (2015).

[279]G. S. Zeng, C. L. Liu, and S. H. Chen, "Effect of substrate biasing on the epitaxial growth and structural properties of rf magnetron sputtered germanium buffer layer on silicon," Coatings **11**, 1060 (2021).

[280]Z. Liu, X. Hao, J. Huang, M. Ho-Baillie, and M. A. Green, "Reduction of threading dislocation density in sputtered Ge/Si(100) epitaxial films by continuous-wave diode laser-induced recrystallization," ACS Appl. Energy Mater. **1**, 1893 (2018).

[281]W. Yeh, A. Matsumoto, K. Sugihara, and H. Hayase, "Sputter epitaxial growth of flat germanium film with low threading-dislocation density on silicon (001)," ECS J. Solid State Sci. Technol. **3**, Q195 (2014).

[282]S. M. Pietralunga, M. Feré, M. Lanata, D. Piccinin, G. Radnóczi, F. Misják, A. Lamperti, M. Martinelli, and P. M. Ossi, "Heteroepitaxial sputtered Ge on Si (100): Nanostructure and interface morphology," Europhys. Lett. **88**, 28005 (2009).

[283]S. Otsuka, S. Mori, Y. Morita, N. Uchida, Y. Liu, S. O'uchi, H. Fuketa, S. Migita, M. Masahara, and T. Matsukawa, "Structural and electrical characterization of epitaxial Ge thin films on Si(001) formed by sputtering," Jpn. J. Appl. Phys., Part 1 **56**, 04CB01 (2017).

[284]M. Steglich, C. Patzig, L. Berthold, F. Schrempel, K. Füchsel, T. Höche, E.-B. Kley, and A. Tünnermann, "Heteroepitaxial Ge-on-Si by DC magnetron sputtering," AIP Adv. **3**, 072108 (2013).

[285]G. Bajor, K. C. Cadien, M. A. Ray, J. E. Greene, and P. S. Vijayakumar, "Growth of high quality epitaxial Ge films on (100)Si by sputter deposition," Appl. Phys. Lett. **40**, 696 (1982).

04 January 2025 10:11:00

[286] Y. Arroyo Rojas Dasilva, R. Kozak, R. Erni, and M. D. Rossell, "Structural defects in cubic semiconductors characterized by aberration-corrected scanning transmission electron microscopy," Ultramicroscopy **176**, 11 (2017).

[287] Y. B. Bolkhovityanov and L. V. Sokolov, "Ge-on-Si films obtained by epitaxial growing: Edge dislocations and their participation in plastic relaxation," Semicond. Sci. Technol. **27**, 043001 (2012).

[288] J. S. Speck, M. A. Brewer, G. Beltz, A. E. Romanov, and W. Pompe, "Scaling laws for the reduction of threading dislocation densities in homogeneous buffer layers," J. Appl. Phys. **80**, 3808 (1996).

[289] A. Marzegalli, M. Brunetto, M. Salvalaglio, F. Montalenti, G. Nicotra, M. Scuderi, C. Spinella, M. De Seta, and G. Capellini, "Onset of plastic relaxation in the growth of Ge on Si(001) at low temperatures: Atomic-scale microscopy and dislocation modeling," Phys. Rev. B **88**, 165418 (2013).

[290] The slip plane is the plane containing both the dislocation line and b, within which a dislocation can glide.[474] Gliding involves the switching of interatomic bonds, with no diffusion.[287]

[291] A. Sakai, T. Tatsumi, and K. Aoyama, "Growth of strain-relaxed Ge films on Si (001) surfaces," Appl. Phys. Lett. **71**, 3510 (1997).

[292] F. Rovaris, M. H. Zoellner, P. Zaumseil, A. Marzegalli, L. Di Gaspare, M. De Seta, T. Schroeder, P. Storck, G. Schwalb, G. Capellini, and F. Montalenti, "Dynamics of crosshatch patterns in heteroepitaxy," Phys. Rev. B **100**, 085307 (2019).

[293] E. P. Kvam, D. M. Maher, and C. J. Humphreys, "Variation of dislocation morphology with strain in Ge_xSi_{1-x} epilayers on (100)Si," J. Mater. Res. **5**, 1900 (1990).

[294] J. Zou, X. Z. Liao, D. J. H. Cockayne, and Z. M. Jiang, "Alternative mechanism for misfit dislocation generation during high-temperature Ge(Si)/Si (001) island growth," Appl. Phys. Lett. **81**, 1996 (2002).

[295] Y. Huangfu, W. Zhan, X. Hong, X. Fang, G. Ding, and H. Ye, "Heteroepitaxy of Ge on Si(001) with pits and windows transferred from free-standing porous alumina mask," Nanotechnology **24**, 185302 (2013).

[296] D. Leonhardt, S. Ghosh, and S. M. Han, "Origin and removal of stacking faults in Ge islands nucleated on Si within nanoscale openings in SiO_2," J. Appl. Phys. **110**, 073516 (2011).

[297] M. Y. Gutkin, K. N. Mikaelyan, and I. A. Ovidko, "Generation and evolution of partial misfit dislocations and stacking faults in thin-film heterostructures," Phys. Solid State **43**, 42 (2001).

[298] E. Maras, O. Trushin, A. Stukowski, T. Ala-Nissila, and H. Jónsson, "Global transition path search for dislocation formation in Ge on Si(001)," Comput. Phys. Commun. **205**, 13 (2016).

[299] A. E. Romanov, W. Pompe, G. Beltz, and J. S. Speck, "Modeling of threading dislocation density reduction in heteroepitaxial layers: II. Effective dislocation kinetics," Phys. Status Solidi B **199**, 33 (1997).

[300] O. Skibitzki, M. H. Zoellner, F. Rovaris, M. A. Schubert, Y. Yamamoto, L. Persichetti, L. Di Gaspare, M. De Seta, R. Gatti, F. Montalenti, and G. Capellini, "Reduction of threading dislocation density beyond the saturation limit by optimized reverse grading," Phys. Rev. Mater. **4**, 103403 (2020).

[301] R. Hull, J. C. Bean, R. E. Leibenguth, and D. J. Werder, "Role of strained layer superlattices in misfit dislocation reduction in growth of epitaxial $Ge_{0.5}Si_{0.5}$ alloys on Si(100) substrates," J. Appl. Phys. **65**, 4723 (1989).

[302] L. B. Freund and S. Suresh, *Thin Film Materials* (Cambridge University Press, 2004).

[303] V. T. Gillard, W. D. Nix, and L. B. Freund, "Role of dislocation blocking in limiting strain relaxation in heteroepitaxial films," J. Appl. Phys. **76**, 7280 (1994).

[304] B. Pichaud, M. Putero, and N. Burle, "Elemental dislocation mechanisms involved in the relaxation of heteroepitaxial semiconducting systems," Phys. Status solidi A **171**, 251 (1999).

[305] E. A. Stach, R. Hull, R. M. Tromp, F. M. Ross, M. C. Reuter, and J. C. Bean, "In-situ transmission electron microscopy studies of the interaction between dislocations in strained SiGe/Si (001) heterostructures," Philos. Mag. A **80**, 2159 (2000).

[306] V. Terzieva, L. Souriau, M. Caymax, D. P. Brunco, A. Moussa, S. Van Elshocht, R. Loo, F. Clemente, A. Satta, and M. Meuris, "Benefits and side effects of high temperature anneal used to reduce threading dislocation defects in epitaxial Ge layers on Si substrates," Thin Solid Films **517**, 172 (2008).

[307] Y. Yamamoto, P. Zaumseil, M. A. Schubert, and B. Tillack, "Influence of annealing conditions on threading dislocation density in Ge deposited on Si by reduced pressure chemical vapor deposition," Semicond. Sci. Technol. **33**, 124007 (2018).

[308] At 300K, the TECs of Ge and Si are respectively $5.9 \times 10^{-6}\,°C^{-1}$ and $2.6 \times 10^{-6}\,°C^{-1}$.

[309] R. Hull and J. C. Bean, "New insights into the microscopic motion of dislocations in covalently bonded semiconductors by in-situ transmission electron microscope observations of misfit dislocations in thin strained epitaxial layers," Phys. Status Solidi A **138**, 533 (1993).

[310] L. Wei, Y. Miao, Y. Ding, C. Li, H. Lu, and Y.-F. Chen, "Ultra high hole mobility in Ge films grown directly on Si (100) through interface modulation," J. Cryst. Growth **548**, 125838 (2020).

[311] Y. H. Tan and C. S. Tan, "Growth and characterization of germanium epitaxial film on silicon (001) using reduced pressure chemical vapor deposition," Thin Solid Films **520**, 2711 (2012).

[312] Y. Yamamoto, P. Zaumseil, T. Arguirov, M. Kittler, and B. Tillack, "Low threading dislocation density Ge deposited on Si (100) using RPCVD," Solid-State Electron. **60**, 2 (2011).

[313] V. A. Shah, A. Dobbie, M. Myronov, and D. R. Leadley, "High quality relaxed Ge layers grown directly on a Si(0 0 1) substrate," Solid-State Electron. **62**, 189 (2011).

[314] D. Choi, Y. Ge, J. S. Harris, J. Cagnon, and S. Stemmer, "Low surface roughness and threading dislocation density Ge growth on Si (0 0 1)," J. Cryst. Growth **310**, 4273 (2008).

[315] A. Nayfeh, C. O. Chui, K. C. Saraswat, and T. Yonehara, "Effects of hydrogen annealing on heteroepitaxial-Ge layers on Si: Surface roughness and electrical quality," Appl. Phys. Lett. **85**, 2815 (2004).

[316] H.-Y. Yu, S. Cheng, J.-H. Park, A. K. Okyay, M. C. Onbaşlı, B. Ercan, Y. Nishi, and K. C. Saraswat, "High quality single-crystal germanium-on-insulator on bulk Si substrates based on multistep lateral over-growth with hydrogen annealing," Appl. Phys. Lett. **97**, 063503 (2010).

[317] T. Nishimura, S. Kabuyanagi, W. Zhang, C. H. Lee, T. Yajima, K. Nagashio, and A. Toriumi, "Atomically flat planarization of Ge(100), (110), and (111) surfaces in H_2 annealing," Appl. Phys. Express **7**, 051301 (2014).

[318] A. Toriumi and T. Nishimura, "Germanium CMOS potential from material and process perspectives: Be more positive about germanium," Jpn. J. Appl. Phys. **57**, 010101 (2018).

[319] S. Kobayashi, Y. Nishi, and K. Saraswat, "Effect of isochronal hydrogen annealing on surface roughness and threading dislocation density of epitaxial Ge films grown on Si," Thin Solid Films **518**, S136 (2010).

[320] J. Hartmann, A. Abbadie, J. Barnes, J. Fédéli, T. Billon, and L. Vivien, "Impact of the H_2 anneal on the structural and optical properties of thin and thick Ge layers on Si; Low temperature surface passivation of Ge by Si," J. Cryst. Growth **312**, 532 (2010).

[321] L. Barbisan, A. Marzegalli, and F. Montalenti, "Atomic-scale insights on the formation of ordered arrays of edge dislocations in Ge/Si(001) films via molecular dynamics simulations," Sci. Rep. **12**(1), 3235 (2022).

[322] A. Kumar, J. Demeulemeester, J. Bogdanowicz, J. Bran, D. Melkonyan, C. Fleischmann, F. Gencarelli, Y. Shimura, W. Wang, R. Loo, and W. Vandervorst, "On the interplay between relaxation, defect formation, and atomic Sn distribution in $Ge_{1-x}Sn_x$ unraveled with atom probe tomography," J. Appl. Phys. **118**, 025302 (2015).

[323] H. Stanchu, A. V. Kuchuk, Y. I. Mazur, J. Margetis, J. Tolle, J. Richter, S.-Q. Yu, and G. J. Salamo, "X-ray diffraction study of strain relaxation, spontaneous compositional gradient, and dislocation density in GeSn/Ge/Si(100) heterostructures," Semicond. Sci. Technol. **35**, 075009 (2020).

[324] N. Bhargava, M. Coppinger, J. Prakash Gupta, L. Wielunski, and J. Kolodzey, "Lattice constant and substitutional composition of GeSn alloys grown by molecular beam epitaxy," Appl. Phys. Lett. **103**, 041908 (2013).

[325] F. Gencarelli, B. Vincent, J. Demeulemeester, A. Vantomme, A. Moussa, A. Franquet, A. Kumar, H. Bender, J. Meersschaut, W. Vandervorst, R. Loo, M. Caymax, K. Temst, and M. Heyns, "Crystalline properties and strain relaxation mechanism of CVD grown GeSn," ECS J. Solid State Sci. Technol. **2**, P134 (2013).

[326] H. Cai, H. Qian, K. Qian, Y. An, G. Lin, S. Wu, H. Ding, W. Huang, S. Chen, J. Wang, and C. Li, "Thickness-dependent behavior of strain relaxation and Sn

04 January 2025 10:11:00

segregation of GeSn epilayer during rapid thermal annealing," J. Alloys Compd. **904**, 164068 (2022).

[327] H. H. Cheng, W. P. Huang, V. I. Mashanov, and G. Sun, "Local intermixing on Ge/Si heterostructures at low temperature growth," J. Appl. Phys. **108**, 044314 (2010).

[328] D. Huang, R. Ji, L. Yao, J. Jiao, X. Chen, C. Li, W. Huang, S. Chen, and S. Ke, "Strain-induced abnormal Ge/Si inter-diffusion during hetero-epitaxy process," Vacuum **196**, 110735 (2022).

[329] S. Gupta, E. Simoen, R. Loo, Y. Shimura, C. Porret, F. Gencarelli, K. Paredis, H. Bender, J. Lauwaert, H. Vrielinck, and M. Heyns, "Electrical properties of extended defects in strain relaxed GeSn," Appl. Phys. Lett. **113**, 022102 (2018).

[330] J. D. Gallagher, C. L. Senaratne, P. Sims, T. Aoki, J. Menéndez, and J. Kouvetakis, "Electroluminescence from GeSn heterostructure pin diodes at the indirect to direct transition," Appl. Phys. Lett. **106**, 091103 (2015).

[331] F. Wan, C. Xu, X. Wang, G. Xu, B. Cheng, and C. Xue, "Study of strain evolution mechanism in $Ge_{1-x}Sn_x$ materials grown by low temperature molecular beam epitaxy," J. Cryst. Growth **577**, 126399 (2022).

[332] G. Ju, M. Tabuchi, Y. Takeda, and H. Amano, "Role of threading dislocations in strain relaxation during GaInN growth monitored by real-time X-ray reflectivity," Appl. Phys. Lett. **110**, 262105 (2017).

[333] F. Castioni, L. Henry, L. Casiez, N. Bernier, V. Reboud, J. Chretien, N. Pauc, V. Calvo, J. Richy, A. Jannaud, V. Delaye, E. Robin, J.-M. Hartmann, and P. Bayle-Guillemaud, "Impact of strain on Si and Sn incorporation in (Si)GeSn alloys by STEM analyses," J. Appl. Phys. **132**, 195306 (2022).

[334] J. R. Weber, A. Janotti, and C. G. Van de Walle, "Defects in germanium," in *Photonics and Electronics with Germanium*, edited by K. Wada and L. C. Kimerling (Wiley-VCH Verlag GmbH & Co. KGaA, Weinheim, Germany, 2015), pp. 1–23.

[335] The concentration of vacancies is given by $N = N_0 * \exp(-E_f/kT)$, where N_0 is the density of sites the defect can occupy and E_f is the formation energy. At 300K, with $N_0 = 4.41 \times 10^{22}$ at/cm^{-3}, this expression yields $N \ll 1$ at/cm^{-3}, while at 600K, typically used for GeSn growth, it yields $N \sim 0.02$ at/cm^{-3}.

[336] E. N. Sgourou, A. Daskalopulu, L. H. Tsoukalas, G. Stamoulis, R. V. Vovk, and A. Chroneos, "Seventy-five years since the point-contact transistor: Germanium revisited," Appl. Sci. **12**, 11993 (2022).

[337] K. Kuitunen, F. Tuomisto, J. Slotte, and I. Capan, "Divacancy clustering in neutron-irradiated and annealed n-type germanium," Phys. Rev. B **78**, 033202 (2008).

[338] V. Markevich, A. Peaker, S. Lastovskii, L. Murin, V. Litvinov, V. Emtsev, and L. Dobaczewski, "Interstitial-related defect reactions in electron-irradiated oxygen-rich Ge crystals: A DLTS study," Physica B **404**, 4533 (2009).

[339] H. Gossmann, P. Asoka–Kumar, T. C. Leung, B. Nielsen, K. G. Lynn, F. C. Unterwald, and L. C. Feldman, "Point defects in Si thin films grown by molecular beam epitaxy," Appl. Phys. Lett. **61**, 540 (1992).

[340] H. Jorke, H.-J. Herzog, and H. Kibbel, "Kinetics of ordered growth of Si on Si (100) at low temperatures," Phys. Rev. B **40**, 2005 (1989).

[341] Y. Bai, M. T. Bulsara, and E. A. Fitzgerald, "Photoluminescence and secondary ion mass spectrometry investigation of unintentional doping in epitaxial germanium thin films grown on III-V compound by metal-organic chemical vapor deposition," J. Appl. Phys. **111**, 013502 (2012).

[342] K. M. Shoukri, Y. M. Haddara, A. P. Knights, and P. G. Coleman, "Impact of growth conditions on vacancy-type defects in silicon–germanium structures grown by molecular-beam epitaxy," Appl. Phys. Lett. **86**, 131923 (2005).

[343] J. Slotte, I. Makkonen, and F. Tuomisto, "Review–Defect identification with positron annihilation spectroscopy in narrow band gap semiconductors," ECS J. Solid State Sci. Technol. **5**, P3166 (2016).

[344] H. av Skardi, A. Bro Hansen, A. Mesli, and A. Nylandsted Larsen, "The divacancy in particle-irradiated, strain-relaxed SiGe," Nucl. Instrum. Methods Phys. Res., Sect. B **186**, 195 (2002).

[345] J. Slotte, S. Kilpeläinen, N. Segercrantz, K. Mizohata, J. Räisänen, and F. Tuomisto, "In situ positron annihilation spectroscopy analysis on low–temperature irradiated semiconductors, challenges and possibilities," Phys. Status Solidi A **218**, 2000232 (2021).

[346] J. Slotte and F. Tuomisto, "Advances in positron annihilation spectroscopy of Si, Ge and their alloys," Mater. Sci. Semicond. Process. **15**, 669 (2012).

[347] M. Christian Petersen, A. Nylandsted Larsen, and A. Mesli, "Divacancy defects in germanium studied using deep-level transient spectroscopy," Phys. Rev. B **82**, 075203 (2010).

[348] M. Elsayed, N. Arutyunov, R. Krause-Rehberg, G. Oganesyan, and V. Kozlovski, "Formation and annealing of vacancy-P complexes in proton-irradiated germanium," Acta Mater. **100**, 1–10 (2015).

[349] J. R. Weber, A. Janotti, P. Rinke, and C. G. Van de Walle, "Dangling-bond defects and hydrogen passivation in germanium," Appl. Phys. Lett. **91**, 142101 (2007).

[350] C. Van de Walle, J. Weber, and A. Janotti, "Role of hydrogen at germanium/dielectric interfaces," Thin Solid Films **517**, 144 (2008).

[351] P. Clauws, "Oxygen related defects in germanium," Mater. Sci. Eng.: B **36**, 213 (1996).

[352] I. Chambouleyron and A. R. Zanatta, "Nitrogen in germanium," J. Appl. Phys. **84**(1), 1–30 (1998).

[353] S. Brotzmann, H. Bracht, J. L. Hansen, A. N. Larsen, E. Simoen, E. E. Haller, J. S. Christensen, and P. Werner, "Diffusion and defect reactions between donors, C, and vacancies in Ge. I. Experimental results," Phys. Rev. B **77**, 235207 (2008).

[354] A. Chroneos, "Isovalent impurity-vacancy complexes in germanium," Phys. Status Solidi B **244**, 3206 (2007).

[355] A. Chroneos, "Effect of germanium substrate loss and nitrogen on dopant diffusion in germanium," J. Appl. Phys. **105**, 056101 (2009).

[356] N. Kuganathan, R. W. Grimes, and A. Chroneos, "Nitrogen-vacancy defects in germanium," AIP Adv. **12**, 045110 (2022).

[357] V. P. Markevich, V. V. Litvinov, L. Dobaczewski, J. L. Lindström, L. I. Murin, S. V. Vetrov, I. D. Hawkins, and A. R. Peaker, "Vacancy-oxygen complex in Ge crystals," Physica B **340–342**, 844 (2003).

[358] J. Kujala, T. Südkamp, J. Slotte, I. Makkonen, F. Tuomisto, and H. Bracht, "Vacancy-donor complexes in highly n-type Ge doped with As, P and Sb," J. Phys. Condens. Matter **28**, 335801 (2016).

[359] A. Vohra, A. Khanam, J. Slotte, I. Makkonen, G. Pourtois, C. Porret, R. Loo, and W. Vandervorst, "Heavily phosphorus doped germanium: Strong interaction of phosphorus with vacancies and impact of tin alloying on doping activation," J. Appl. Phys. **125**, 225703 (2019).

[360] A. Vohra, A. Khanam, J. Slotte, I. Makkonen, G. Pourtois, R. Loo, and W. Vandervorst, "Evolution of phosphorus-vacancy clusters in epitaxial germanium," J. Appl. Phys. **125**, 025701 (2019).

[361] A. Carvalho, V. Torres, V. Markevich, J. Coutinho, V. Litvinov, A. Peaker, R. Jones, and P. Briddon, "Identification of stable and metastable forms of centers in germanium," Physica B **401–402**, 192 (2007).

[362] A. Chroneos, H. Bracht, R. W. Grimes, and B. P. Uberuaga, "Vacancy-mediated dopant diffusion activation enthalpies for germanium," Appl. Phys. Lett. **92**, 172103 (2008).

[363] F. Auret, P. J. van Rensburg, M. Hayes, J. Nel, S. Coelho, W. Meyer, S. Decoster, V. Matias, A. Vantomme, and D. Smeets, "Electrical characterization of defects in heavy-ion implanted n-type Ge," Nucl. Instrum. Methods Phys. Res., Sect. B **257**, 169 (2007).

[364] H. Höhler, N. Atodiresei, K. Schroeder, R. Zeller, and P. H. Dederichs, "Vacancy complexes with oversized impurities in Si and Ge," Phys. Rev. B **71**, 035212 (2005).

[365] S. Decoster, S. Cottenier, U. Wahl, J. G. Correia, and A. Vantomme, "Lattice location study of ion implanted Sn and Sn-related defects in Ge," Phys. Rev. B **81**, 155204 (2010).

[366] E. Kamiyama, K. Sueoka, O. Nakatsuka, N. Taoka, S. Zaima, K. Izunome, and K. Kashima, "Analysis for positions of Sn atoms in epitaxial $Ge_{1-x}Sn_x$ film in low temperature depositions," Thin Solid Films **557**, 173 (2014).

[367] D. Rainko, D. Stange, N. von den Driesch, C. Schulte-Braucks, G. Mussler, Z. Ikonic, J. M. Hartmann, M. Luysberg, S. Mantl, D. Grützmacher, and D. Buca, "(Si)GeSn nanostructures for light emitters," Proc. SPIE **9891**, 98910W (2016).

[368] S. Su, W. Wang, B. Cheng, G. Zhang, W. Hu, C. Xue, Y. Zuo, and Q. Wang, "Epitaxial growth and thermal stability of $Ge_{1-x}Sn_x$ alloys on Ge-buffered Si (001) substrates," J. Cryst. Growth **317**, 43 (2011).

[369] In Ref. 368, they claim χ_{min} is equal for Sn and Ge, but precise values are not reported.

[370] R. Roucka, R. Beeler, J. Mathews, M. Y. Ryu, Y. Kee Yeo, J. Menéndez, and J. Kouvetakis, "Complementary metal-oxide semiconductor-compatible detector

04 January 2025 10:11:00

materials with enhanced 1550 nm responsivity via Sn-doping of Ge/Si(100)," J. Appl. Phys. **109**, 103115 (2011).

[371]C. I. Ventura, J. D. Fuhr, and R. A. Barrio, "Nonsubstitutional single-atom defects in the $Ge_{1-x}Sn_x$ alloy," Phys. Rev. B **79**, 155202 (2009).

[372]Y. Shimura, N. Tsutsui, O. Nakatsuka, A. Sakai, and S. Zaima, "Low temperature growth of $Ge_{1-x}Sn_x$ buffer layers for tensile-strained Ge layers," Thin Solid Films **518**, S2 (2010).

[373]A. Chroneos, C. Jiang, R. W. Grimes, U. Schwingenschlögl, and H. Bracht, "Defect interactions in $Sn_{1-x}Ge_x$ random alloys," Appl. Phys. Lett. **94**, 252104 (2009).

[374]F. Tuomisto and I. Makkonen, "Defect identification in semiconductors with positron annihilation: Experiment and theory," Rev. Mod. Phys. **85**, 1583 (2013).

[375]S. Assali, M. Elsayed, J. Nicolas, M. O. Liedke, A. Wagner, M. Butterling, R. Krause-Rehberg, and O. Moutanabbir, "Vacancy complexes in nonequilibrium germanium-tin semiconductors," Appl. Phys. Lett. **114**, 251907 (2019).

[376]J. Slotte, F. Tuomisto, J. Kujala, A. M. Holm, N. Segercrantz, S. Kilpeläinen, K. Kuitunen, E. Simoen, F. Gencarelli, R. Loo, and Y. Shimura, "(Invited) Positron annihilation spectroscopy on open-volume defects in group IV semiconductors," ECS Trans. **64**, 241 (2014).

[377]E. Kamiyama, S. Nakagawa, T. Ohmura, T. Asano, O. Nakatsuka, N. Taoka, S. Zaima, K. Izunome, and K. Kashima, "Effect of Sn atoms on incorporation of vacancies in epitaxial $Ge_{1-x}Sn_x$ film grown at low temperature," Appl. Phys. Express **7**, 021302 (2014).

[378]A. Chroneos, C. A. Londos, and H. Bracht, "A-centers and isovalent impurities in germanium: Density functional theory calculations," Mater. Sci. Eng. B **176**, 453 (2011).

[379]O. Nakatsuka, Y. Shimura, W. Takeuchi, N. Taoka, and S. Zaima, "Development of epitaxial growth technology for $Ge_{1-x}Sn_x$ alloy and study of its properties for Ge nanoelectronics," Solid-State Electron. **83**, 82 (2013).

[380]E. Kamiyama, K. Sueoka, K. Terasawa, T. Yamaha, O. Nakatsuka, S. Zaima, K. Izunome, K. Kashima, and H. Uchida, "Atom probe tomography study on $Ge_{1-x-y}Sn_xC_y$ hetero-epitaxial film on Ge substrates," Thin Solid Films **592**, 54 (2015).

[381]A. Khanam, A. Vohra, J. Slotte, I. Makkonen, R. Loo, G. Pourtois, and W. Vandervorst, "A demonstration of donor passivation through direct formation of V-As i complexes in As-doped $Ge_{1-x}Sn_x$," J. Appl. Phys. **127**, 195703 (2020).

[382]V. P. Markevich, A. R. Peaker, B. Hamilton, V. V. Litvinov, Y. M. Pokotilo, S. B. Lastovskii, J. Coutinho, A. Carvalho, M. J. Rayson, and P. R. Briddon, "Tin-vacancy complex in germanium," J. Appl. Phys. **109**, 083705 (2011).

[383]V. P. Markevich, A. R. Peaker, B. Hamilton, V. V. Litvinov, Y. M. Pokotilo, A. N. Petukh, S. B. Lastovskii, J. Coutinho, M. J. Rayson, and P. R. Briddon, "Radiation-induced defect reactions in tin-doped Ge crystals," Solid State Phenom. **178–179**, 392 (2011).

[384]A. Vohra, I. Makkonen, G. Pourtois, J. Slotte, C. Porret, E. Rosseel, A. Khanam, M. Tirrito, B. Douhard, R. Loo, and W. Vandervorst, "Source/drain materials for Ge nMOS Devices: Phosphorus activation in epitaxial Si, Ge, $Ge_{1-x}Sn_x$ and $Si_yGe_{1-x-y}Sn_x$," ECS J. Solid State Sci. Technol. **9**, 044010 (2020).

[385]S. Ghosh, G. Sun, T. A. Morgan, G. T. Forcherio, H.-H. Cheng, and G.-E. Chang, "Dark current analysis on GeSn p-i-n photodetectors," Sensors **23**, 7531 (2023).

[386]S. Xu, "Germanium-tin photo detectors for applications in the two micron wavelength range," Ph.D. thesis (National University of Singapore, 2019).

[387]Y.-H. Hsieh, W.-Y. Hsieh, H.-H. Tseng, Y.-K. Liu, H. H. Cheng, and G.-E. Chang, "Enhanced infrared optical absorption in GeSn alloys for full-telecommunication photodetection," in *International Photonics and Optoelectronics Meetings* (OSA, Washington, DC, 2012), Vol. 95, Paper No. ITh3B.3.

[388]From Ref. 149, the dependence of the absorption coefficient can be approximated to $\alpha \propto (E - E_g)^{-1/2}$. Given the bowing behavior of $E_{g,GeSn}$, the data is fitted using the square root of a second-degree polynomial $f(x_{Sn})$.

[389]Q. Zhang, Y. Liu, J. Yan, C. Zhang, Y. Hao, and G. Han, "Theoretical investigation of tensile strained GeSn waveguide with Si_3N_4 liner stressor for mid-infrared detector and modulator applications," Opt. Express **23**, 7924 (2015).

[390]H. Tran, W. Du, S. A. Ghetmiri, A. Mosleh, G. Sun, R. A. Soref, J. Margetis, J. Tolle, B. Li, H. A. Naseem, and S.-Q. Yu, "Systematic study of $Ge_{1-x}Sn_x$

absorption coefficient and refractive index for the device applications of Si-based optoelectronics," J. Appl. Phys. **119**, 103106 (2016).

[391]H. Li, C. Chang, H. H. Cheng, G. Sun, and R. A. Soref, "Disorder-induced enhancement of indirect absorption in a GeSn photodetector grown by molecular beam epitaxy," Appl. Phys. Lett. **108**, 191111 (2016).

[392]V. R. D'Costa, Y. Fang, J. Mathews, R. Roucka, J. Tolle, J. Menéndez, and J. Kouvetakis, "Sn-alloying as a means of increasing the optical absorption of Ge at the C - and L -telecommunication bands," Semicond. Sci. Technol. **24**, 115006 (2009).

[393]H. Kumar and R. Basu, "Noise analysis of group IV material-based heterojunction phototransistor for fiber-optic telecommunication networks," IEEE Sens. J. **18**, 9180 (2018).

[394]A. K. Pandey, R. Basu, and G. E. Chang, "Gain performance of GeSn based n-p-n heterojunction phototransistor," in Proceedings of the International Conference on Numerical Simulation of Optoelectronic Devices (NUSOD) (2018).

[395]A. K. Pandey, R. Basu, and G. E. Chang, "Optimized $Ge_{1-x}Sn_x$/Ge multiple-quantum-well heterojunction phototransistors for high-performance SWIR photodetection," IEEE Sens. J. **18**, 5842 (2018).

[396]R. Roucka, J. Mathews, C. Weng, R. Beeler, J. Tolle, J. Menendez, and J. Kouvetakis, "High-performance near-IR photodiodes: A novel chemistry-based approach to Ge and Ge-Sn devices integrated on silicon," IEEE J. Quantum Electron. **47**, 213 (2011).

[397]G.-E. Chang, R. Basu, B. Mukhopadhyay, and P. K. Basu, "Design and modeling of GeSn-based heterojunction phototransistors for communication applications," IEEE J. Sel. Top. Quantum Electron. **22**, 425 (2016).

[398]W. Wang, Y. Dong, S. Y. Lee, W. K. Loke, X. Gong, S. F. Yoon, G. Liang, and Y. C. Yeo, "Germanium-Tin heterojunction phototransistor: Towards high-efficiency low-power photodetection in short-wave infrared range," in Digest of Technical Papers - Symposium on VLSI Technology (2016).

[399]P. Tao, W. Tang, Y. Wang, J. Shi, H. H. Cheng, and X. Wu, "Optoelectronic properties for the compressively strained $Ge_{1-x}Sn_x$ films grown on Ge(004)," Mater. Res. Express **7**, 035902 (2020).

[400]S. Adachi, "Optical dispersion relations for GaP, GaAs, GaSb, InP, InAs, InSb, $Al_xGa_{1-x}As$, and $In_{1-x}Ga_xAs_yP_{1-y}$," J. Appl. Phys. **66**, 6030 (1989).

[401]E. Simoen, F. De Stefano, G. Eneman, B. De Jaeger, C. Claeys, and F. Crupi, "On the temperature and field dependence of trap-assisted tunneling current in Ge p+n junctions," IEEE Electron Device Lett. **30**, 562 (2009).

[402]C. Claeys, E. Simoen, G. Eneman, K. Ni, A. Hikavyy, R. Loo, S. Gupta, C. Merckling, A. Alian, and M. Caymax, "Review–Device assessment of electrically active defects in high-mobility materials," ECS J. Solid State Sci. Technol. **5**, P3149 (2016).

[403]O. Madelung, "Elements of the IVth group and IV-IV compounds," in *Semiconductors: Data Handbook* (Springer, Berlin, Heidelberg, 2004), pp. 7–70.

[404]E. Simoen, G. Brouwers, R. Yang, G. Eneman, M. B. Gonzalez, F. Leys, B. D. Jaeger, J. Mitard, D. Brunco, L. Souriau, N. Cody, S. Thomas, L. Lajaunie, M. David, and M. Meuris, "Is there an impact of threading dislocations on the characteristics of devices fabricated in strained–Ge substrates?," Phys. Status Solidi C **6**, 1912 (2009).

[405]E. Simoen, C. Claeys, A. Oliveira, P. Agopian, J. Martino, B. Hsu, G. Eneman, E. Rosseel, R. Loo, H. Arimura, N. Horiguchi, W.-C. Wen, and H. Nakashima, "Device-based threading dislocation assessment in germanium hetero-epitaxy," in *34th Symposium on Microelectronics Technology and Devices (SBMicro)* (IEEE, 2019), Vol. 50, pp. 1–6.

[406]B. Son, Y. Lin, K. H. Lee, Q. Chen, and C. S. Tan, "Dark current analysis of germanium-on-insulator vertical p-i-n photodetectors with varying threading dislocation density," J. Appl. Phys. **127**, 203105 (2020).

[407]M. B. Gonzalez, G. Eneman, G. Wang, B. De Jaeger, E. Simoen, and C. Claeys, "Analysis of the temperature dependence of trap-assisted tunneling in Ge pFET junctions," J. Electrochem. Soc. **158**, H955 (2011).

[408]G. Eneman, E. Simoen, R. Yang, B. De Jaeger, G. Wang, J. Mitard, G. Hellings, D. Brunco, R. Loo, K. De Meyer, M. R. Caymax, C. Claeys, M. Meuris, and M. Heyns, "Defects, junction leakage and electrical performance of Ge pFET devices," ECS Trans. **19**, 195 (2009).

[409]N. A. DiLello, D. K. Johnstone, and J. L. Hoyt, "Characterization of dark current in Ge-on-Si photodiodes," J. Appl. Phys. **112**, 054506 (2012).

04 January 2025 10:11:00

[410]P. N. Grillot, S. A. Ringel, and E. A. Fitzgerald, "Effect of composition on deep levels in heteroepitaxial Ge$_x$Si$_{1-x}$ layers and evidence for dominant intrinsic recombination-Generation in relaxed ge layers on Si," J. Electron. Mater. **25**, 1028 (1996).

[411]E. Simoen, P. Clauws, and J. Vennik, "DLTS of grown-in dislocations in p- and n- type high-purity germanium," Solid State Commun. **54**, 1025 (1985).

[412]M. Sande, L. Goethem, L. Laet, and H. Guislain, "Dislocations in high-purity germanium and its relation to γ-ray detector performance," Appl. Phys. A **40**, 257 (1986).

[413]S. A. Shevchenko, "Electrical conductivity of germanium with dislocation grids," J. Exp. Theor. Phys. **88**, 66 (1999).

[414]J. Vanhellemont, J. Lauwaert, A. Witecka, P. Śpiewak, I. Romandic, and P. Clauws, "Experimental and theoretical study of the thermal solubility of the vacancy in germanium," Physica B **404**, 4529 (2009).

[415]I. Capan, B. Pivac, I. Hawkins, V. Markevich, A. Peaker, L. Dobaczewski, and R. Jačimović, "Neutron-irradiation-induced defects in germanium: A Laplace deep level transient spectroscopy study," Vacuum **84**, 32 (2009).

[416]J. Fage-Pedersen, A. N. Larsen, and A. Mesli, "Irradiation-induced defects in Ge studied by transient spectroscopies," Phys. Rev. B **62**, 10116 (2000).

[417]S. M. M. Coelho, F. D. Auret, P. J. Janse van Rensburg, and J. M. Nel, "Electrical characterization of defects introduced in n-Ge during electron beam deposition or exposure," J. Appl. Phys. **114**, 173708 (2013).

[418]E. Simoen, B. Vincent, C. Merckling, F. Gencarelli, L.-K. Chu, and R. Loo, "Deep-level transient spectroscopy of MOS capacitors on GeSn epitaxial layers," ECS Trans. **50**, 279 (2013).

[419]F. H. Baumann and W. Schröter, "Deformation-induced defects in p-Type germanium," Phys. Status Solidi A **79**, K123 (1983).

[420]V. P. Markevich, I. D. Hawkins, A. R. Peaker, V. V. Litvinov, L. I. Murin, L. Dobaczewski, and J. L. Lindström, "Electronic properties of vacancy-oxygen complex in Ge crystals," Appl. Phys. Lett. **81**, 1821 (2002).

[421]M. Hogsed, K. Choe, N. Miguel, B. Wang, and J. Kouvetakis, "Radiation-induced electron and hole traps in Ge$_{1-x}$Sn$_x$ (x = 0–0.094)," J. Appl. Phys. **127**, 065708 (2020).

[422]C. Nyamhere, A. Das, F. Auret, A. Chawanda, C. Pineda-Vargas, and A. Venter, "Deep level transient spectroscopy (DLTS) study of defects introduced in antimony doped Ge by 2MeV proton irradiation," Physica B **406**, 3056 (2011).

[423]E. E. Haller, W. L. Hansen, and F. S. Goulding, "Physics of ultra-pure germanium," Adv. Phys. **30**, 93 (1981).

[424]I. A. Gulyas, C. A. Stephenson, Q. Meng, S. R. Bank, and M. A. Wistey, "The carbon state in dilute germanium carbides," J. Appl. Phys. **129**, 055701 (2021).

[425]L. Dobaczewski, K. B. Nielsen, N. Zangenberg, B. B. Nielsen, A. R. Peaker, and V. P. Markevich, "Donor level of bond-center hydrogen in germanium," Phys. Rev. B **69**, 245207 (2004).

[426]M. Stavola, "Hydrogen in silicon and germanium," in *Proceedings of the 5th International Symposium on Advanced Science and Technology of Silicon Materials (JSPS Si Symposium)*, Kona, Hawaii (JSPS, 2008), pp. 337–343.

[427]F. Berg Rasmussen, R. Jones, and S. Öberg, "Nitrogen in germanium: Identification of the pair defect," Phys. Rev. B **50**, 4378 (1994).

[428]S. Gupta, E. Simoen, H. Vrielinck, C. Merckling, B. Vincent, F. Gencarelli, R. Loo, and M. Heyns, "Identification of deep levels associated with extended and point defects in GeSn epitaxial layers using DLTs," ECS Trans. **53**, 251 (2013).

[429]L. I. Khirunenko, M. G. Sosnin, A. V. Duvanskii, N. V. Abrosimov, and H. Riemann, "Divacancy-tin related defects in irradiated germanium," J. Appl. Phys. **123**, 161595 (2018).

[430]M.-Y. Ryu, Y. K. Yeo, M. Ahoujja, T. Harris, R. Beeler, and J. Kouvetakis, "Degenerate parallel conducting layer and conductivity type conversion observed from p-Ge$_{1-y}$Sn$_y$ (y = 0.06%) grown on n-Si substrate," Appl. Phys. Lett. **101**, 131110 (2012).

[431]P. Ščajev, V. Soriūtė, G. Kreiza, T. Malinauskas, S. Stanionytė, P. Onufrijevs, A. Medvids, and H.-H. Cheng, "Temperature dependent carrier lifetime, diffusion coefficient, and diffusion length in Ge$_{0.95}$Sn$_{0.05}$ epilayer," J. Appl. Phys. **128**, 115103 (2020).

[432]W. Takeuchi, T. Asano, Y. Inuzuka, M. Sakashita, O. Nakatsuka, and S. Zaima, "Characterization of shallow- and deep-level defects in undoped Ge$_{1-x}$Sn$_x$ epitaxial layers by electrical measurements," ECS J. Solid State Sci. Technol. **5**, P3082 (2016).

[433]B. Baert, S. Gupta, F. Gencarelli, R. Loo, E. Simoen, and N. D. Nguyen, "Electrical characterization of p-GeSn/n-Ge diodes with interface traps under dc and ac regimes," Solid-State Electron. **110**, 65 (2015).

[434]M. Carroll, J. Sheng, and J. C. Verley, "Low-temperature hetero-epitaxial growth of Ge on Si by high density plasma chemical vapor deposition," MRS Proc. **934**, 902 (2006).

[435]A. Stesmans, T. Nguyen Hoang, and V. V. Afanas'ev, "Hydrogen interaction kinetics of Ge dangling bonds at the Si$_{0.25}$Ge$_{0.75}$/SiO$_2$ interface," J. Appl. Phys. **116**, 044501 (2014).

[436]S. J. Pearton and J. M. Kahn, "Dislocations in germanium: Effects of plasma hydrogenation," Phys. Status Solidi A **78**, K65 (1983).

[437]B. J. Coomer, P. Leary, M. Budde, B. B. Nielsen, R. Jones, S. Öberg, and P. R. Briddon, "Vacancy-hydrogen complexes in germanium," Mater. Sci. Eng. B **58**, 36 (1999).

[438]Kusumandari, N. Taoka, W. Takeuchi, M. Fukudome, M. Sakashita, O. Nakatsuka, and S. Zaima, "Broad defect depth distribution in germanium substrates induced by CF$_4$ plasma," Appl. Phys. Lett. **103**, 033511 (2013).

[439]S.-Y. Wen, L. He, Y.-H. Zhu, and J.-W. Luo, "Excimer laser annealing suppresses the bubbles in the recrystallization of argon-implantation induced amorphous germanium," J. Appl. Phys. **133**, 045703 (2023).

[440]C. Schulte-Braucks, K. Narimani, S. Glass, N. Von Den Driesch, J. M. Hartmann, Z. Ikonic, V. V. Afanas'ev, Q. T. Zhao, S. Mantl, and D. Buca, "Correlation of bandgap reduction with inversion response in (Si)GeSn/high-k/metal stacks," ACS Appl. Mater. Interfaces **9**, 9102 (2017).

[441]L. I. Khirunenko, Y. V. Pomozov, M. G. Sosnin, N. V. Abrosimov, and H. Riemann, "The interaction between divacancies and shallow dopants in irradiated Ge:Sn," AIP Conf. Proc. **1583**, 75–79 (2014).

[442]M. Kaukonen, R. Jones, S. Öberg, and P. R. Briddon, "Tin-vacancy complexes in silicon," Phys. Rev. B **64**, 245213 (2001).

[443]M. Oehme, K. Kostecki, K. Ye, S. Bechler, K. Ulbricht, M. Schmid, M. Kaschel, M. Gollhofer, R. Körner, W. Zhang, E. Kasper, and J. Schulze, "GeSn-on-Si normal incidence photodetectors with bandwidths more than 40 GHz," Opt. Express **22**, 839 (2014).

[444]T. Mizoguchi, T. Imajo, J. Chen, T. Sekiguchi, T. Suemasu, and K. Toko, "Composition dependent properties of p- and n-type polycrystalline group-IV alloy thin films," J. Alloys Compd. **887**, 161306 (2021).

[445]B. Julsgaard, N. von den Driesch, P. Tidemand-Lichtenberg, C. Pedersen, Z. Ikonic, and D. Buca, "Carrier lifetime of GeSn measured by spectrally resolved picosecond photoluminescence spectroscopy," Photonics Res. **8**, 788 (2020).

[446]C. Schulte-Braucks, "Investigation of GeSn as novel group IV semiconductor for electronic applications," Ph.D. thesis (Forschungszentrum Jülich, 2017).

[447]O. Nakatsuka, N. Tsutsui, Y. Shimura, S. Takeuchi, A. Sakai, and S. Zaima, "Mobility behavior of Ge$_{1-x}$Sn$_x$ layers grown on silicon-on-insulator substrates," Jpn. J. Appl. Phys., Part 1 **49**, 04DA10 (2010).

[448]Vacancies cannot form upon cooling down in equilibrium conditions, as thermodynamics predict they are less stable compared to room temperature.

[449]L. Rebohle, S. Prucnal, and W. Skorupa, "A review of thermal processing in the subsecond range: Semiconductors and beyond," Semicond. Sci. Technol. **31**, 103001 (2016).

[450]S. Ghosh, B. Mukhopadhyay, G. Sen, and P. K. Basu, "Performance analysis of GeSn/SiGeSn quantum well infrared photodetector in terahertz wavelength region," Physica E **115**, 113692 (2020).

[451]D. Schroder, "The concept of generation and recombination lifetimes in semiconductors," IEEE Trans. Electron Devices **29**, 1336 (1982).

[452]E. Gaubas and J. Vanhellemont, "Dependence of carrier lifetime in germanium on resisitivity and carrier injection level," Appl. Phys. Lett. **89**, 142106 (2006).

[453]N. Derhacobian, P. Fine, J. T. Walton, Y. K. Wong, C. S. Rossington, and P. N. Luke, "Determination of surface recombination velocity and bulk lifetime in detector grade silicon and germanium crystals," IEEE Trans. Nucl. Sci. **41**, 1026 (1994).

[454]S. Saito, F. Y. Gardes, A. Z. Al-Attili, K. Tani, K. Oda, Y. Suwa, T. Ido, Y. Ishikawa, S. Kako, S. Iwamoto, and Y. Arakawa, "Group IV light sources to

04 January 2025 10:11:00

enable the convergence of photonics and electronics," Front. Mater. **1**, 15 (2014).

[455] J. J. Sheng, D. Leonhardt, S. M. Han, S. W. Johnston, J. G. Cederberg, and M. S. Carroll, "Empirical correlation for minority carrier lifetime to defect density profile in germanium on silicon grown by nanoscale interfacial engineering," J. Vac. Sci. Technol. B **31**, 051201 (2013).

[456] R. Geiger, J. Frigerio, M. J. Süess, D. Chrastina, G. Isella, R. Spolenak, J. Faist, and H. Sigg, "Excess carrier lifetimes in Ge layers on Si," Appl. Phys. Lett. **104**, 062106 (2014).

[457] G. Grzybowski, R. Roucka, J. Mathews, L. Jiang, R. T. Beeler, J. Kouvetakis, and J. Menéndez, "Direct versus indirect optical recombination in Ge films grown on Si substrates," Phys. Rev. B **84**, 205307 (2011).

[458] M. K. Hudait, S. W. Johnston, M. B. Clavel, S. Bhattacharya, S. Karthikeyan, and R. Joshi, "High carrier lifetimes in epitaxial germanium-tin/Al(In)As heterostructures with variable tin compositions," J. Mater. Chem. C **10**, 10530 (2022).

[459] S. Kako, K. Oda, T. Ido, and Y. Arakawa, "Excess carrier lifetime in epitaxially grown layers of germanium on silicon," in *IEEE 12th International Conference on Group IV Photonics (GFP)* (IEEE, 2015), pp. 171–172.

[460] G. Daligou, A. Attiaoui, S. Assali, P. Del Vecchio, and O. Moutanabbir, "Radiative carrier lifetime in GeSn midinfrared emitters," Phys. Rev. Appl. **20**, 064001 (2023).

[461] E. Rogowicz, J. Kopaczek, J. Kutrowska-Girzycka, M. Myronov, R. Kudrawiec, and M. Syperek, "Carrier dynamics in thin Germanium–Tin epilayers," ACS Appl. Electron. Mater. **3**, 344 (2021).

[462] E. Vitiello, S. Rossi, C. A. Broderick, G. Gravina, A. Balocchi, X. Marie, E. P. O'Reilly, M. Myronov, and F. Pezzoli, "Continuous-wave magneto-optical determination of the carrier lifetime in coherent Ge$_{1-x}$Sn$_x$/Ge heterostructures," Phys. Rev. Appl. **14**, 064068 (2020).

[463] S. D. Cesari, A. Balocchi, E. Vitiello, P. Jahandar, E. Grilli, T. Amand, X. Marie, M. Myronov, and F. Pezzoli, "Spin-coherent dynamics and carrier lifetime in strained Ge$_{1-x}$Sn$_x$ semiconductors on silicon," Phys. Rev. B **99**, 035202 (2019).

[464] R. Geiger, Ph.D. thesis (ETH, 2016).

[465] S. A. Srinivasan, M. Pantouvaki, P. Verheyen, G. Lepaee, P. Absil, J. Van Campenhout, and D. Van ThouAout, "Carrier lifetime assessment in integrated Ge waveguide devices," in *IEEE 12th International Conference on Group IV Photonics (GFP)* (IEEE, 2015), pp. 167–168.

[466] B. R. Conley, J. Margetis, W. Du, H. Tran, A. Mosleh, S. A. Ghetmiri, J. Tolle, G. Sun, R. Soref, B. Li, H. A. Naseem, and S.-Q. Yu, "Si based GeSn photoconductors with a 1.63 A/W peak responsivity and a 2.4 μm long-wavelength cutoff," Appl. Phys. Lett. **105**, 221117 (2014).

[467] Pseudomorphic refers to a film that grows epitaxially without relaxing the strain induced by a lattice-mismatched substrate. Lattice-matched refers to epitaxial growth in absence of lattice mismatch.

[468] S. Dominici, H. Wen, F. Bertazzi, M. Goano, and E. Bellotti, "Numerical study on the optical and carrier recombination processes in GeSn alloy for E-SWIR and MWIR optoelectronic applications," Opt. Express **24**, 26363 (2016).

[469] S. Ghosh, D. Leonhardt, and S. M. Han, "Effect of threading dislocation density and dielectric layer on temperature-dependent electrical characteristics of high-hole-mobility metal semiconductor field effect transistors fabricated from wafer-scale epitaxially grown p-type germanium on silicon substrates," J. Appl. Phys. **115**, 094507 (2014).

[470] X. Liu, A. Giunto, J. D. Hutchinson, N. Humblot, D. Damry, R. L. Milot, A. Fontcuberta i Morral, and J. Boland, "THz characterization of GeSn monocrystalline thin films," in *47th International Conference on Infrared, Millimeter and Terahertz Waves (IRMMW-THz)* (2022).

[471] S. Prucnal, Y. Berencén, M. Wang, L. Rebohle, R. Böttger, I. A. Fischer, L. Augel, M. Oehme, J. Schulze, M. Voelskow, M. Helm, W. Skorupa, and S. Zhou, "Ex situ n+ doping of GeSn alloys via non-equilibrium processing," Semicond. Sci. Technol. **33**, 065008 (2018).

[472] R. Cheng, Z. Chen, S. Yuan, M. Takenaka, S. Takagi, G. Han, and R. Zhang, "Mobility enhancement techniques for Ge and GeSn MOSFETs," J. Semicond. **42**, 023101 (2021).

[473] T. Imajo, K. Moto, R. Yoshimine, T. Suemasu, and K. Toko, "High hole mobility ($|\geq 500$ cm^{-2}V^{-1}s^{-1}) polycrystalline Ge films on GeO$_2$-coated glass and plastic substrates," Appl. Phys. Express **12**, 015508 (2019).

[474] D. Hull and D. Bacon, *Introduction to Dislocations* (Elsevier, 2011).